The Pennsylvania State University

The Graduate School

Department of Materials Science and Engineering

DESIGN OF NEW ANION EXCHANGE MEMBRANES FOR ELECTROCHEMICAL APPLICATIONS

A Dissertation in

Materials Science and Engineering

by

Liang Zhu

© 2016 Liang Zhu

Submitted in Partial Fulfillment
of the Requirements
for the Degree of

Doctor of Philosophy

May 2016

The dissertation of Liang Zhu was reviewed and approved* by the following:

Michael A. Hickner
Associate Professor of Materials Science and Engineering
Dissertation Advisor
Chair of Committee

Qing Wang
Professor of Materials Science and Engineering

Evangelos Manias
Professor of Materials Science and Engineering

Enrique Gomez
Associate Professor of Chemical Engineering

Suzanne Mohney
Professor of Materials Science and Engineering and Electrical Engineering
Chair, Intercollege Graduate Degree Program in Materials Science and Engineering
Head of the Department of Department or Graduate Program

*Signatures are on file in the Graduate School

ABSTRACT

Anion exchange membranes (AEMs) are polymer-based electrolyte solids that conduct anions (OH^-, HCO_3^-, Cl^-, *et al.*), with positively charged groups bound covalently to the polymer backbones. There has been a strong and growing worldwide interest in the use of anion exchange membranes for electrochemical energy conversion and storage systems. Anion exchange membrane fuel cells (AEMFCs) have been regarded as promising energy conversion devices for stationary and mobile applications due to their potential low cost. To realize high-performance AEMFCs, new polymeric membranes are needed that are highly conductive and chemically stable. Herein, cross-linked, multication side chain, and fluorene side chain AEMs based on poly(2,6-dimethyl-1,4-phenylene oxide)s (PPO) were synthesized. PPO was chosen as an AEM substrate because of its ease of functionalization at large scale and relatively good stability and membrane properties.

To produce anion conductive and durable polymer electrolytes for alkaline fuel cell applications, a series of cross-linked quaternary ammonium functionalized poly(2,6-dimethyl-1,4-phenylene oxide)s with mass-based ion exchange capacities (IEC) ranging from 1.80 to 2.55 mmol/g were synthesized via thiol-ene click chemistry. From small angle X-ray scattering (SAXS), it was found that the cross-linked membranes developed micro-phase separation between the polar PPO backbone and the hydrophobic alkyl side chains. The ion conductivity, dimensional stability, and alkaline durability of the cross-linked membranes were evaluated. The hydroxide ion conductivity of the cross-linked samples reached 60 mS/cm in liquid water at room temperature. The chemical stabilities of the membranes were evaluated under severe, accelerated aging conditions and degradation was quantified by measuring ion conductivity changes during aging. The cross-linked membranes retained their relatively high ion conductivity and good mechanical properties both in 1 M and 4 M NaOH at 80 °C after 500 h. Attenuated total

reflection (ATR) spectra were used to study the degradation pathways of the membranes, and it was discovered that β-hydrogen (Hofmann) elimination was likely to be the major pathway for degradation in these membranes.

Side-chain containing AEMs with one, two or three cations per side chain were designed and synthesized, enabling a study of how the degree of polymer backbone functionalization and arrangement of cations on the side chain impact AEM properties. A systematic study of anion exchange membranes (AEMs) with multiple cations per side chain site was conducted to demonstrate how this motif can boost both the conductivity and stability of poly(2,6-dimethyl-1,4-phenylene oxide)-based AEMs. The highest conductivity, up to 99 mS/cm at room temperature, was observed for a triple-cation side chain AEM with 5 or 6 methylene groups between cations. This conductivity was considerably higher than AEM samples based on benzyltrimethyl ammonium or benzyldimethylhexyl ammonium groups with only one cation per side chain site. In addition to high conductivity, the multication side chain AEMs showed good alkaline and dimensional stabilities. High retention of ion exchange capacity (IEC) (93% retention) and ionic conductivity (90% retention) were observed for the triple-cation side chain AEMs during degradation testing in 1 M NaOH at 80 °C for 500 h. Based on the high-performance triple-cation side chain AEM, a Pt-catalyzed fuel cell with a peak power density of 364 mW/cm^2 was achieved at 60 °C under 100% related humidity.

Anion-conductive copolymers, poly(2,6-dimethyl-1,4-phenylene oxide)s containing fluorene side chains with pendant alkyltrimethylammonium groups, were synthesized via Suzuki-Miyaura coupling of aryl bromides with fluorene-boronic acids. The quaternized copolymers produced ductile, transparent membranes which were soluble in dimethyl formamide, dimethyl sulfoxide and methanol at room temperature. The fluorene side chain-containing membranes showed considerably higher hydroxide ion conductivities, up to 176 mS/cm at 80 °C, compared to that of typical anion exchange membranes based on the benzyltrimethyl ammonium moiety.

The results of titration and hydroxide ion conductivity measurements demonstrated excellent chemical stability of the fluorene side chain-containing anion exchange membranes (AEMs), even after 1000 h immersion in 1 M NaOH at 80 °C. The results of this study suggest a scalable route for the preparation of AEMs for practical alkaline fuel cell applications.

A unique approach was employed to toughen AEMs by crosslinking the AEMs using commercial Jeffamine additives. Compared to the BTMA40 membrane, the 10% Jeffamine cross-linked membrane demonstrated significantly higher elongation at break. To be specific, the hydrated BTMA40 membrane showed a 51.7% elongation at break, while the 10% Jeffamine cross-linked membrane had a 166.8 % elongation at break. Clearly, the introducing of hydrophilic cross-linked network greatly enhanced the toughness of the AEMs.

Overall, this thesis details a number of strategies for the large-scale production of PPO-based anion exchange membranes. These strategies will be useful in going forward in the design and deployment of hydroxide, bromide, bicarbonate, and chloride-conducting membranes for water purification and electrochemical technology.

TABLE OF CONTENTS

List of Figures ix

List of Tables xv

List of Schemes xvi

Acknowledgements xvii

Chapter 1 Introduction to Anion Exchange Membranes 1

1.1 Introduction 1
1.2 Working Mechanism of an H_2-O_2 Type AEMFC 3
1.3 Motivation for This Work 4
1.4 References 12

Chapter 2 Literature Review of Anion Exchange Membranes 15

2.1 Introduction 15
2.2 Anion Exchange Membranes with Different Side Chains 15
2.2.1 Anion Exchange Membranes with Single-Cation Side Chains 15
2.2.2 AEMs Based on Poly (2, 6-dimethyl-1, 4-phenylene oxide) 22
2.2.3 AEMs Based on Poly (olefin)s 24
2.2.4 Fluorene-Containing AEMs 26
2.2.5 Other AEM Structures 28
2.2.2 Anion Exchange Membrane with Multication Side Chains 29
2.2.3 Anion Exchange Membranes with Modified Ammonium Cations 33
2.3 Crosslinking of AEMs 39
2.4 Chemical Degradation of Anion Exchange Membranes 48
2.4.1 Degradation of AEMs Cations 48
2.4.2 Degradation of AEMs Polymer Backbones 51
2.5 Summary 53
2.6 Reference 55

Chapter 3 Experimental Details of Polymer Synthesis, Membrane Preparation and Characterization. 59

3.1. Introduction 59
3.2 Materials 59
3.3 Synthesis and Characteriazation of Side Chain Containing PPO Copolymers 60
3.3.1 Synthesis of Side Chain Containing PPO Copolymer 60
3.4 Characterization of Side Chain Containing PPO Copolymer and Membranes 60
3.4.1 Nuclear Magnetic Resonance Spectroscopy 61
3.4.2 Membrane Preparation 61
3.4.3 Conductivity Measurements 61
3.4.5 Water Uptake 62

3.4.6 Titrated Gravimetric IEC Measuring. 63
3.4.6 Calculation of the Diffusion Coefficient (D) and Dilute Ion Diffusivity (D_0) 63
3.4.7 Mechanical Property Measurements 64
3.4.8 Morphological Characterization of the AEMs 65
3.4.9 FTIR Spectra 65
3.4.10 Gel Fraction for Cross-linked AEMs 66
3.4.11 Membrane-Electrode Assembly Fabrication and Fuel Cell testing. 66
3.5 References 67

Chapter 4 Cross-linking of Comb-Shaped Polymer Anion Exchange Membranes via Thiol-ene Click Chemistry 68

4.1 Introduction 68
4.2 Experimental Section 70
4.3 Results and Discussion 72
4.4 Conclusions 89
4.5 References 91

Chapter 5 Multication Side Chain Anion Exchange Membranes 94

5.1 Introduction 94
5.2 Experimental Section 95
5.3 Results and Discussion 99
5.4 Conclusions 126
5.5 References 127

Chapter 6 Poly(2,6-dimethyl-1,4-phenylene oxide)s With Fluorene Side Chains for Anion Exchange Membranes 130

6.1 Introduction 130
6.2 Experimental Section 131
6.3 Results and Discussion 134
6.4 Conclusions 149
6.5 References 151

Chapter 7 Hydrophilic Robust Anion Exchange Membranes 153

7.1 Introduction 153
7.2 Experimental Section 153
7.3 Results and Discussion 155
7.4 Conclusions 164
7.5 References 166

Chapter 8 Summary and Future Research Directions 167

8.1 Summary and Conclusions 167
8.1.1 Cross-linking of Comb-Shaped Polymer Anion Exchange Membranes via Thiol-ene Click Chemistry 168
8.1.2 MultiCation Side Chain Anion Exchange Membranes 168

8.1.3 Poly(2,6-dimethyl-1,4-phenylene oxide)s With Fluorene Side Chains for Anion Exchange Membranes 169
8.1.4 Jeffamine cross-linked robust Anion Exchange Membranes 170
8.2 Future Research Direction 170

LIST OF FIGURES

Figure 1.1 Schematic depiction of an AEM based fuel cell with a Ni-catalyzed anode, an Ag-catalyzed cathode, and hydrogen feed. © National Academy of Sciences, 2008.[18] ...3

Figure 1.2 Synthesis of cross-linked comb-shaped AEMs, X*x*Y*y*C*z*, with one alkyl side chain using thiol-ene click chemistry. 6

Figure 1.3 Multication side chain AEMs based on PPO. 7

Figure 1.4 Chemical degradation pathways for the tetraalkyammonium cation small molecules. 8

Figure 1.5 Chemical structures of tetraalkyammonium small molecule AEM analogs and polymers studied by Nuñez, *et al*.[46] 9

Figure 1.6 Synthetic strategy for the fluorene single-side chains poly (2,6-dimethyl-1,4-phenylene oxide). 10

Figure 2.1 Synthetic strategy of SEBS AEMs. © ELSEVIER, 2010.[3] 16

Figure 2.2 Synthesis of quaternized SEBS via iridium-catalyzed aromatic C-H borylation and palladium-catalyzed Suzuki cross-coupling. © American Chemical Society, 2015.[12] 17

Figure 2.3 Synthetic route of quaternary ammonium polysulphone in hydroxide form. © WILEY-VCH Verlag GmbH & Co. KGaA, Weinheim, 2010.[13] 18

Figure 2.4 Synthetic route of quaternary ammonium-containing polymers from bromination of tetramethyl bisphenol A-based PS. © American Chemical Society, 2010.[4] 19

Figure 2.5 Synthetic route of trimethylbenzylammonium functionalized PS via C-H borylation and Suzuki coupling reactions. © American Chemical Society, 2014.[14] 20

Figure 2.6 Chemical structure of imidazolium functionalized polysulfone AEM. © The Royal Society of Chemistry, 2011.[15] 21

Figure 2.7 Chemical structure of the tri(2,4,6-trimethoxyphenyl) polysulfone-methylene quaternary phosphonium hydroxide (TPQPOH). © WILEY-VCH Verlag GmbH & Co. KGaA, Weinheim, 2009.[16] 22

Figure 2.8 Synthetic route for the poly (2, 6-dimethyl-1, 4-phenylene oxide)-*b*-poly (vinylbenzyltrimethylammonium) diblock copolymers based AEMs. © American Chemical Society, 2015.[18] 23

Figure 2.9 Synthetic procedure for tetraalkylammonium-functionalized polyethylene AEMs. © American Chemical Society, 2010.[19] 24

Figure 2.10 Synthetic procedure for phosphonium-functionalized polyethylene AEMs. © American Chemical Society, 2012.[20] 25

Figure 2.11 Synthetic route of QPE. © American Chemical Society, 2011.[21] 26

Figure 2.12 Chemical structure of poly (arylene ether sulfone)s containing tetra-quaternary ammonium hydroxide on fluorenyl group (QAPAES-OH). © ELSEVIER, 2012.[22] 27

Figure 2.13 Chemical structure of multivalent metal-cation-based AEMs and synthetic route. © American Chemical Society, 2012.[26] 28

Figure 2.14 Chemical structure of hydroxide-conducting AEMs based on benzimidazolium hydroxide. © American Chemical Society, 2012.[27] 29

Figure 2.15 Synthetic route for the QAPS and DQAPS. © The Royal Society of Chemistry, 2013.[28] 30

Figure 2.16 Chemical structure of GQ-PEEK. © WILEY-VCH Verlag GmbH & Co. KGaA, Weinheim, 2014.[29] 31

Figure 2.17 Graphical illustrations and chemical structures of (a) conventionally QAPPO AEM and (b) functionalized PPO bearing quaternary ammonium groups (PPO-TQA). © The Royal Society of Chemistry, 2014.[30] 32

Figure 2.18 Chemical structure of comb-shaped CyDx copolymers. © American Chemical Society, 2013.[31] 33

Figure 2.19 Chemical stability of the quaternary ammonium cation of CyDx and BTMAx membranes after immersion in 1 M NaOH solution at 80 °C. © American Chemical Society, 2013.[31] 34

Figure 2.20 Synthetic route of the AEMs containing ammonium groups via flexible spacers (gQAPPO); (A)iridium catalyzed Miyaura; (B) bromination of PPO; (C) Suzuki coupling catalyzed by palladium; (D) quaternization and hydroxide exchange of gPPO membrane. © The Royal Society of Chemistry, 2015.[32] 35

Figure 2.21 Synthetic route for PPO modified with heptyltrimethylammonium side chains (PPO-7Q) via lithiation, bromoalkylation and quaternization. (i)*n*-BuLi, THF, -78 °C (ii) 1,6-dibromohexane, THF, -78 °C, (iii) trimethylamine, NMP, -78 °C; NaOH. © The Royal Society of Chemistry, 2015.[33] 36

Figure 2.22 Polymer structures of fluorene-based AEMs. © American Chemical Society, 2015.[34] 37

Figure 2.23 Chemical structure of polyfluorene ionomer. © American Chemical Society, 2011.[35] 37

Figure 2.24 Synthetic route of AEMs based on quaternized polypropylene. © The Royal Society of Chemistry, 2015.[36] 38

Figure 2.25 Chemical structure of the cross-linked AEMs prepared by amination agent of mixing diamine (with longer alkyl chain). © ELSEVIER, 2011.[52] 40

Figure 2.26 Synthetic route for the alkaline Ionic liquid(IL)-based anion exchange membranes. © American Chemical Society, 2010.[53] 40

Figure 2.27 Monomer structure and synthetic route of the cross-linked AEMs. © American Chemical Society, 2010.[54] 41

Figure 2.28 Hydroxide conductivity of cross-linked AEMs prepared by Coates *et al.*and Nafion-112 in liquid water as a function of temperature. © American Chemical Society, 2010.[54] 42

Figure 2.29 Synthetic route for the cross-linked comb-shaped AEMs via olefin metathesis with Grubbs II catalyst. © The Royal Society of Chemistry, 2014.[55] 43

Figure 2.30 (a) Swelling ratio as a function of degree of crosslinking at 60 °C and 80 °C; (b) hydroxide conductivity of the XxYy and reported AEMs (circles) at different swelling ratio. © The Royal Society of Chemistry, 2014.[55] 43

Figure 2.31 Chemical structure of the self-crosslinked TPQPOH (SCL-TPQPOH). © The Royal Society of Chemistry, 2011.[8] 44

Figure 2.32 Swelling degree of TPQPOH and SCL-TPQPOH AEMs at 60 ^{o}C. © The Royal Society of Chemistry, 2011.[8] 45

Figure 2.33 Chemical structures for alkaline functional groups attached to the polysulfone backbone. (A) Quaternary ammonium (QA). (B) Tertiary amino (TA). (C) A new type of QA generated upon solidification (*x*QA), crosslinking two nearest chains. © The Royal Society of Chemistry, 2011.[56] 46

Figure 2.34 (A) the ionic conductivity and swelling degree plot of *x*TQAPS . (B) the stability testing of *x*TQAPS in hot water. © The Royal Society of Chemistry, 2010.[56] ..47

Figure 2.35 Possible degradation pathways of AEMs based on PPO in alkaline environment. 48

Figure 2.36 Degradation pathways of poly(sulfones) backbone in alkaline media: (A) OH^- attack at quaternary carbon to yield to phenylpropane alcohol, and (B) displacement by OH^- of the aryl ethers to generate phenols. Red lines indicates electron delocalizatioin. ©2013 National Academy of Sciences, 2013.[64] 52

Figure 2.37 Computational and experimental results of alkaline stability of benzyl trimethyl ammonium functionalized polyaromatics. © American Chemical Society, 2014.[65] 53

Figure 4.1 ^{1}H NMR of crosslinkable comb-shaped X80Y*y* in bromine salt form in DMSO-d_6. 75

Figure 4.2 FTIR spectra of uncross-linked and cross-linked membranes. 76

Figure 4.3 Liquid water uptake (a) and swelling ratio (b) of membranes in OH^- form as a function of degree of cross-linking at room temperature. 77

Figure 4.4 Liquid water uptake (a) and swelling ratio (b) of membranes in OH^- form as a function of temperature. 78

Figure 4.5 Hydroxide conductivity of cross-linked and BTMA membranes as a function of (a) IEC (ion exchange capacity) and (b) hydration number λ 79

Figure 4.6 Hydroxide conductivity of membranes as a function of (a) IEC (ion exchange capacity) and (b) hydration number λ (moles of water per mole of quaternary ammonium group) in water at room temperature. Conductivities were measured with samples exposed to liquid water. 80

Figure 4.7 Hydroxide conductivity of X80Y*x*C6 and BTMA30 membranes as a function of temperature. Conductivities were measured with samples exposed to liquid water. 81

Figure 4.8 Bicarbonate conductivity of AEMs as a function of temperature and the computed Arrhenius activation energies. 82

Figure 4.9 Water volume fraction dependence of the effective hydroxide conductivity in the water channels (σ') in water at room temperature 83

Figure 4.10 SAXS profiles of dry polymer membranes in the bromide form. 84

Figure 4.11 Ratio of the diffusion coefficient, D, to the dilute solution diffusivity, D_0, as a function of hydration number for membranes in the hydroxide form. 85

Figure 4.12 Chemical stability of the quaternary ammonium cation of X60Y30C6 and uncross-linked X60Y30C6 in 1 M and 4 M NaOH solution at 80 °C, and OH^- conductivity as a function of duration time measured at 20 °C. 87

Figure 4.13 ATR spectra of treated X60Y15C6 membrane (a) ATR spectra of functional group region (b) fingerprint region. 88

Figure 5.1 ^{1}H NMR of 1-(*N',N'*-dimethylamino)-6-(*N,N,N*-trimethylammonium) dodecane bromide in $CHCl_3$-d_1. 101

Figure 5.2 ^{1}H NMR of 1-(*N',N'* - dimethylamino)-6,11-(*N,N,N*-trimethylammonium) undecane bromide in $CHCl_3$-d_1. 102

Figure 5.3. ^{1}H NMR of D40NC6NC6 in bromide salt form in DMSO-d_6. 103

Figure 5.4 ^{1}H NMR of T30NC6NC5N in bromide salt form in DMSO-d_6. 104

Figure 5.5 IEC values as a function of the degree of polymer backbone functionalization and side chain type. 107

Figure 5.6 Liquid water uptake (a) and swelling ratio (b) of membranes in OH^- form as a function of IEC at room temperature. 108

Figure 5.7 Liquid water uptake (a) and swelling ratio (b) of membranes in OH^- form as a function temperature. 109

Figure 5.8 Hydroxide conductivity of multication and single-cation AEMs in liquid water at 20 °C as a function of IEC. 110

Figure 5.9 Hydroxide conductivity of AEMs as a function of temperature. 111

Figure 5.10 Hydroxide conductivity of AEMs in an Arrhenius-type temperature plot showing activation energies in kJ/mol. 112

Figure 5.11 SAXS profiles of dry membranes in the bromide form. 113

Figure 5.12. SAXS profiles of triple-cation and BTMA40 AEMs in the bromide form. 114

Figure 5.13TEM images of dry membranes in the bromide form (a) BTMA40; (b) S60NC6; (c) D30NC6NC6; (d) T20NC6NC5N. 115

Figure 5.14 Water volume fraction dependence of the effective hydroxide conductivity in the water channels (σ') in liquid water at room temperature. 116

Figure 5.15 Ratio of the diffusion coefficient, D, to the dilute solution diffusivity, D_0, as a function of hydration number for membranes in the hydroxide form. 117

Figure 5.16 OH^- mobility ratios (D/D_0) of multication and single-cation AEMs as a function of OH^- concentrations in liquid water at 20 °C. 118

Figure 5.17 Stability of the T20NC6NC5N, D30NC6NC6, S60NC6 and BTMA40 samples in 1 M NaOH solution at 80 °C; (a) IEC and (b) OH^- conductivity as a function of duration time measured at 20 °C. 119

Figure 5.18. ^1H NMR spectra of D30NC6NC6 before and after stability tests in 1 M NaOH solution at 80 °C. 120

Figure 5.19 OH^- conductivity measured at 20 °C for the T20NC6NC5N, D30NC6NC6, S60NC6 and BTMA40 samples in 4 M NaOH solution at 80 °C as a function of degradation time. 121

Figure 5.20 Water uptake (a) and Hydroxide conductivity (b) of multication AEMs with different length of spacers at 20 °C as a function of IEC. 123

Figure 5.21 Stability of the T20NC6NC5N, T20NC6NC5N, D30NC6NC6, and D30NC3NC6 samples in 1 M NaOH solution at 80 °C; (a) IEC and (b) OH^- conductivity as a function of duration time measured at 20 °C. 124

Figure 5.22 Fuel cell performance of the AEM samples under H_2/O_2 conditions. 125

Figure 6.1 ^{1}H NMR of 2-bromo-9, 9-bis(6'-bromohexyl) fluorene in $CHCl_3$-d_1. 138

Figure 6.2 ^{1}H NMR of 2-dioxaboralane-9, 9-bis(6'-bromohexyl)fluorene in $CHCl_2CHCl_2$-d_2. 139

Figure 6.3 ^{1}H NMR of 40PPO-flurorene (PPOF) in $CHCl_2CHCl_2$-d_2. 140

Figure 6.4^{1}H NMR of 40PPOFC6N in DMSO-d_6. 141

Figure 6.5. ^{1}H NMR of 40PPOFC6NC6 in DMSO-d_6.....142

Figure 6.6 Liquid water uptake of membranes in OH^- form as a function of (a) IEC and (b) temperature. 143

Figure 6.7 Hydroxide conductivity of PPOF and BTMA40 membranes in liquid water at 20 °C as a function of (a) IEC (in mmol/g) and (b) hydration number (λ). 145

Figure 6.8 Hydroxide conductivity of PPOF and BTMA40 membranes (a) as a function of temperature and (b) Arrhenius-type temperature plot showing activation energies in kJ/mol.....146

Figure 6.9 Chemical stability of the quaternary ammonium cation in 50PPOC6NC6, 50PPOC6N, and BTMA40 during immersion in 1 M NaOH solution at 80 °C. (a) OH^- conductivity measured at 20 °C and (b) IEC as a function of time. 148

Figure 7.1 FTIR spectra of PPO, brominated PPO, Jeffamine and cross-linked membranes. 156

Figure 7.2 Stress-strain curves for J10PPO and BTMA40 hydrated AEMs.....157

Figure 7.3 Maximum tensile stress for Jeffamine cross-linked and BTMA40 hydrated AEMs. 158

Figure 7.4 Maximum elongation at break for Jeffamine cross-linked and BTMA40 hydrated AEMs. 159

Figure 7.5 Hydroxide conductivity of Jeffamine cross-linked and BTMA AEMs in liquid water at 20 °C as a function of IEC.....160

Figure 7.6 Hydroxide conductivity of Jeffamine cross-linked and BTMA AEMs in liquid water at 20 °C as a function of hydration number (λ). 161

Figure 7.7 TEM images of dry membranes in the bromide form (a) BTMA40; (b) J10PPO.....162

Figure 7.8 Chemical stability of the quaternary ammonium cation of Jeffamine cross-linked and BTMA40 samples in 1 M NaOH solution at 80 °C, OH^- conductivity as a function of duration time measured at 20 °C. 163

LIST OF TABLES

Table 2.1 Alkaline stability of various small molecule analogs at 160 °C in 6 M NaOH. © WILEY-VCH Verlag GmbH & Co. KGaA, Weinheim, 2015.[62] 50

Table 4.1 Ion exchange capacity, water uptake, swelling and conducting behaviors of cross-linked AEMs.....74

Table 5.1 Properties of the multication side chain PPO membranes. 106

Table 6.1 Suzuki-Miyaura couplings of aryl bromide of PPO with boronic acid.....136

Table 6.2 Mechanical properties of hydrated PPOF and BTMA30 AEMs. 136

Table 6.3 Ion exchange capacity, water uptake, swelling and ionic conductivity of PPOF AEMs. 137

Table 7.1 Ion exchange capacity, water uptake, ionic conductivity and mechanical properties of Jeffamine cross-linked AEMs.....165

LIST OF SCHEMES

Scheme 4.1 Synthesis of cross-linked comb-shaped AEMs, X*x*Y*y*C*z*, with one alkyl side chain using thiol-ene click chemistry. 72

Scheme 4.2 Possible degradation pathways of the quaternary ammonium cations in the membranes. 86

Scheme 5.1 Chemical structures of BTMA40 and S60NC6. 99

Scheme 5.2 Synthetic route for multication sidechain AEMs. 100

Scheme 6.1 Synthetic route for fluorene side chain ionomers. (a) 50 wt % NaOH, tetrabutylammonium, 65 °C, 7 h; (b) Pd(dppf)Cl_2, KOAc, dioxane, 75 °C, 12 h; (c) $Pd(OAc)_2$, K_3PO_4, XPhos, toluene/water, 100 °C, 24 h; (d) 50 °C, 24 h; (e) 60 °C, 72 h. 135

Scheme 7.1 Synthetic route of the Jeffamine cross-linked AEMs. 155

ACKNOWLEDGEMENTS

I would, first and foremost, like to thank my advisor, Dr. Michael Hickner, for providing me with the research opportunity to pursue my PhD degree. Under his patient guidance over the years, I have become better in polymer science and engineering, more than I expected. Without the combined guidance and support of Dr. Hickner, I wouldn't have grown as a scientist. I would also like to give my gratitude to my committee members, Dr. Qing Wang, Dr. Evangelos Manias, and Dr. Enrique Gomez for serving on my committee and for their expertise that helped the dissertation completion.

I would also like to thank the Hickner Research Group for their support in research during the course of PhD study, particularly Li Nanwen, Melanie Disabb-Miller, Lizhu Wang, Douglas Kushner, Tawanda J. Zimudzi and Jing Pan. Thanks Nanwen for teaching how to synthesize brominated PPO and membrane characterization. I also recognized the help from Tawanda J. Zimudzi in FTIR characterization of membranes.

Last, I would also like to give thanks to my family for supporting me though the ups and downs that come with life and schooling. I cherish your support and sacrifices.

Chapter 1

Introduction to Anion Exchange Membranes

1.1 Introduction

Anion exchange membranes are solid polymer electrolytes that conduct anions, for exampleOH$^-$, HCO_3^-, Cl$^-$, with positively charged groups bound covalently to the polymer backbones.[1] There has been a strong and growing worldwide interest in the use of anion exchange membranes for electrochemical energy conversion and storage systems.[1] A key part of the research in this burgeoning sub-field is the development of polymeric anion exchange membranes that are highly conductive, electrochemically stable, and scalable to quantities that can be applied for cell engineering.[2] Currently, there are very few commercially available anion exchange membranes and none are highly suited to electrochemical technology. Therefore, the community is looking to develop a consensus on the best design parameters to move new polymer structures into this space.

Fuel cell technology offers clean, efficient, and reliable power generation for electronic devices used in a wide range of applications such as mobile, transportation, and stationary technologies. In a fuel cell, electricity is generated by means of an electro-chemical reaction that is promoted by an overall negative Gibb's free energy of reaction between the fuel and the oxidant. Compared to batteries, fuel cells can directly convert the fuels into electric energy without the need for electrical power storage and the capacity of the system can be adjusted by the fuel feeds and chemical fuel storage. In addition, fuel cells have 10 times the power density of lithium ion batteries. Polymer membrane-based fuel cell technology such as proton exchange

membrane fuel cells (PEMFC) and anion exchange membrane fuel cells (AEMFC) are regarded as one of the most promising solutions to resolve rising energy demands in the 21st century while reducing negative environmental impact associated with traditional sources of hydrocarbon energy.[3-5]

The solid polymeric membrane in a fuel cell, which serves as an ion transport medium and separator for isolation of the cathode and anode, is a key component in the performance of the cell. During the process of fuel cell operation, the polymeric membrane durability is of great importance to the functional life of the fuel cell. An ideal membrane for fuel cell applications should demonstrate high ionic conductivity, good dimensional stability, low fuel crossover, chemical and mechanical stability, and facile assemble into fuel cells.[6,7] The most frequently used PEM in PEMFCs is Nafion®, a perfluorinated sulfonic acid resin with pendant sulfonic acid side groups, produced by DuPont.[7,8] Nafion®, which has high efficient proton conduction, good mechanical properties, and excellent chemical stability, ensures high discharge performance and durability of PEM fuel cells. However, the widespread use of PEMFCs based on Nafion® has been hindered. Firstly, the high cost and environmental incompatibility of processing the perfluorinated material limits the large-scale commercialization of PEMs based on Nafion.[9] Secondly, precious metals, such as Pt, which are stable and highly efficient under strongly acidic environments, are essential as electrocatalysts in PEM fuel cells and substantially drive up the price of the system.[9]

To break the reliance on precious metal catalysts, alkaline membrane fuel cells (AEMFCs) with anion exchange membranes (AEMs) operating at high pH are currently being studied for their potential to use non-precious metal catalysts.[10,11] Advantages of anion exchange membrane fuel cells (AEMFCs) over PEMFCs include an enhancement of the kinetics of the electrode reactions, especially at the cathode, and more options for cathode catalysts such as

nonprecious transition metals, leading to a performance improvement and reduction in device cost.[12-17] Due to these advantages, in the past decade researchers has been focused on developing materials and cell operational technologies for AEMFCs. Among them, studies on high-performance polymeric AEMs have gained a lot of attention.

1.2 Working Mechanism of an H_2-O_2 Type AEMFC

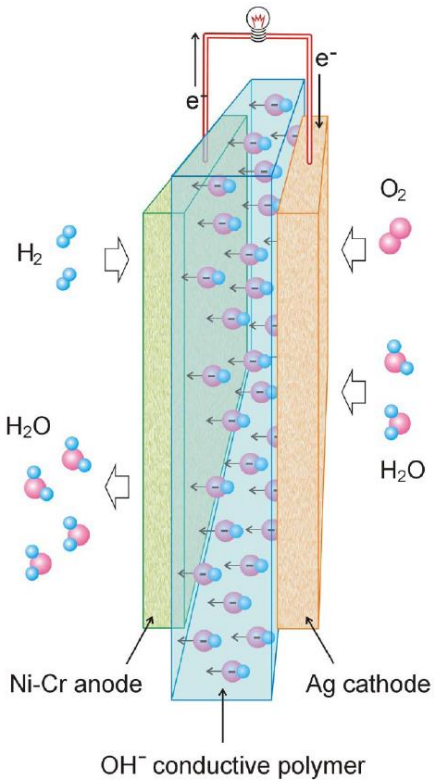

Figure 1.1 Schematic depiction of an AEM based fuel cell with a Ni-catalyzed anode, an Ag-catalyzed cathode, and hydrogen feed. © National Academy of Sciences, 2008.[18]

As shown in Figure 1.1, AEMFC convert hydrogen fuel to electrical energy based on the following reactions: [18]

Cathode reaction: $O_2 + 2\ H_2O + 4\ e^- \rightarrow 4\ OH^-$

Anode reaction: $2\ H_2 + 4\ OH^- \rightarrow 4\ H_2O + 4\ e^-$

Overall reaction: $2\ H_2 + O_2 \rightarrow 2\ H_2O$

At the cathodic side of an H_2-O_2 type AEMFC, O_2 is reduced in the presence of H_2O to produce 4 OH^-, which transports through the polymeric AEM to the anodic side of the cell. At the anode, H_2 reacts with 4 OH^-, and is oxidized to produce H_2O.[18] The overall reaction of H_2-O_2 type AEMFC is reaction of H_2 and O_2 to generate H_2O, heat, and electrical energy. [18]

Obviously, AEMFCs consist of two kinds of key materials. Catalysts are needed for the cathode and anode to enable the electrochemical reactions. Additionally, a polymeric AEM, which serves as both the ion transport medium and the separator for isolating the cathode and anode are needed for effective separation of the electrodes and low ionic resistance in the cell.

1.3 Motivation for This Work

The performance of AEMFCs is dependent on the properties of AEMs. In order to obtain highly efficient and durable AEMFCs, AEMs should meet the following requirements:[14]

1) high hydroxide ionic conductivity (no lower than 10^{-2} S/cm at room temperature, expected to be higher than 10^{-1} S/cm under AEMFC operating conditions).[14]
2) high chemical and thermal stability (under fuel cell operating conditions, e.g., 80 °C) with no obvious degradation of polymer backbones and positively charged groups. [14]
3) excellent mechanical strength (≥10 MPa at room temperature) and low swelling degree (less than 30 %) under the operating conditions. [14]
4) capability of being used in form of solution, i.e, ionomer solution, which can be used to prepare polymer impregnated electrodes and membrane electrode assembly (MEA). [14]

In previous report by Li,[19] *et al*., comb-shaped polymers based on a backbone of poly(2,6-dimethy-1,4-phenylene oxide) with different lengths of alky side chains pendant to the backbone for AEMs were synthesized. These kinds of polymers showed good hydroxide conductivity and alkaline stability.[19,20] However, due to the increase of ion exchange capacity (IEC), membranes with degree of functionalization (DF) $\geq$ 70 could not be obtained in the pursuit of higher performances AEMs. In order to achieve sufficient ion conductivity for AEM applications, high ion-exchange capacities (IEC) are essential for anion exchange membranes. However, increasing the IEC values is always accompanied by high water uptake, leading to severe dimensional swelling, or even dissolution.[21,22] This trade-off between dimensional stability and ion conductivity creates a need for methods to enhance dimensional stability without compromising ion conductivity.[23] Cross-linking has been reported as an effective method to enhance the dimensional stability of the membrane and to increase the fuel resistance crossover in the preparation of AEMs.[23-37] In this work, side chains with double bonds were introduced, and photochemical strategies (UV) to crosslink the polymers and limit dimensional swelling (Figure 1.2). The advantages of using the thiol-ene click reaction as a strategy for cross-linking are its robustness and efficiency without yielding any harmful byproducts or residue that must be removed from the membrane after the cross-linking reaction has occurred.[38] Also, UV-initiated thiol-ene chemistry was shown to proceed quantitatively with a high degree of specificity within a short time.[38]

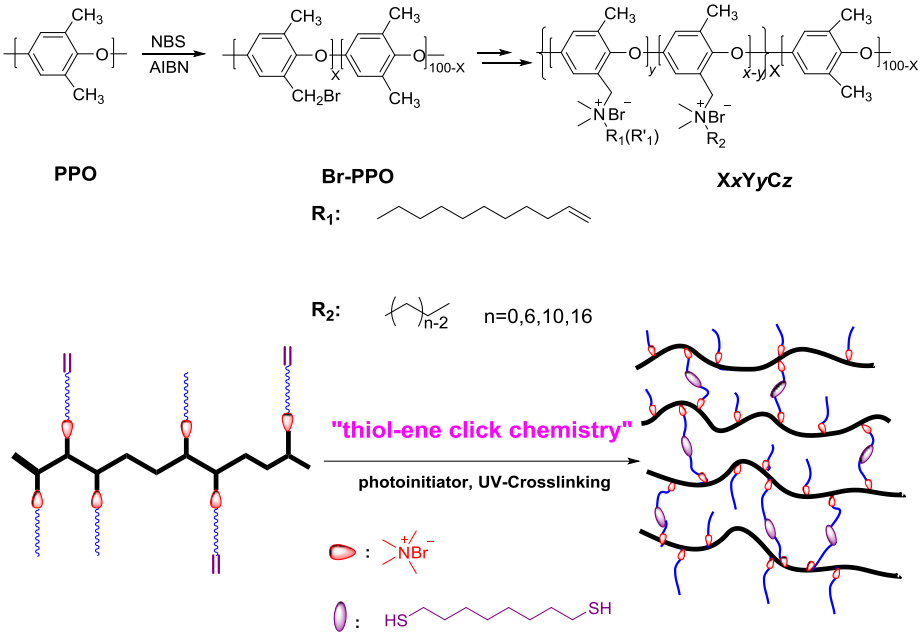

Figure 1.2 Synthesis of cross-linked comb-shaped AEMs, X*x*Y*y*C*z*, with one alkyl side chain using thiol-ene click chemistry.

AEMs are a new class of solid polymer electrolytes enabling the use of nonprecious metal catalysts as the electrodes in the fuel cell devices. However, the design of the AEMs has faced a dilemma - how to enhance the ion conducting and maintain the stability of the AEMs simultaneously? Usually, to obtain higher ion conductivity, more cationic functional groups must be grafted to the polymer backbone, severely damaging the chemical inertness of the polymer backbone and inducing more degradation of the AEMs under alkaline conditions. One of the strategies to disentangle the issue of increasing functionalization that causes degradation is to incorporate two cations on each grafted functional side chains in order to reduce the grafting degree of functional groups along the backbone. Reducing the degree of functionalization while increasing the charge number of the cationic groups was reported as a method to balance the ionic conductivity and the other required properties of AEMs.[39-42] Zhuang, [39] *et al*. reported a polysulfone (PSF)-based AEM with double quaternary ammonium groups (DQAPS) side chains.

Compared to typical AEMs, *i.e.*, quaternary ammonium polysulfone (QAPS), DQAPS enabled higher IECs without increasing the DF, and demonstrated higher hydroxide conductivity as well as higher dimensional and alkaline stability.[39] Although DQAPS showed promising properties as AEMs, the hydroxide conductivity of DQAPS was not high enough. More importantly, the report did not detail systematic studies to demonstrate the effect of the arrangement of the charges on the performance of the AEMs. In addition, the reported AEM backbone was polysulfone which was demonstrated less stable than the PPO backbone.[20] In this work, we synthesized a series of poly(2,6-dimethy 1,4-phenylene oxide)-based AEMs with different kinds of cationic side chains to investigate the relationship between the degree of functionalization (DF), the structure of the side chain (charge number and charge arrangement), and the AEM performance in terms of ionic conductivity, swelling degree, and chemical stability of the material (Figure 1.3).

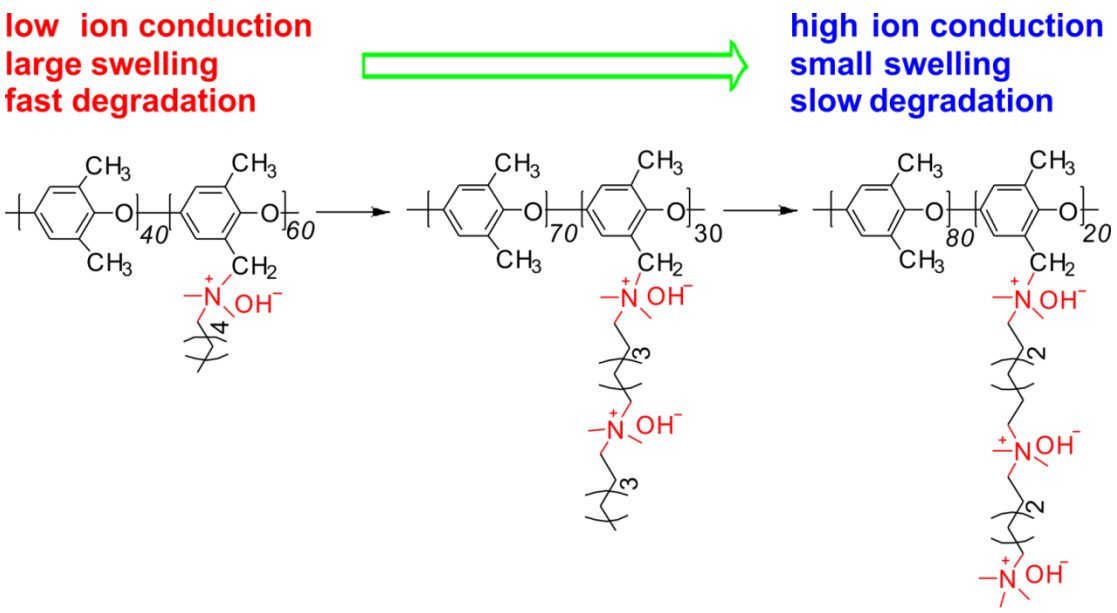

Figure 1.3 Multication side chain AEMs based on PPO.

Although AEMFCs have the potential to replace PEMFCs for usage in mobile vehicles and portable applications, the chemical and electro-chemical stabilities of the cations in AEMs under high temperature and high pH environment limit the applications[51] where this technology

can be applied. Benzyltrimethylammonium cations, for example, which are commonly employed as functional groups for transporting hydroxide ions in AEMs, can undergo irreversible reaction to give small molecules, such as methanol and trimethylamine. The irreversible formation of such neutral molecules leads to the loss of ion conductivity, mechanical strength and functionality of the AEMs.[43] The reaction between the cations and hydroxide is the ultimate limitation preventing the AEM fuel cells from being widely used. Thus, it is desirable to design and develop AEMs which possess high alkaline stability under operating conditions.

The main chemical degradation pathways for the tetraalkyammonium cations include eliminations(E2) ,[44] substitutions(S_N2) ,[45] and Stevens or Sommelet-Hauser rearrangements,[44] as shown in Figure 1.4.

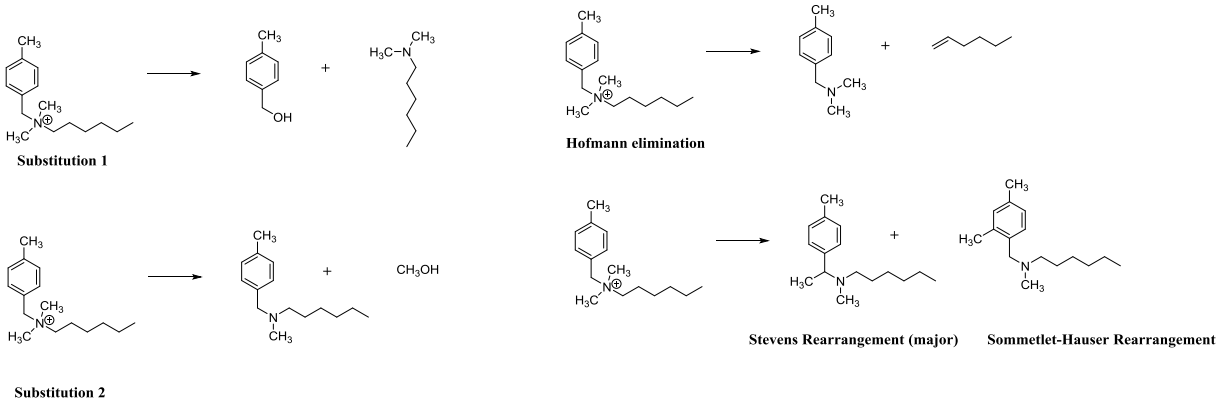

Figure 1.4 Chemical degradation pathways for the tetraalkyammonium cation small molecules.

Nuñez,[46] *et al*. has had a systematically studied of the degradation pathways and mechanisms of tetraalkylammonium cations on small molecule AEM analogs and polymers. The chemical structures of tetraalkyammonium small molecule AEM analogs and polymers studied were shown in Figure 1.5.

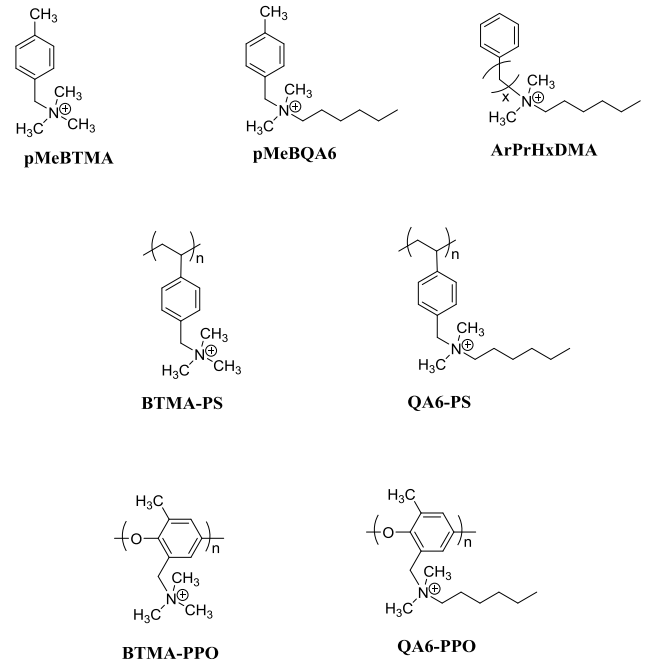

Figure 1.5 Chemical structures of tetraalkyammonium small molecule AEM analogs and polymers studied by Nuñez, *et al*.[46]

These researchers designed an accelerated degradation method based on hydroxide attack to investigate the stability of important structures that are building blocks of AEMs. They found that the presence of an interstitial spacer in ArPrHxDMA limited the possibility of Stevens and Sommelet-Hauser rearrangement.[46] As the substitution at the benzyl position was the major degradation route for in both of small molecules and polymers, Nuñez, [46] *et al*. studied the effect of the interstitial n-alkyl spacers between the aromatic and the trimethyammonium cation as well. It was found that the addition of an interstitial spacer obviously enhanced the stability of both the ArPrHxDMA and ArPrTMA compounds.[46] The authors concluded that it appeared that both interstitial spacers and terminal pendent n-alkyl groups enhanced the stability of the tetraalkylammonium, but the interstitial spacers seems to make the greatest contribution to eliminate the benzyl substitution in the benzyl-linked ammonium small molecules and polymers. [46] In addition, the alkaline degradation investigation on AEM polymer backbone demonstrated

that poly (phenylene oxide) provided a more stable polymer backbone than polystyrene architectures at 120°C.[46]

Inspired by these results, we designed fluorene-containing side chain AEMs, which is shown in Figure 1.6, in order to obtain n-alkyl interstitial spacers tetraalkylammonium cations AEMs. In this work, anion-conductive copolymers, poly(2,6-dimethyl-1,4-phenylene oxide)s containing fluorene side chains with pendant alkyltrimethylammonium groups, were synthesized via Suzuki-Miyaura coupling of aryl bromides with fluorene-boronic acids. The relationship among water uptake, IEC and ionic conductivities of these advance AEMs were investigated. The long-term alkaline stability of the AEMs was evaluated by treating the AMEs with argon-saturated 1 M NaOH solution at 80 °C for 1000 hours.

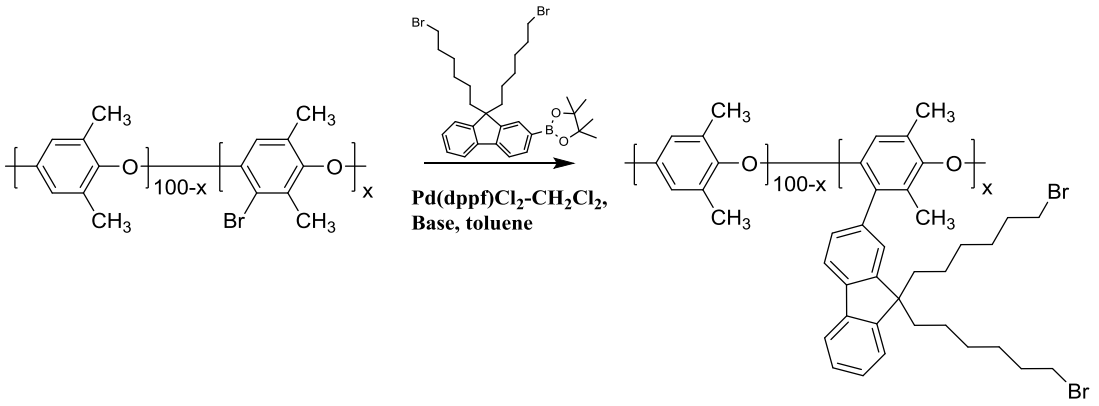

Figure 1.6 Synthetic strategy for the fluorene single-side chains poly (2,6-dimethyl-1,4-phenylene oxide).

Compared to their counterpart PEMs, AEMs generally exhibit inferior properties, such as lower mobility of OH^- and less developed phase-segregated morphology of aromatic polymers. In order to enhance the ionic conductivity and maintain an acceptable swelling ratio, researchers have been employed the strategies of crosslinking and controlling the phase-segregated morphology to fabricate desirable AEMs. In addition, although the rigid aromatic polymer

backbones ensure good tensile strength (higher than 20 MPa), the poor flexibility (lower than 30% elongation at break) of the AEMs is unsatisfactory for fuel cell applications. Under a low relative humidity environment, the poor flexibility makes AEMs brittle, causing problems during MEA fabrication. Also, the long-term fuel cell performance closely relies on the flexibility of AEMs since the fuel cell is operated under conditions such as wet-dry cycling. Herein, we employ a unique approach to toughen AEMs by crosslinking the AEMs using commercial hydrophilic Jeffamine cross-linkers.

1.4 References

(1) Varcoe, J. R.; Atanassov, P.; Dekel, D. R.; Herring, A. M.; Hickner, M. A.; Kohl, P. A.; Kucernak, A. R.; Mustain, W. E.; Nijmeijer, K.; Scott, K.; Xu, T.; Zhuang, L. *Energy Environ. Sci*. **2014**, 7, 3135.

(2) Zhu, L.; Pan, J.; Hickner, M. A. *ECS Trans.* **2015**, 69, 403.

(3) Appleby, A. J.; Foulkes, F. R. Fuel Cell Handbook; Van Nostrand Reinhold: New York, 1989.

(4) Carratte, L.; Friedlich, K. A.; Stimming, U. *Fuel Cells* **2001**, *1*, 5.

(5) Steele, B. C. H.; Heinzel, A. *Nature* **2001**, *414*, 345.

(6) Borup, R.; et al. *Chem. Rev*. **2007**, 107, 3904.

(7) Diat, O.; Gebel, G. *Nat. Mater.* **2008**, *7*, 13.

(8) Curtin, D. E.; Lousenberg, R. D.; Henry, T. J.; Tangeman, P. C.;Tisack, M. E. *J. Power Sources* **2004**, *131*, 41.

(9) Tanaka, M.; Fukasawa, K.; Nishino, E.; Yamaguchi, S.; Yamada, K.; Tanaka, H.; Bae, B.; Miyatake, K.; Watanabe, M. *J. Am. Chem. Soc*. **2011**, 133, 10646.

(10) Xu, T. *J. Membr. Sci.* **2005**, *263*, 1.

(11) Hickner, M. A. *Mater. Today* **2010**, *13*, 34.

(12) Olson, T. S.; Pylypenko, S.; Atanassov, P.; Asazawa, K.; Yamada, H.; Tanaka, H. *J. Phys. Chem. C* **2010**, *114*, 5049.

(13) Sanabria-Chinchilla, J.; Asazawa, K.; Sakamoto, T.; Yamada, K.; Tanaka, T.; Strasser, P. *J. Am. Chem. Soc.* **2011**, *133*, 5425.

(14) Pan, J.; Chen, C.; Zhuang, L.; Lu, *J. Acc. Chem. Res*. **2012**, *45*, 473.

(15) Wang, Y. -J.; Qiao, J.; Baker, R.; Zhang, J. *Chem. Soc. Rev.* **2013**, *42*, 5768.

(16) Varcoe, J. R.; Slade, R. C. T.; Wright, G. L.; Chen, Y. L. *J. Phys. Chem. B* **2006**, *110*, 21041.

(17) Wu, X.; Scott, K. *J. Power Sources* **2012**, *206*, 14.

(18) Lu, F.; Pan, J.; Huang, A.; Zhuang, L.; Lu, J. T. *Proc. Natl. Acad. Sci. U.S.A.* **2008**, *105*, 20611.

(19) Li, N. W.; Leng, Y. J.; Hickner, M. A.; Wang, C. Y. *J. Am. Chem. Soc*. **2013**, *135*, 10124

(20) Amel, A.; Zhu, L.; Hickner, M.; Ein-Eli, Y. *J. Electrochem. Soc*. **2014**, *161*, F615.

(21) Pan, J.; Lu, S.; Li, Y.; Huang, A.; Zhuang, L.; Lu, J. *Adv. Funct. Mater.* **2009**, *19***,** 1.

(22) Tsai, T. H.; Ertem, S. P.; Maes, A. M.; Seifert, S.; Herring, A. M.; Coughlin, E. B. *Macromolecules* **2015**, *48*, 655.

(23) Pan, J.; Zhu, L.; Han, J.; Hickner, M. A. *Chem. Mater.* **2015**, *27*, 6689**.**

(24) Zhang, M.; Liu, J.; Wang, Y.; An, L.; Guiver, M. D.; Li, N. J. Mater. Chem. A **2015**, *3*, 12284.

(25) Zhuo, Y. Z.; Lai, A. N.; Zhang, Q. G.; Zhu, A. M.; Ye, M. L.; Liu, Q. L. *J. Membr. Sci.* **2015**, *491*, 138.

(26) Lin, B.; Chu, F.; Ren, Y.; Jia, B.; Yuan, N.; Shang, H.; Feng, T.; Zhu, Y.; Ding, J. *J. Power Sources* **2014**, *266*, 186.

(27) Li, N.; Wang, L.; Hickner, M. A. *Chem. Commun.* **2014**, *50*, 4092.

(28) Lin, B.; Dong, H.; Li, Y.; Si, Z.; Gu, F.; Yan, F. *Chem. Mater.* **2013**, *25*, 1858.

(29) Lin, X.; Liu, Y.; Poynton, S. D.; Ong, A. L.; Varcoe, J. R.; Wu, L.; Li, Y.; Liang, X.; Li, Q.; Xu, T. *J. Power Sources* **2013**, *233*, 259.

(30) Zhao, Y.; Yu, H.; Yang, D.; Li, J.; Shao, Z.; Yi, B. *J. Power Sources* **2013**, *221*, 247.

(31) Zhou, J. F.; Unlu, M.; Anestis-Richard, I.; Kohl, P. A. *J. Membr. Sci.* **2010**, *350*, 286.

(32) Yang, C. C.; Chiu, S. J.; Chien, W. C.; Chiu, S. S. *J. Power Sources* **2010**, *195*, 2212.

(33) Lin, B.; Qiu, L.; Lu, J.; Yan, F. *Chem. Mater.* **2010**, *22*, 6718.

(34) Xiong, Y.; Fang, J.; Zeng, Q. H.; Liu, Q. L. *J. Membr. Sci.* **2008**, *311*, 319.

(35) Stoica, D.; Ogier, L.; Akrour, L.; Alloin, F.; Fauvarque,J. F. *Electrochim. Acta,* **2007**, *53*, 1596.

(36) Wu, Y. H.; Wu, C. M.; Xu, T. W.; Yu F.; Fu, Y. X. *J. Membr. Sc.*, **2008**, *321*, 299.

(37) Park, J. S.; Park, S. H.; Yim, S. D.; Yoon, Y. G.; Lee, W. Y.; Kim, C. S. *J. Power Sources* **2008**, *178*, 620.

(38) Killops, K. L.; Campos, L. M.; Hawker, C. J. *J. Am. Chem. Soc.* **2008**, *130*, 5062.

(39) Pan, J.; Li, Y.; Han, J.; Li, G.; Tan, L.; Chen, C.; Zhuang, L. *Energy Environ. Sci.* **2013**, *6*, 2912.

(40) Yan, Y.; Wang, J.; Gu, S. Polymers with side chains having cationic groups, useful in hydroxide/anion exchange membrane. U.S. Patent, 20140107237 A1, April 02, 2014.

(41) Si, J.; Lu, S.; Xu, X.; Peng, S.; Xiu, R.; Xiang, Y. *ChemSusChem*. **2014**, *7*, 3389.

(42) Li, Q.; Liu, L.; Miao, Q.; Jin, B.; Bai, R. *Chem. Commun.* **2014**, *50*, 2791.

(43) Chempath, S.; Einsla, B. R.; Pratt, L. R.; Macomber, C. S.; Boncella, J. M.; Rau, J. A.; Pivovar, B. S. *J. Phys. Chem. C* , **2008**, *112*, 3179.

(44) Chempath, S.; Boncella, J. M.; Pratt, L. R.; Henson, N.; Pivovar, B. S. *J. Phys. Chem. C*, **2010**, *114*, 11977.

(45) Modern Physical Organic Chemistry; University Science Books, 2006.

(46) Nuñez, S. A.; Hickner, M. A. *ACS Macro Letters* **2012**, *2*, 49. And Nuñez, S. A. Ph.D. Thesis, Penn State University, 2015.

Chapter 2

Literature Review of Anion Exchange Membranes

2.1 Introduction

In addition to catalyst, high-performance polymeric membranes are key materials in electrochemical technology and ensure high discharge performance and durability of PEM fuel cells. In 1960s, the commercialization of Nafion®, a perfluorinated sulfonic acid resin produced by DuPont, boosted the development and research of PEM fuel cells in the following decades. Compared to PEMs, however, the commercialization of AEMs for fuel cell applications is still in the initial stages and faces materials and engineering challenges. Until now, there are no commercial AEMs meet the requirements for fuel cell devices. Thus, in the past decade, much effort has been placed on developing materials and cell operational technologies for AEM fuel cells. Among them, studies on high-performance polymeric AEMs have gained a lot of attention.

2.2 Anion Exchange Membranes with Different Side Chains

2.2.1 Anion Exchange Membranes with Single-Cation Side Chains

Poly(styrene)s and poly(divinylbenzene)s were typical polymer backbones for AEM materials.[1-11]

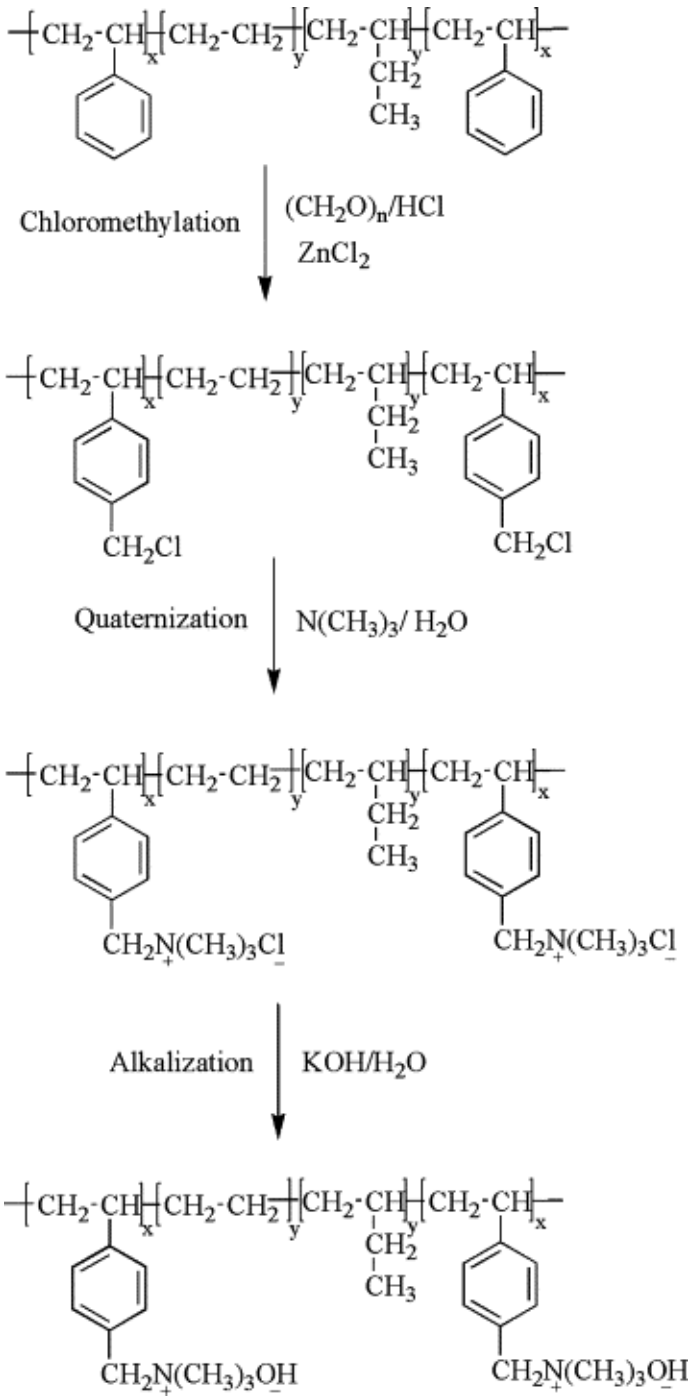

Figure 2.1 Synthetic strategy of SEBS AEMs. © ELSEVIER, 2010.[3]

Zeng,[3] *et al.* reported AEMs using polystyrene-block-poly(ethylene-ran-butyl)-block-polystyrene (SEBS) as staring material (Figure 2.1). Chloromethyl groups were introduced into the SEBS by using paraformaldehyde and hydrochloric acid in the presence of $ZnCl_2$ catalyst.[3] The reaction of chloromethyl groups with trimethylamine gave the quaternized SEBS which was converted to an AEM by immersion 1 M KOH solution.[3] This kind of AEMs exhibited low hydroxide conductivity (9.37 mS/cm) in deionized water at 80 °C due to the low IEC.[3]

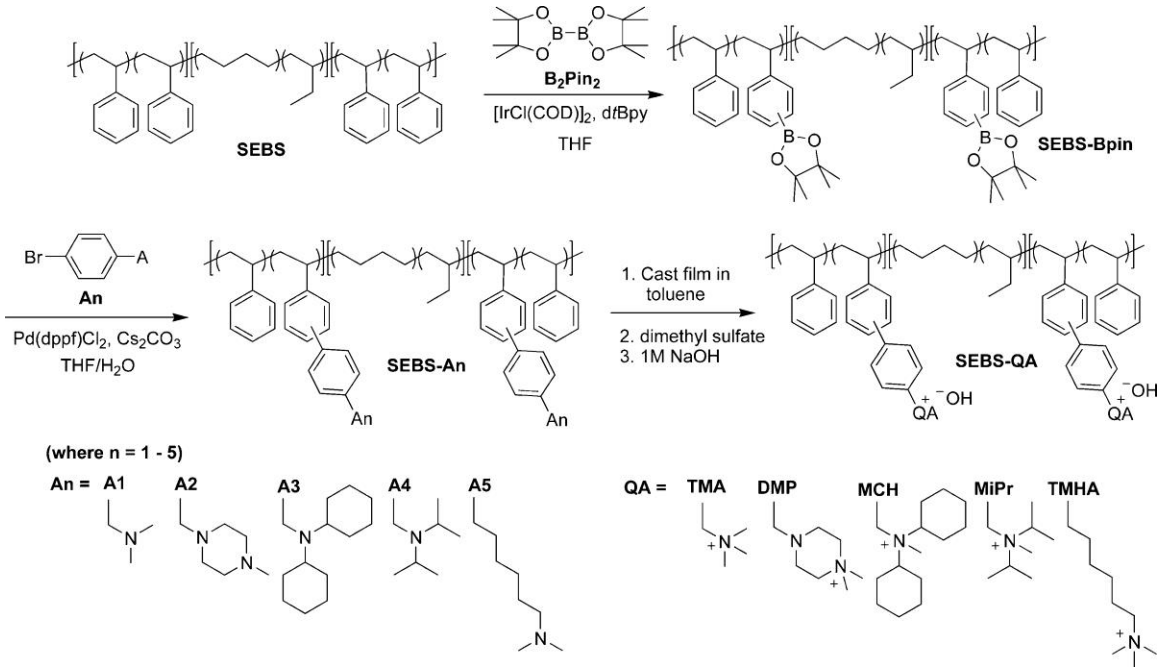

Figure 2.2 Synthesis of quaternized SEBS via iridium-catalyzed aromatic C-H borylation and palladium-catalyzed Suzuki cross-coupling. © American Chemical Society, 2015.[12]

Recently, Mohanty,[12] *et al.* reported AEMs based on the chemically stable and elastomeric triblock copolymer, polystyrene-*b*-poly(ethylene-*co*-butylene)-*b*-polystyrene (SEBS), which demonstrated high hydroxide conductivity and chemical stability (Figure 2.2). The SEBS triblock copolymer was functionalized via iridium-catalyzed aromatic C-H borylation and palladium-catalyzed Suzuki cross-coupling. This kind of AEM exhibited hydroxide conductivity as high as 45 mS/cm in deionized water at 30 °C with IEC = 2.41 mmol/g.[12] The H_2-O_2 fuel cell

of the membrane electrode assembly (MEA) based on quaternized SEBS using Pt/C as catalysts exhibited peak power density of 240 mW/cm^2 at 80 °C.[12]

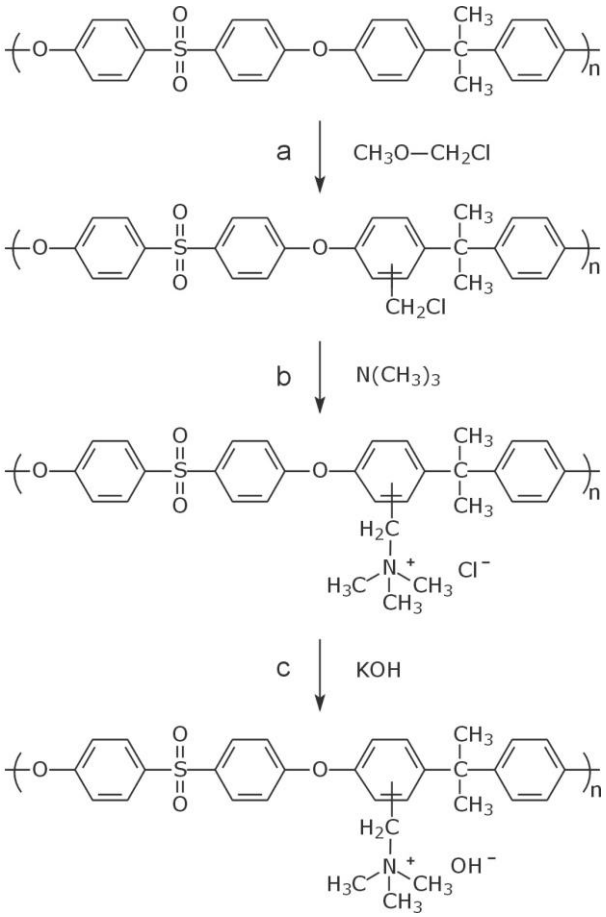

Figure 2.3 Synthetic route of quaternary ammonium polysulphone in hydroxide form. © WILEY-VCH Verlag GmbH & Co. KGaA, Weinheim, 2010.[13]

In the reported polymeric materials for AEMs, poly(arylene ether)s have been the most frequently used polymer backbones. Among them, polysulfones (PS) have garnered a lot of attention due to their toughness, chemical stability and easy modification. Typically, the preparation of PS AEMs consists of three steps, as shown in Figure 2.3. Firstly, chloromethyl groups were introduced to aromatic position of PS backbone via electrophilic substitution reaction in the presence of lewis acid. Secondly, chloromethylated PSs reacted with

trimethylamine to give the quaternized PSs, which were AEMs in the Cl^- form. Finally, the quaternized PSs were converted to PS AEMs by immersing 1 M KOH solution. The PS AEMs exhibited hydroxide conductivity which was on the order of 10^{-2} S/cm at room temperature.[13]

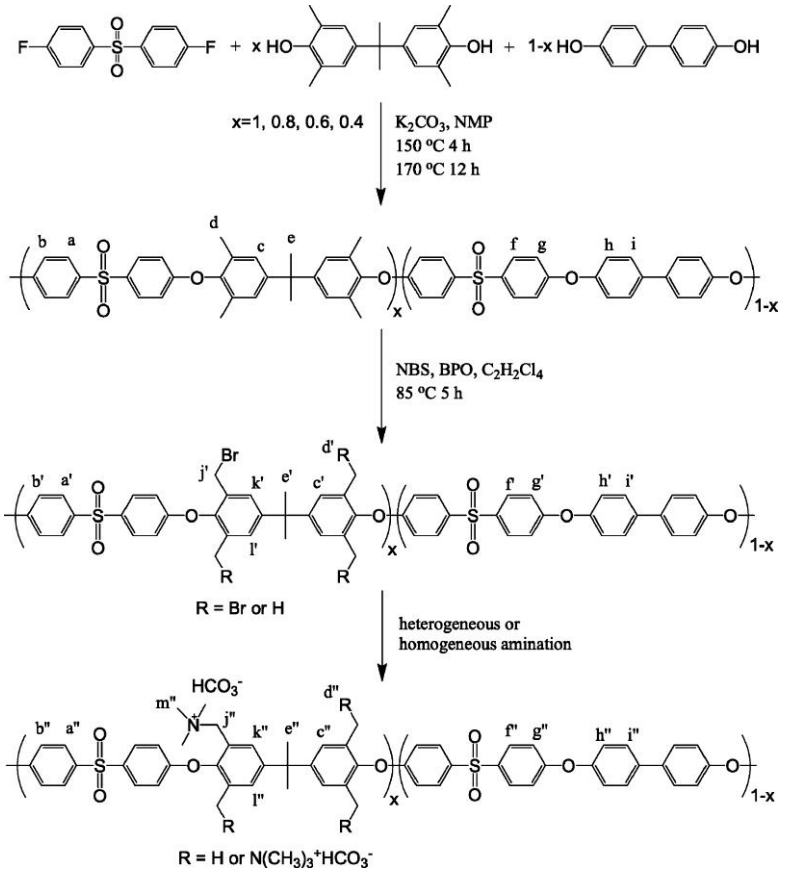

Figure 2.4 Synthetic route of quaternary ammonium-containing polymers from bromination of tetramethyl bisphenol A-based PS. © American Chemical Society, 2010.[4]

In many reports, the PS-based AEMs were prepared via chloromethylation and quaternization of the benzylchloromethyl groups. However, producing new PS-based AEMs via the chloromethylation reaction has been hindered because of the use of toxic and carcinogenic chloromethyl methyl ether. Yan,[4a] and Hibbs,[4b] *et al*. introduced the benzylmethyl moieties into polymer during the polymer synthesis, thereby circumventing postmodification of poly(sulfone)s

by chloromethylation (Figure 2.4). The ionic conductivity and water uptake of the PS-based AEMs could be turned over a wide range by controlling the distribution of the cationic groups.

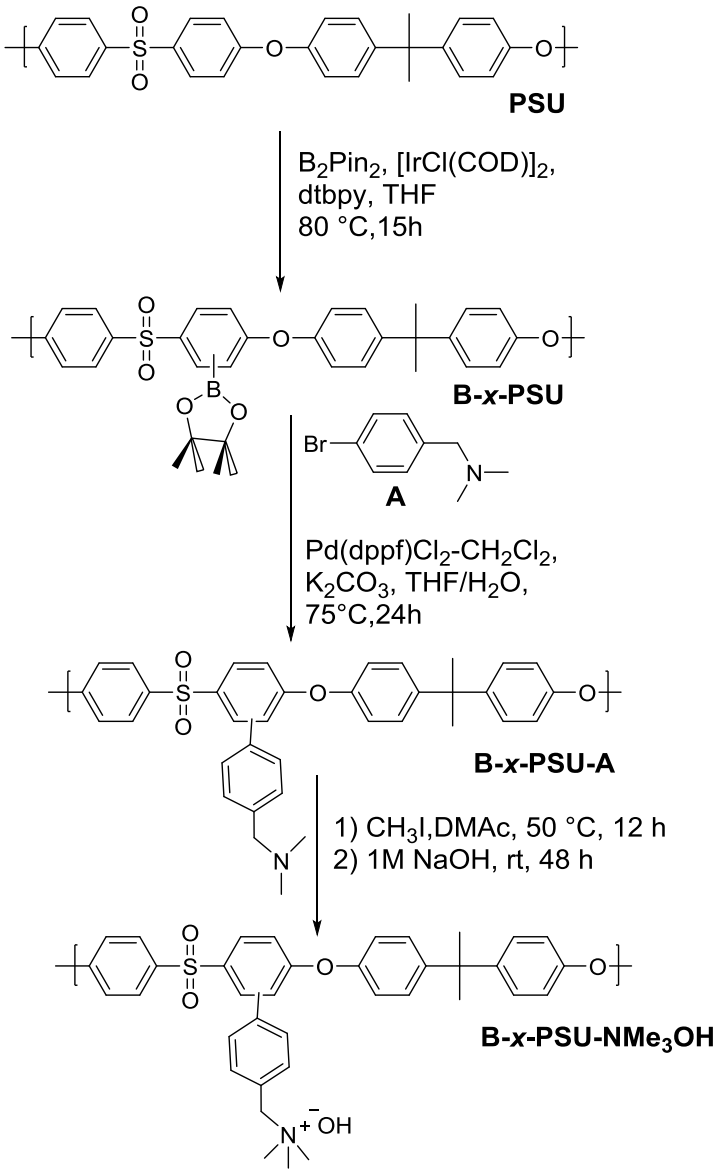

Figure 2.5 Synthetic route of trimethylbenzylammonium functionalized PS via C-H borylation and Suzuki coupling reactions. © American Chemical Society, 2014.[14]

Recently, Mohanty, [14] *et al.* reported the preparation of PS-based AEMs by methods of iridium-catalyzed C-H borylation followed by palladium-catalyzed Suzuki coupling. The side

reactions could be minimized and the degree of functionalization of the polysulfones could be easily controlled due to the use of mild reaction conditions.[14] Compared to the corresponding AEMs materials prepared via chloromethylation, these kinds of AEMs exhibited lower water uptake, while maintaining similar ionic conductivity.[14] These kind of AEMs exhibited hydroxide conductivity as high as 56 mS/cm) in deionized water at 30 °C with IEC = 2.64 mmol/g.[14]

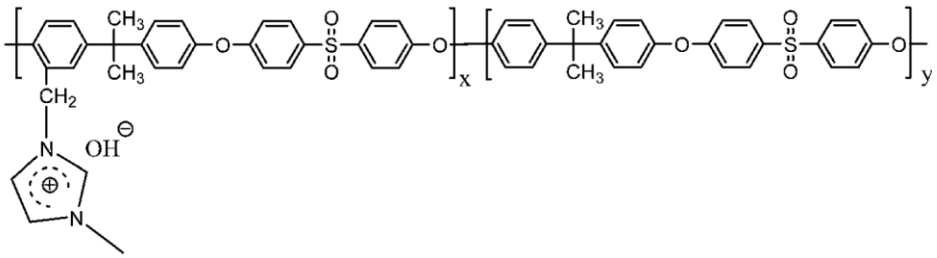

Figure 2.6 Chemical structure of imidazolium functionalized polysulfone AEM. © The Royal Society of Chemistry, 2011.[15]

A series of PSf-ImOH AEMs (Figure 2.6) with different IECs were synthesized by Zhang,[15] *et al.* via functionalization of chloromethylated polysulfone with methylimidazole. When the IECs were increased from 1.39 mmol/g to 2.64 mmol/g , the hydroxide conductivity of the PSf-ImOH AMEs increased from 16.1 mS/cm to 20.7 mS/cm.[15] Meanwhile, large increases of swelling ratio were observed for the PSf-ImOH AEMs when the IECs were increased from 1.39 mmol/g to 2.64 mmol/g, indicating the increasing of ionic conductivity was at cost of mechanical strength. [15] The H_2-O_2 fuel cell based on PSf-ImOH AEMs using Pt/C as catalysts exhibited peak power density of 16 mW/cm^2 at 60 °C.[15]

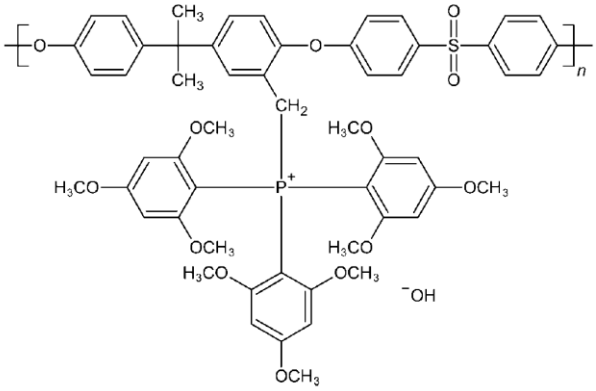

Figure 2.7 Chemical structure of the tri(2,4,6-trimethoxyphenyl) polysulfone-methylene quaternary phosphonium hydroxide (TPQPOH). © WILEY-VCH Verlag GmbH & Co. KGaA, Weinheim, 2009.[16]

Gu,[16] *et al.* synthesized a new quaternary phosphonium based polysulfone-AEMs: tri(2,4,6-trimethoxyphenyl) polysulfone-methylene quaternary phosphonium hydroxide (TPQPOH) (Figure 2.7), which was soluble in low-boiling-point water-soluble solvents. For this kind of AEMs, hydroxide conductivity as high as 45 mS/cm could be achieved in deionized water at 30 °C with IEC = 1.17 mmol/g.[16] The H_2-O_2 fuel cell based on TPQPOH AMEs using Pt/C as catalysts exhibited a peak power density of 258 mW/cm^2 at 70 °C.[16] Although TPQPOH AEMs demonstrated high ionic conductivity, the large swelling ratio at elevated temperature could not ensure the mechanical strength of the AEM materials during the fuel cell operating conditions.

2.2.2 AEMs Based on Poly (2, 6-dimethyl-1, 4-phenylene oxide)

Poly (2, 6-dimethyl-1, 4-phenylene oxide) is a good polymer membrane backbone candidate for its high thermal, mechanical and chemical stabilities. Additionally, it is possible to have modifications on both aryl and benzyl positions because of its unique repeat unit structure.[17] For example, reactions such as the free-radical substitution of hydrogen from the benzyl position

of PPO; electrophilic substitution on the aryl positions of PPO; metalation of PPO with organometallic compounds; modification and functionalization of PPO from the terminal hydroxyl groups are possible.[17]

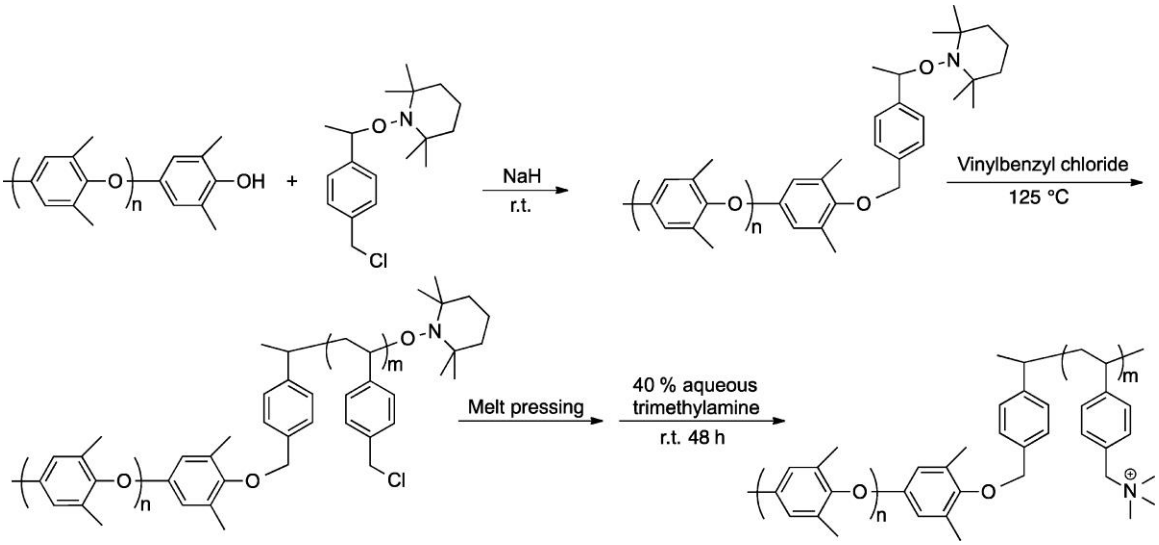

Figure 2.8 Synthetic route for the poly (2, 6-dimethyl-1, 4-phenylene oxide)-*b*-poly (vinylbenzyltrimethylammonium) diblock copolymers based AEMs. © American Chemical Society, 2015.[18]

Yang,[18] *et al.* synthesized poly (2, 6-dimethyl-1, 4-phenylene oxide)-*b*-poly (vinylbenzyltrimethylammonium) diblock copolymers based AEMs through growing poly(vinylbenzyl chloride) (PVBC) blocks from a PPO macroinitiator using nitroxide-mediated polymerization, shown in Figure 2.8. These kind of AEMs exhibited hydroxide conductivity as high as 132 mS/cm in deionized water at 60 °C with IEC = 2.9 mmol/g.[18] In addition, no significant loss of hydroxide conductivity was observed for the AEMs after exposure to 1 M KOH over 13 days at 60 °C.[18]

2.2.3 AEMs Based on Poly (olefin)s

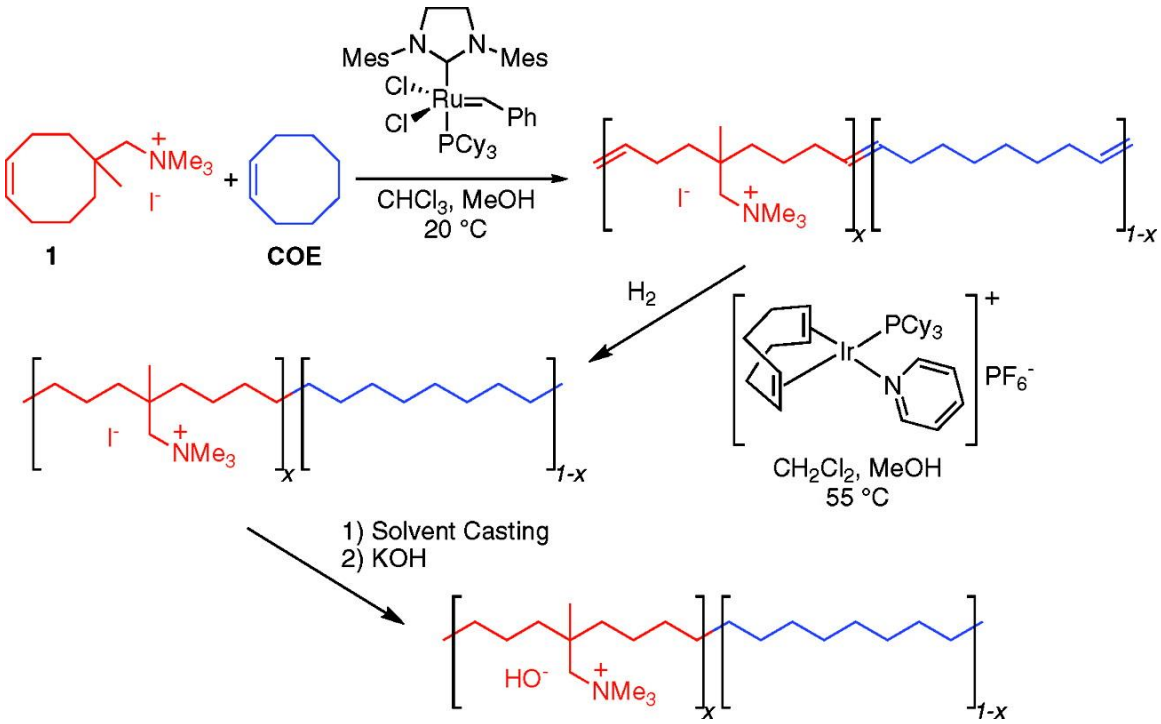

Figure 2.9 Synthetic procedure for tetraalkylammonium-functionalized polyethylene AEMs. © American Chemical Society, 2010.[19]

Kostalik,[19] *et al.* reported a solvent processable, tetraalkylammonium-functionalized polyethylene based AEMs through the ring-opening metathesis polymerization (ROMP). The AEMs was synthesized from tetraalkylammonium-functionalized monomer (compound 1 in Figure 2.9) and cyclooctene by using Grubb's second generation catalyst.[19] These kind of AEMs exhibited hydroxide conductivity as high as 40 mS/cm in deionized water at 20 °C with IEC = 1.29 mmol/g.[19] In addition, the excellent solubility of the polymer materials in aqueous alcohols extended the promising application for use as both AEMs and ionomer electrode.[19]

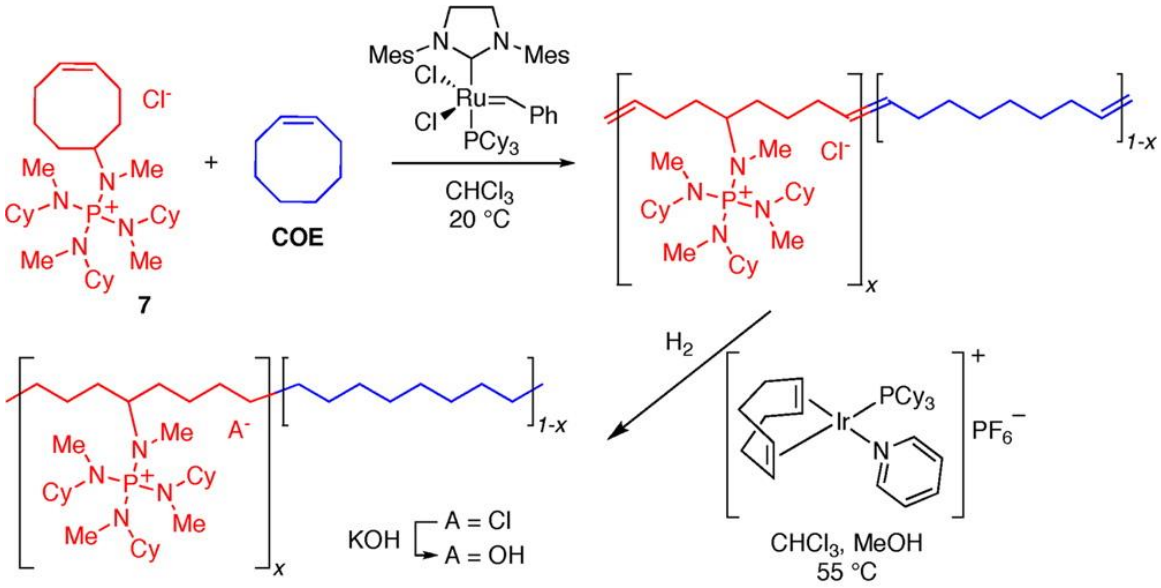

Figure 2.10 Synthetic procedure for phosphonium-functionalized polyethylene AEMs. © American Chemical Society, 2012.[20]

In the development of highly chemical stabile AEMs, Noonan,[20] *et al.* designed a new kind of highly chemical stable AEMs based on tetrakis(dialkylamino)phosphonium-functionalized polyethylene due to the excellent chemical stability of bulky $[P(N(Me)Cy)_4]^+$ (Figure 2.10). The tetrakis(dialkylamino)phosphonium-functionalized AEM exhibited an hydroxide conductivity of 22 mS/cm in deionized water at 22 °C with IEC = 0.67 mmol/g.[20] No significant loss of hydroxide conductivity was observed for the AEMs after exposure to 15 M KOH for 20 weeks at room temperature.[20] In addition, the AEMs only lost 20 % of their hydroxide conductivity after exposure to 1 M KOH for 22 days at 80 °C.[20]

2.2.4 Fluorene-Containing AEMs

Recently, AEMs containing fluorenly groups have been proven to not only have good chemical, thermal and chemical stability, but these types of AEMs have also been shown to have high hydroxide ion conductivity.[21-25]

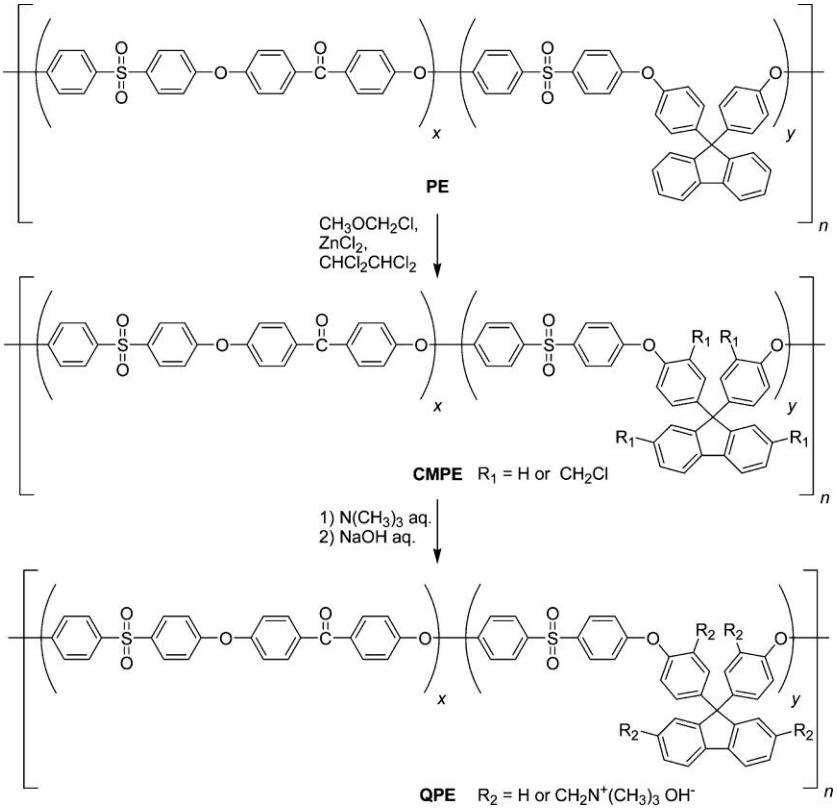

Figure 2.11 Synthetic route of QPE. © American Chemical Society, 2011.[21]

Tanaka,[21] *et al.* synthesized poly (arylene ether)s containing quaternized ammonio-substituted fluorene groups via block copolycondensation of fluorene-containing oligomers and oligo(arylene ether sulfone ketone)s (Figure 2.11). The IEC of the AEMs could be tunable over a wide range due to the large amount of quaternizable positions on fluorene-containing units.[21] When the IEC was 1.93 mmol/g, the AEM containing multiblock exhibited hydroxide conductivity as high as 0.144 S/cm at 80 °C.[21] Tanaka,[21] *et al.* ascribed the high ionic

conductivity to developed hydrophobic/hydrophilic phase separation and interconnected ion transport channels, facilitating the ion-transport efficiency. Despite the incorporation of a hydrophobic block into the copolymer, the swelling behavior and mechanical properties were still dependent on the IEC rather than on the sequential main chain structure. Thus, incorporation of a multiblock copolymer structure with highly ionized hydrophilic blocks proved to be effective for enhancing the ion conductivity of AEMs without sacrificing mechanical stability.[21] The hydrazine/O_2 fuel cell performance of the MEA exhibited a peak power density of 297 $mWcm^{-2}$ at 80 °C.[21]

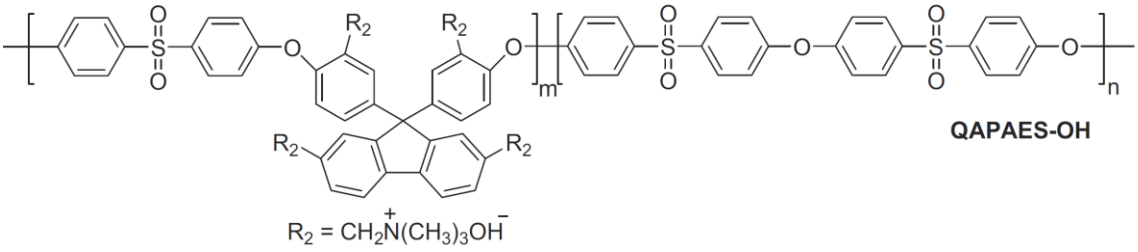

Figure 2.12 Chemical structure of poly (arylene ether sulfone)s containing tetra-quaternary ammonium hydroxide on fluorenyl group (QAPAES-OH). © ELSEVIER, 2012.[22]

Seo,[22] *et al.* synthesized AEMs based on poly (arylene ether sulfone)s containing tetra-quaternary ammonium hydroxide on fluorenyl group (QAPAES-OH) via polycondensation, chloromethylation, quaternization, and ion exchange reactions (Figure 2.12). When the IEC was 1.73 mmol/g, the QAPAES-OH exhibited a hydroxide conductivity of 0.031 S/cm at 80 °C.[22]

2.2.5 Other AEM Structures

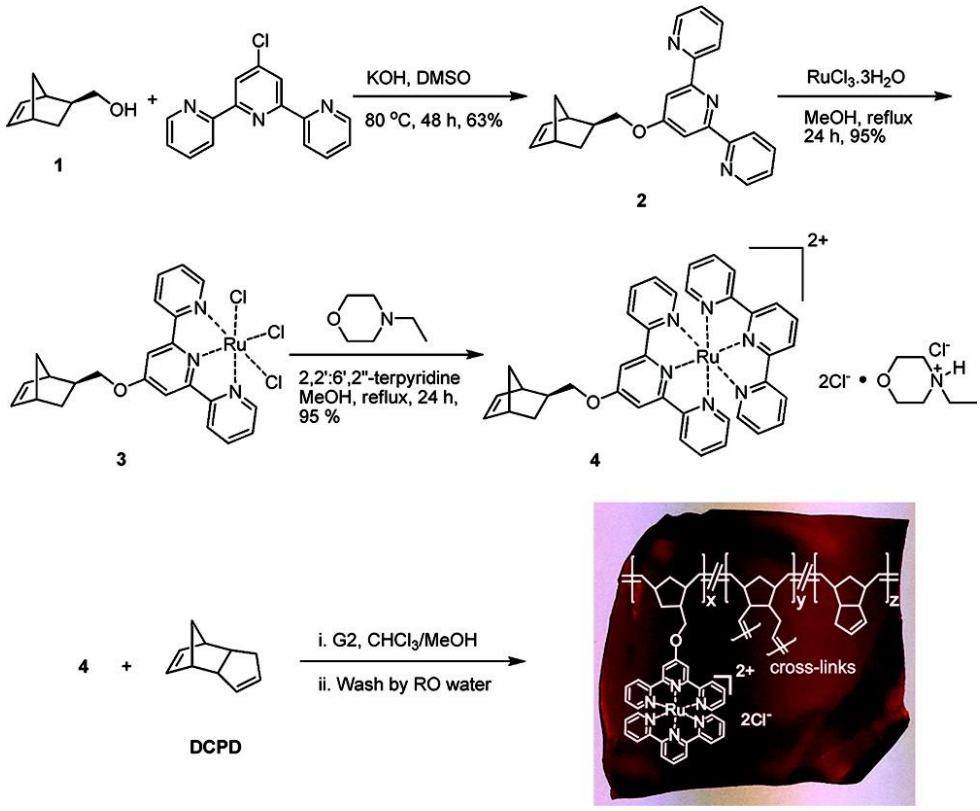

Figure 2.13 Chemical structure of multivalent metal-cation-based AEMs and synthetic route. © American Chemical Society, 2012.[26]

Zha,[26] *et al.* synthesized new multivalent metal-cation-based AEMs via cross-linking a bis(terpyridine) Ru (II) complex-functionalized norbornene and a hydrocarbon comonomer (Figure 2.13). Compared with most ammonium- and phosphonium-based AEMs with single cation-anion pairs, the metal-cation-based AEM has two associated counteranions for each ruthenium complex.[26] The metal-cation-based AEM exhibited hydroxide conductivity of 0.029 S/cm at 30 °C with IEC = 1.4 mmol/g. In addition, the AEM sample with IEC = 1.0 mmol/g shown a tensile strength at break (27 MPa) and tensile stain at break (87%), which were comparable to those of traditional quaternary-ammonium based AEMs.[26] Unfortunately, the single fuel cell performance has not been reported.

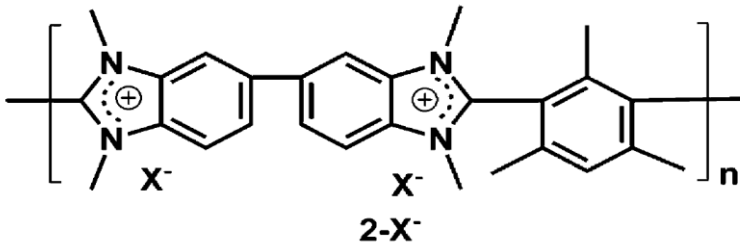

Figure 2.14 Chemical structure of hydroxide-conducting AEMs based on benzimidazolium hydroxide. © American Chemical Society, 2012.[27]

Thomas,[27] *et al.* prepared a stable hydroxide-conducting membrane based on benzimidazolium hydroxide via methylation of poly(benzimidazole) (Figure 2.14). Traditionally, the hydroxide form of poly(benzimidazole) was unstable in alkaline conditions.[27] This polymer was stabilized by steric crowding around the labile benzimidazolium C2 position. The resulting AEMs exhibited hydroxide conductivity up to 0.013 S/cm at 20 °C with an IEC = 1.0 mmol/g.[27]

2.2.2 Anion Exchange Membrane with Multication Side Chains

For common AEMs, high ionic conductivity frequently requires a material with a high IEC. However, high IEC, which usually necessitates a higher grafting degree of the cationic group on the polymer backbone, leads to more water uptake in the material and generally poor mechanical properties.[28-30] AEMs with high IECs and high degrees of functionalization usually exhibit low chemical stability. An increase in the tethered cationic groups along the backbone not only exposes more active sites on the polymer backbone which are vulnerable to OH^- attack, but also the increased degree of functionalization does not allow the formation of hydrophobic domains, which can resist swelling and alleviate degradation by resisting hydroxide intrusion into the material.[28-30]

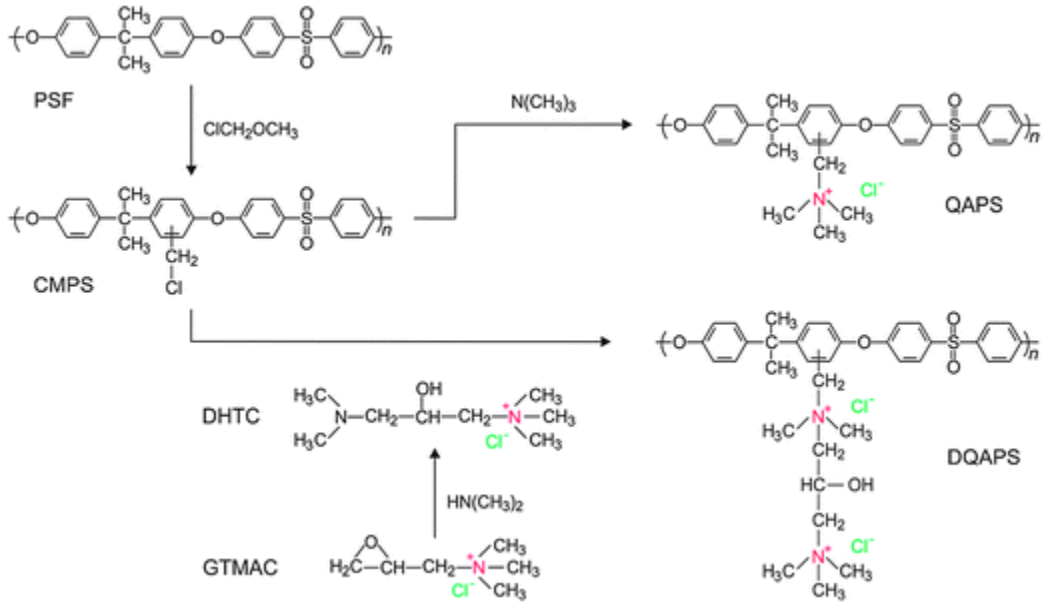

Figure 2.15 Synthetic route for the QAPS and DQAPS. © The Royal Society of Chemistry, 2013.[28]

Reducing the degree of functionalization while increasing the charge number of the cationic groups was reported as a method to balance the ionic conductivity and the other required properties of AEMs.[28-30] Pan,[28] *et al*. investigated a polysulfone (PSF)-based AEM with double quaternary ammonium groups (DQAPS), Figure 2.15. Compared to common AEMs, *i.e.*, quaternary ammonium polysulfone (QAPS), DQAPS enabled higher IECs without increasing the DF, and exhibited higher ionic conductivity as well as a lower swelling degree and higher chemical stability.[28] Although the DQAPS showed promising properties, the previous report did not detail systematic studies to demonstrate the effect of the arrangement of the charges on the performance of the AEMs.

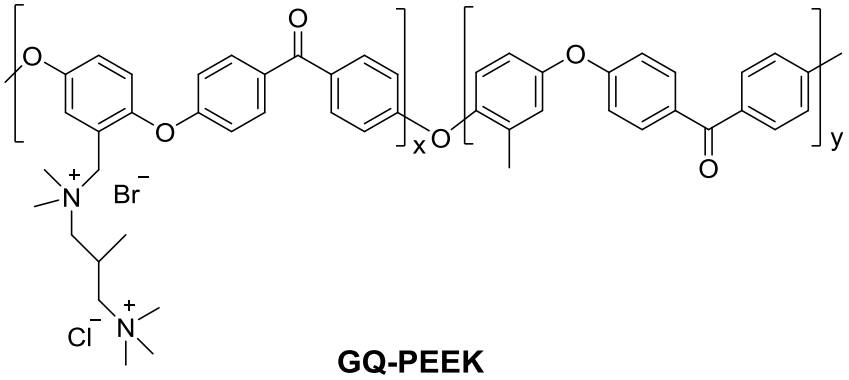

Figure 2.16 Chemical structure of GQ-PEEK. © WILEY-VCH Verlag GmbH & Co. KGaA, Weinheim, 2014.[29]

In order to dismantle the tradeoff between conductivity and dimensional stability in AEM materials, Si,[29] *et al.* synthesized a novel functionalized poly(ether ether ketone) containing double quaternary ammonium side chains (GQ-PEEK, Figure 2.16) via polycondensation, bromination, and quaternization. Compared with functionalized poly(ether ether ketone) containing single quaternary ammonium side chains, GQ-PEEK with a grafting degree of 67% exhibited less swelling (≤ 40% at 25-70 °C) and higher ionic conductivity (0.045 S/cm at 75 °C).[29] The H_2/O_2 fuel cell performance of the MEA with 0.5 mg cm^{-2} Pt/C as both the anode and cathode exhibited a peak power density of 72 $mWcm^{-2}$.[29]

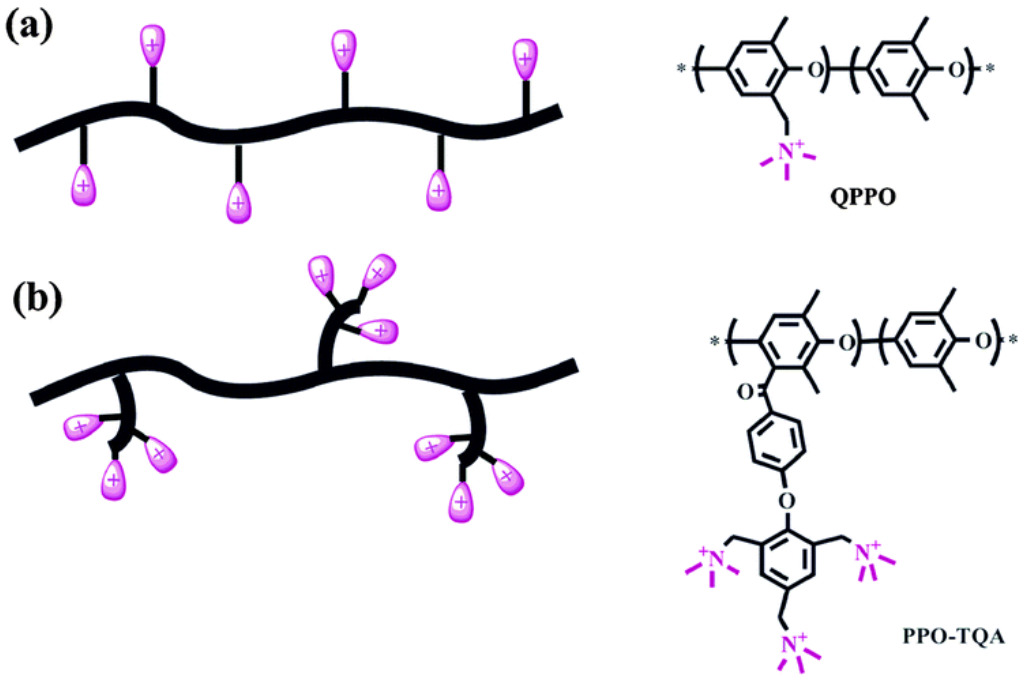

Figure 2.17 Graphical illustrations and chemical structures of (a) conventionally QAPPO AEM and (b) functionalized PPO bearing quaternary ammonium groups (PPO-TQA). © The Royal Society of Chemistry, 2014.[30]

Li,[30] *et al.* synthesized functionalized PPO bearing quaternary ammonium groups (PPO-TQA, Figure 2.17) via incorporating 2,4,6-tri(dimethylaminomethyl)-phenol onto PPO backbone. Compared with conventional QPPO AEMs, the PPO-TQA AEMs possessed higher conductivity, lower swelling ratio and water uptake. When the IEC was 1.50 mmol/g, the PPO-TQA-3 exhibited hydroxide conductivity of 0.072 S/cm and 0.093 S/cm at 30 and 80 °C, respectively.[30] The gQAPPO retained acceptable hydroxide conductivity (0.017 S/cm) after immersion in 1 M NaOH solution at 80 °C for 12 days.[30]

2.2.3 Anion Exchange Membranes with Modified Ammonium Cations

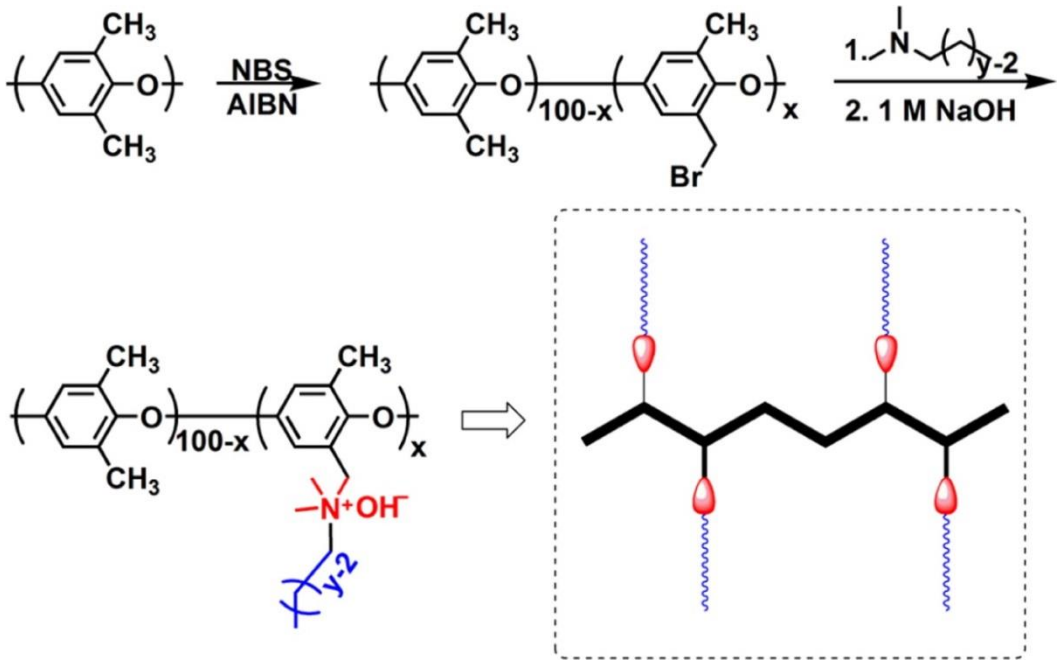

Figure 2.18 Chemical structure of comb-shaped CyDx copolymers. © American Chemical Society, 2013.[31]

Li,[31] *et al.* produced a series of quaternized poly(2,6-dimethyl phenylene oxide)s (PPO) containing terminal pendent n-alkyl group using a Menshutkin reaction (Figure 2.18). Compared to AEMs based on benzyltrimethyl ammonium, the comb-shaped CxDy AEMs exhibited higher hydroxide conductivity due to the formation of highly conductive ionic domains and phase separation.[31] The comb-shaped C6D60 with IEC = 2.75 mmol/g exhibited hydroxide conductivity of 0.043 S/cm at room temperature in water, while the BTMA40 with the similar IEC shown an hydroxide conductivity of 0.024 S/cm under the same condition.[31]

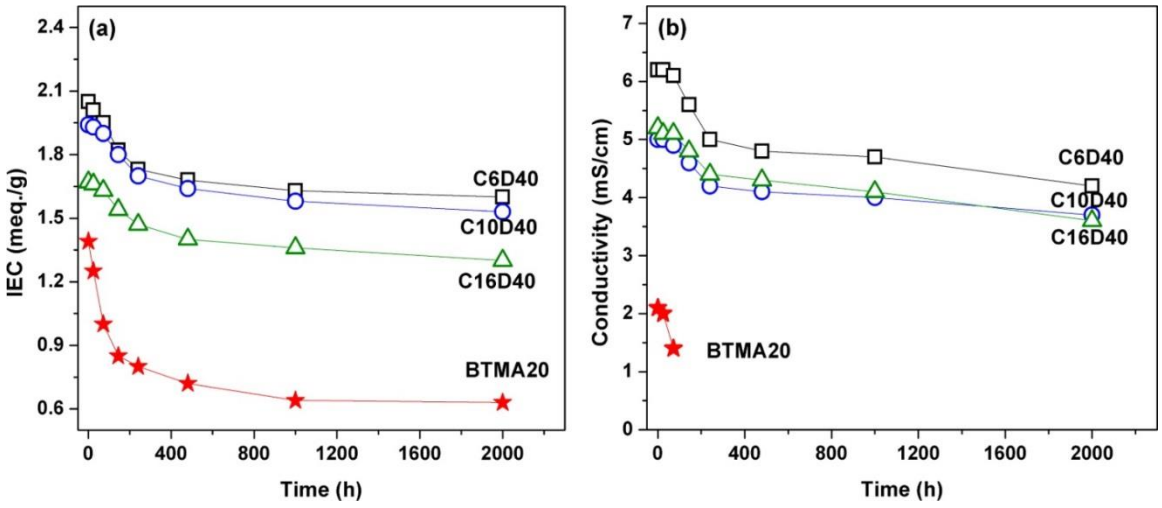

Figure 2.19 Chemical stability of the quaternary ammonium cation of CyDx and BTMAx membranes after immersion in 1 M NaOH solution at 80 °C. © American Chemical Society, 2013.[31]

More importantly, the comb-shaped AEMs demonstrated excellent alkaline stability, which was shown in Figure 2.19.[31] The CxDy comb-shaped samples retained more than 80 % of their bicarbonate conductivities after immersing in 1 M NaOH solution at 80 °C for 2000 h.[31]

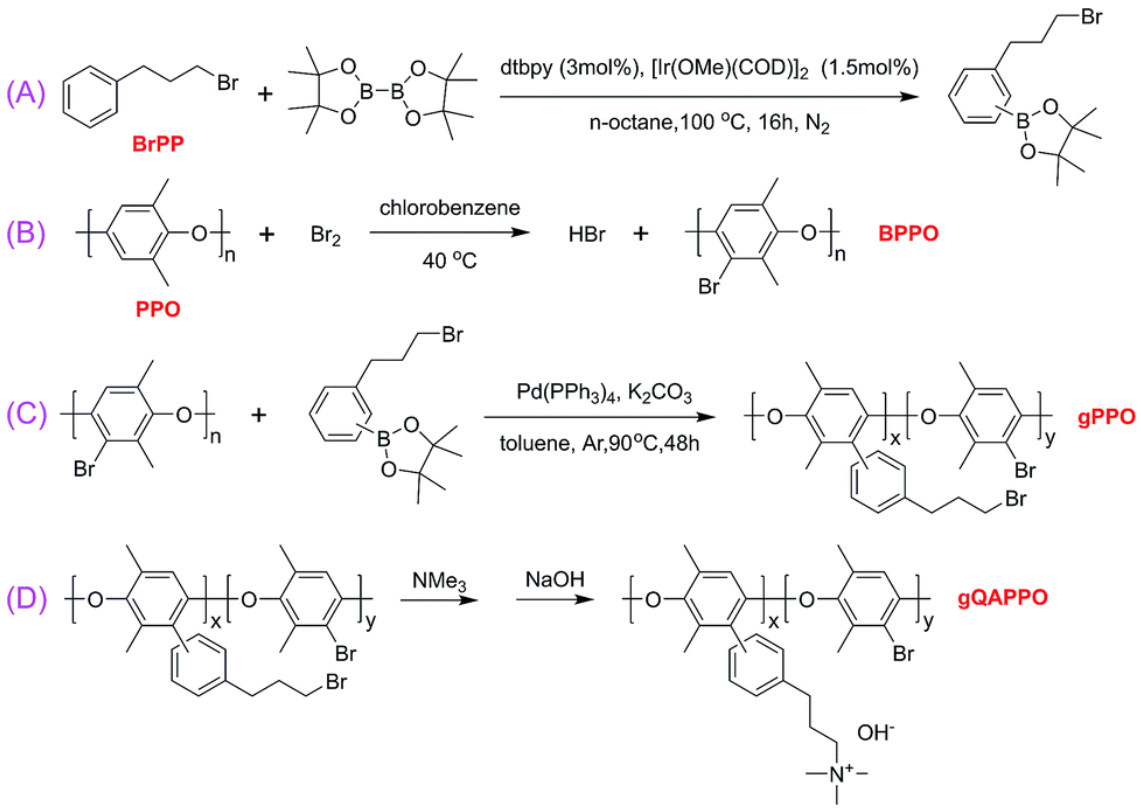

Figure 2.20 Synthetic route of the AEMs containing ammonium groups via flexible spacers (gQAPPO); (A)iridium catalyzed Miyaura; (B) bromination of PPO; (C) Suzuki coupling catalyzed by palladium; (D) quaternization and hydroxide exchange of gPPO membrane. © The Royal Society of Chemistry, 2015.[32]

Yang,[32] *et al.* synthesized AEMs based on functionalized PPO with quaternary ammonium side chains via flexible spacers (gQAPPO) by Suzuki-Miyaura coupling reaction, quaternization and alkalizaition (Figure 2.20). When the IEC was 1.78 mmol/g, the gQAPPO exhibited hydroxide conductivity of 0.027 S/cm and 0.063 S/cm at 30 and 70 °C, respectively.[32] The gQAPPO retained more than 90 % of their hydroxide conductivities after immersing in 1 M NaOH solution at 60 °C for 168 h.[32]

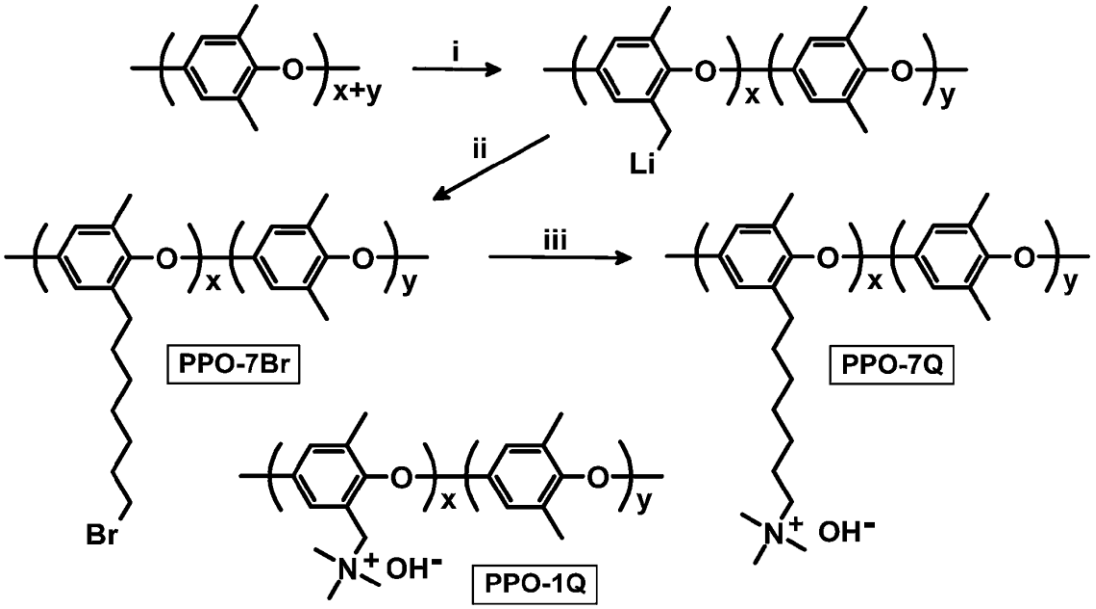

Figure 2.21 Synthetic route for PPO modified with heptyltrimethylammonium side chains (PPO-7Q) via lithiation, bromoalkylation and quaternization. (i)*n*-BuLi, THF, -78 °C (ii) 1,6-dibromohexane, THF, -78 °C, (iii) trimethylamine, NMP, -78 °C; NaOH. © The Royal Society of Chemistry, 2015.[33]

Dang,[33] *et al.* reported AEMs based on PPO modified with heptyltrimethylammonium side chains (PPO-7Q) via lithiation, bromoalkylation and quaternization (Figure 2.21). Compared to the corresponding benzyltrimethylammonium functionalized polymer, significantly enhanced ionic conductivity and alkaline stability was observed for the PPO-7Q with quaternary ammonium groups via flexible alkyl spacers.[33] The phase separated PPO-7Q AEMs reached hydroxide conductivity of 0.035 S/cm at 20 °C and higher than 0.085 S/cm at 80 °C in water.[33] After exposure to 1 M NaOH at 80 °C for 196 h, no detectable degradation was observed for the PPO-7Q, suggesting their high performance as AEMs.[33]

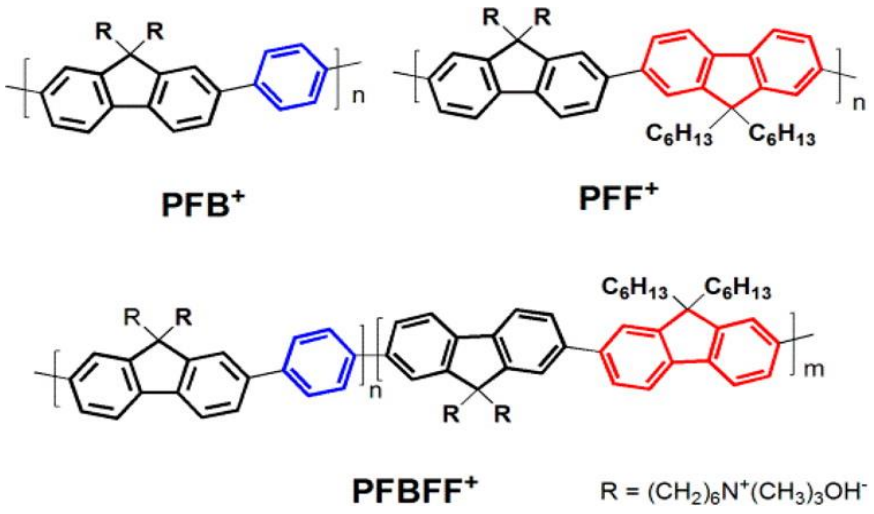

Figure 2.22 Polymer structures of fluorene-based AEMs. © American Chemical Society, 2015.[34]

Recently, Lee,[34] *et al.* reported novel fluorene-based AEMs with long alkyl-tethered quaternary ammonium groups on the side chains via $Pd(PPh_3)_4$-catalyzed Suzuki Couplings (Figure 2.22). Compared to the aryl ether-containing polymers, degradation of the polyfluorene backbone in the strong alkaline conditions was largely restrained due to the replacement of C-O bonds on the polymer backbones.[34] The fluorene-based AEMs exhibited hydroxide conductivity up to 0.124 S/cm at 80 °C with IEC = 3.59 mmol/g.[34] The ^{1}H NMR degradation study of the fluorene-based AEMs demonstrated that there was no backbone degradation or ammonium group loss after exposure to 1 M NaOH at 80 °C for 30 days, suggesting the excellent thermochemical stability in alkaline conditions.[34] In addition, the good solubility and solvent processability of these polyfluorene ionomers enabled their use as both AEMs and ionomer electrode materials.[34]

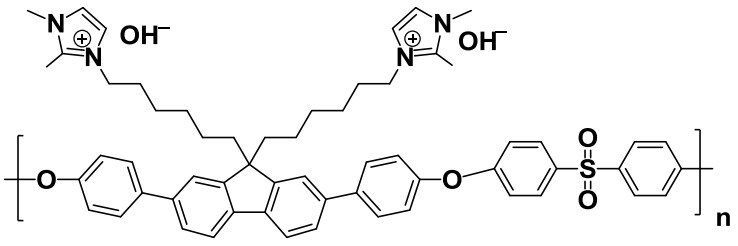

Figure 2.23 Chemical structure of polyfluorene ionomer. © American Chemical Society, 2011.[35]

Lin,[35] *et al.* synthezied fluorene-based AEMs with long alkyl-tethered imidazolium groups on the side chains via polycondensation polymerization, casting from ionomer solution, and followed by immersion in 1 M KOH (Figure 2.23). The polyfuorene ionomer with IEC = 0.98mmol/g exhibited hydroxide conductivity up to 0.428 S/cm at 60 °C.[35] In addition, this AEM possessed a tensile strength (50.41 MPa) and elongation at break (12.63 %), which were comparable to those of traditional imidazolium based AEMs.[35] The AEMs retained their hydroxide conductivity after immersing in 1 M KOH solution at 60 °C for 400 h, indicating the high chemical stability of the AEMs.[35] However, the chemical stability in 1 M KOH solution at 80 °C, which was the fuel cell operating temperature, was not tested.

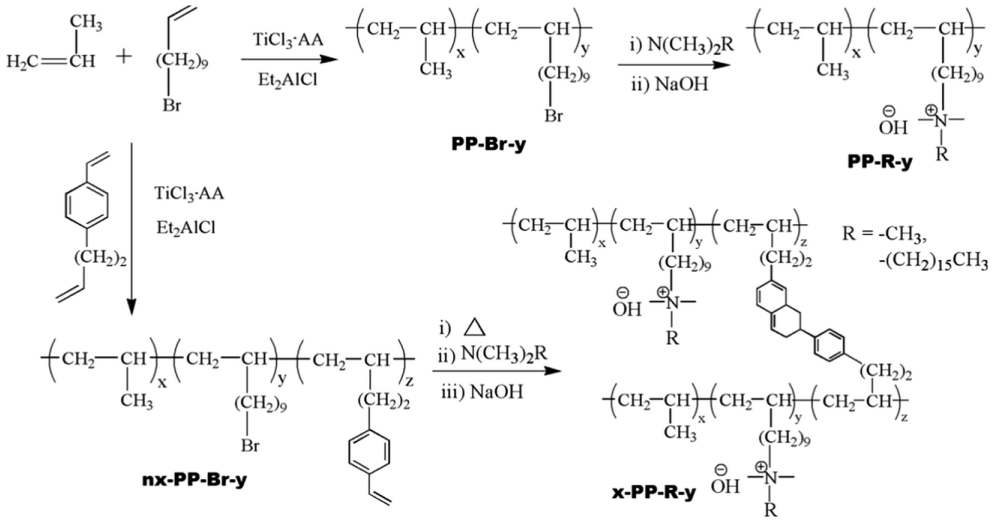

Figure 2.24 Synthetic route of AEMs based on quaternized polypropylene. © The Royal Society of Chemistry, 2015.[36]

Zhang,[36] *et al.* synthesized a series of quaternized polypropylene AEMs with alkyl interstitial spacer by using heterogeneous Ziegler-Natta catalyst (Figure 2.24). These kind of AEMs exhibited hydroxide conductivity up to 19.2 mS/cm in deionized water at 20 °C with IEC = 1.48 mmol/g.[36] More than 85 % of the hydroxide conductivity of the AEMs was retained after exposure to 5 M or 10 M NaOH at 80 °C for 700 h, indicating excellent alkaline stability.[36] In

addition, crosslinked PP-AEMs were obtained at 220 °C by incorporation of a thermally crosslinkable styrenic diene monomer, which exhibited hydroxide conductivity of 56.5 mS/cm in deionized water at 80 °C.[36]

2.3 Crosslinking of AEMs

The performance of AEMFCs is extremely dependent on certain key requirements of the polymer membrane materials: high ion conductivity (> 100 mS/cm), dimensional durability, and chemical stability. Higher charge carrier densities in AEMs are required because of the lower mobility of hydroxide ions compared to protons. In order to achieve sufficient ion conductivity for AEM applications, high ion-exchange capacities (IEC) are essential for anion exchange membranes. However, increasing the IEC values is most often accompanied by high water uptake, leading to severe dimensional swelling, or even dissolution.[37,13] This trade-off between dimensional stability and ion conductivity creates a need for methods to enhance dimensional stability without compromising ion conductivity.[38] Cross-linking has been reported as an effective method to enhance the dimensional stability of the membrane and to increase the fuel resistance crossover in the preparation of AEMs.[38-52]

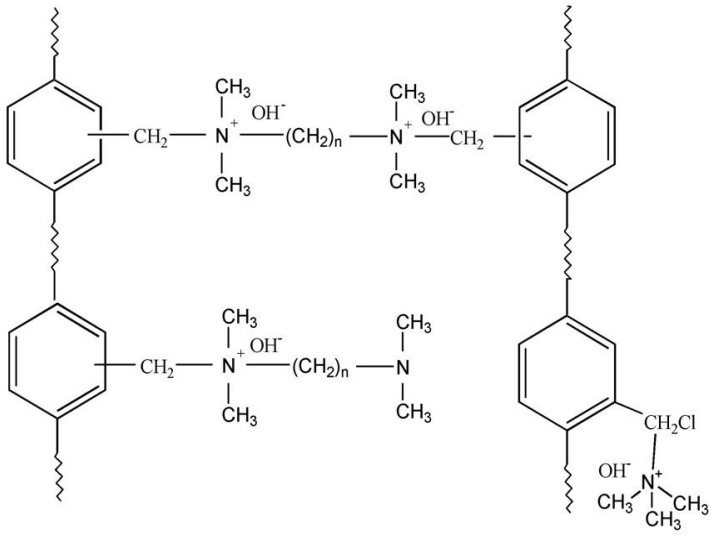

Figure 2.25 Chemical structure of the cross-linked AEMs prepared by amination agent of mixing diamine (with longer alkyl chain). © ELSEVIER, 2011.[52]

Park,[52] *et al.* synthesized a series of cross-linked AEMs using diamine with different alkyl length as crosslinkers, as shown in Figure 2.25. The cross-linked AEMs prepared by amination agent of mixing trimethylamine and *N,N,N',N'*-tetramethyl-1,6-hexanediamine (with longer alkyl chain) shown better hydroxide conductivity (0.012 S/cm at room temperature) and thermal stability than those animated by a diamine.[52] The H_2/air fuel cell performance of the MEA with 0.5 mg cm^{-2} Pt/C at the anode and 2.0 mg cm^{-2} Ag/C at the cathode exhibited a peak power density of 30 $mWcm^{-2}$.[52]

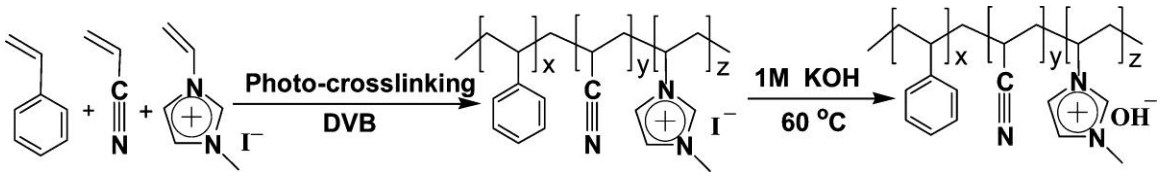

Figure 2.26 Synthetic route for the alkaline Ionic liquid(IL)-based anion exchange membranes. © American Chemical Society, 2010.[53]

Lin, [53] *et al.* synthesized cross-linked AEMs based on alkaline imidazolium-type ionic liquids via in situ cross-linking of 1-vinyl-3-methylimidzolium iodide with styrene and

acrylonitrile, shown in Figure 2.26. For this kind of AEMs, hydroxide conductivity as high as 32.7 mS/cm could be achieved in deionized water at room temperature with IEC = 1.47 mmol/g.[53] These AEMs exhibited excellent chemical stability and mechanical properties. To evaluate the long-term alkaline stability of the AEMs, the samples were immersed in N_2-saturated 1 and 10 M KOH solution at 60 °C for 400 hours.[53] The AEMs maintained the ionic conductivity after 400 h treatment in 1 M KOH solution.[53]

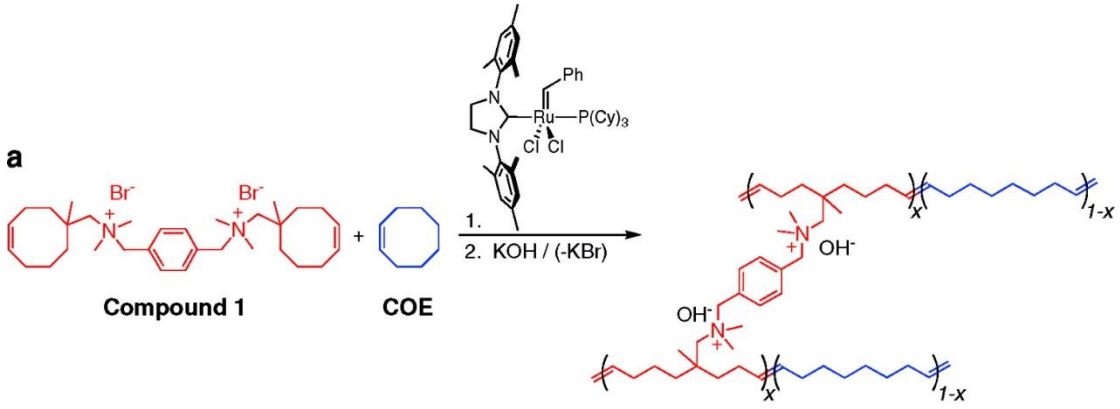

Figure 2.27 Monomer structure and synthetic route of the cross-linked AEMs. © American Chemical Society, 2010.[54]

Robertson,[54] *et al.* incorporated tetraalkylammonium-functionalized cross-links into the polymer main chains by used the Grubbs second generation catalysts, achieving high ion conductivity while retaining good material properties. The cross-linked AEMs were synthesized from cationic compound 1 (Figure 2.27) and cyclooctene in the presence of Grubbs second generation catalysts. The IEC and mechanical strength could be turned by controlling the ratio of cyclooctene.

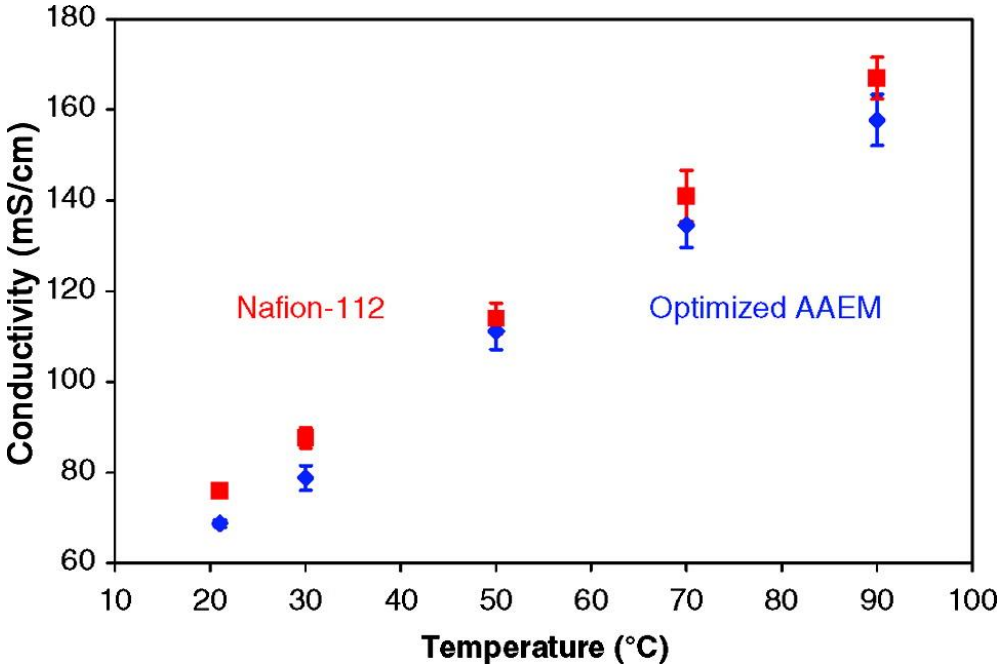

Figure 2.28 Hydroxide conductivity of cross-linked AEMs prepared by Coates *et al.*and Nafion-112 in liquid water as a function of temperature. © American Chemical Society, 2010.[54]

The AEMs demonstrated good ionic conductivity (Figure 2.28), which was comparable to Nafion-112.[54] In addition, the authors of this work believed that these materials would display good long-term stability under alkaline conditions because the tetraalkylammonium ions were devoid of β-hydrogens. [54] However, the resulting polymer became insoluble after crosslinking, which was not compatible with practical fabrication of electrochemical devices. Until now, fuel cell performance of the MEAs based on the cross-linked AEMs was not reported.[54]

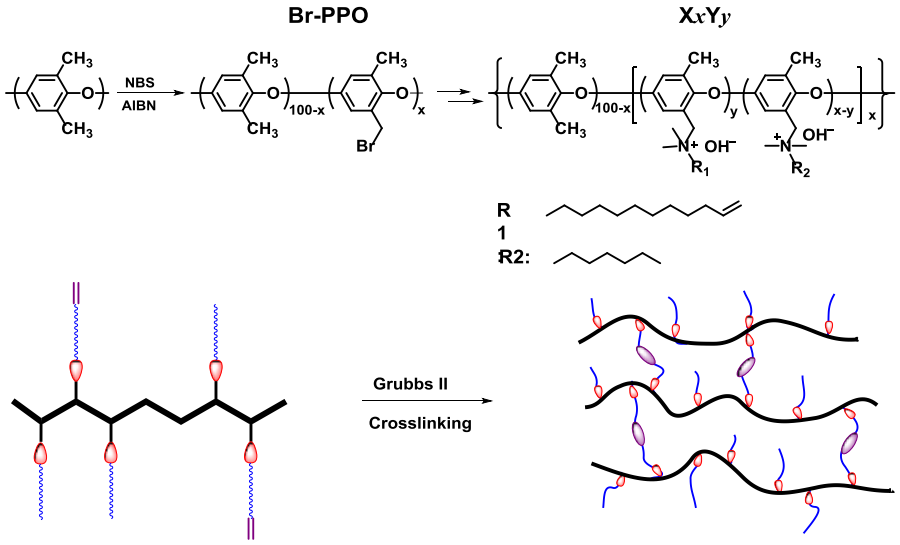

Figure 2.29 Synthetic route for the cross-linked comb-shaped AEMs via olefin metathesis with Grubbs II catalyst. © The Royal Society of Chemistry, 2014.[55]

Li,[55] *et al.* developed one-step crosslinking strategy upon the quaternary ammonium groups using Grubbs II-catalyzed alkene metathesis technique to produce highly base and dimension stable AEMs, shown in Figure 2.29.

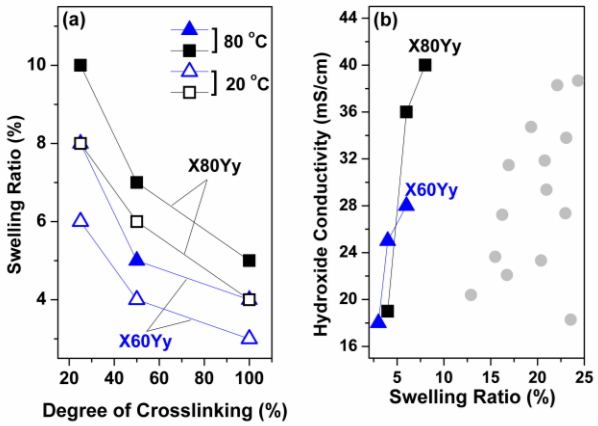

Figure 2.30 (a) Swelling ratio as a function of degree of crosslinking at 60 °C and 80 °C; (b) hydroxide conductivity of the XxYy and reported AEMs (circles) at different swelling ratio. © The Royal Society of Chemistry, 2014.[55]

Compared to the uncrosslinked X80Y40 which could be dissolved in water, the cross-linked exhibited a water uptake of 28.9 % and swelling ratio of 5.4 % (Figure 2.30).[55] In addition, the cross-linked XxYy AEMs exhibited higher hydroxide conductivity than that of reported ones (Figure 2.30).[55] At elevated temperature (80 °C), the cross-linked XxYy membranes demonstrated excellent dimensional and chemical stability.[55] The cross-linked XxYy AEMs remained more than 90 % of their ion conductivity after immersion in 1 M NaOH at 80 °C for 30 days.[55]

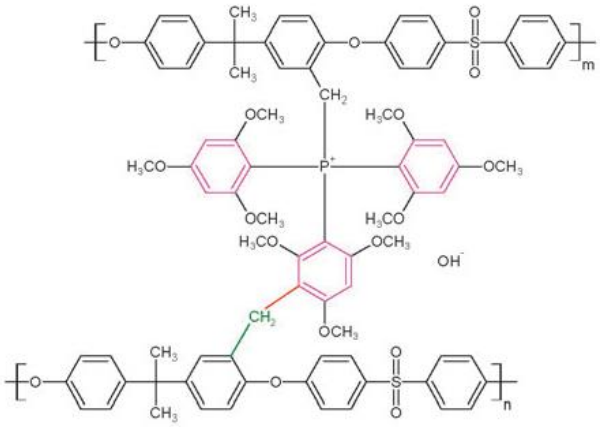

Figure 2.31 Chemical structure of the self-crosslinked TPQPOH (SCL-TPQPOH). © The Royal Society of Chemistry, 2011.[8]

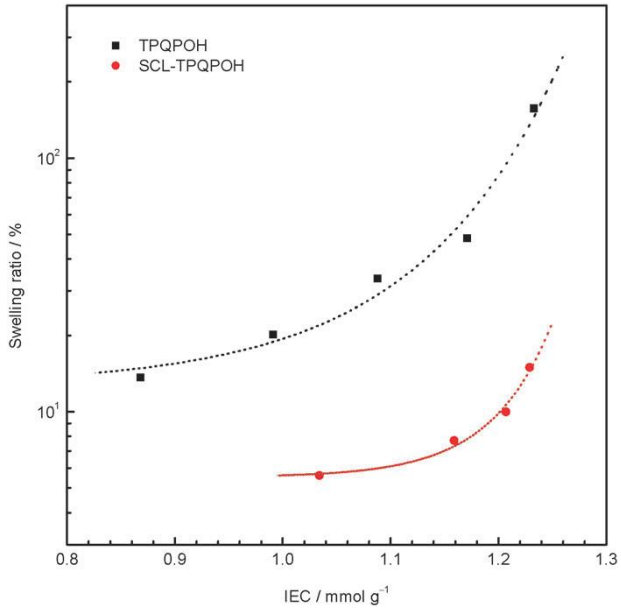

Figure 2.32 Swelling degree of TPQPOH and SCL-TPQPOH AEMs at 60 ^{o}C. © The Royal Society of Chemistry, 2011.[8]

Gu,[16] *et al.* synthesized a new quaternary phosphonium based polysulfone-AEMs: tri(2,4,6-trimethoxyphenyl) polysulfone-methylene quaternary phosphonium hydroxide (TPQPOH), which swelled largely ratio at elevated temperature. In order to enhance the dimensional stability, Gu,[8] *et al.* employed the Friedel–Crafts electrophilic substitution C-alkylation strategy to prepare the self-crosslinked TPQPOH (SCL-TPQPOH, Figure 2.32), which was dimensionally stable, solvent-resistant, and hydroxide-conductive.[8] Compared to the TPQPOH (Figure 2.32), SCL-TPQPOH has greatly enhanced dimensional integrity due to the introduction of the cross-links. The SCL-TPQPOH with an IEC = 1.23 mmol/g exhibited hydroxide conductivity as high 32.7 mS/cm in deionized water at room temperature.[8] More importantly, only a 15 % swelling ratio was observed for this SCL-TPQPOH sample at 60 °C, indicating their potential for use in a fuel cell.[8]

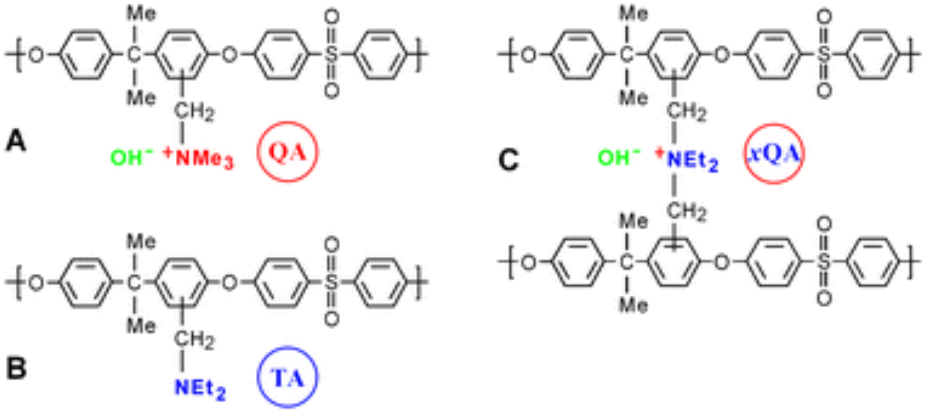

Figure 2.33 Chemical structures for alkaline functional groups attached to the polysulfone backbone. (A) Quaternary ammonium (QA). (B) Tertiary amino (TA). (C) A new type of QA generated upon solidification (*x*QA), crosslinking two nearest chains. © The Royal Society of Chemistry, 2011.[56]

Pan,[56] *et al.* developed a method to prepare the self-crosslinked AEMs (*x*TQAPS) by replacing part of the ammonium group (-NR_3^+) in QAPS with a tertiary amino group (-NR_2, TA), shown in Figure 2.33. The TA groups could react with the residual chloromethyl group of polysulfone backbones to form the cross-linked network at elevated temperature during membrane casting.[56]

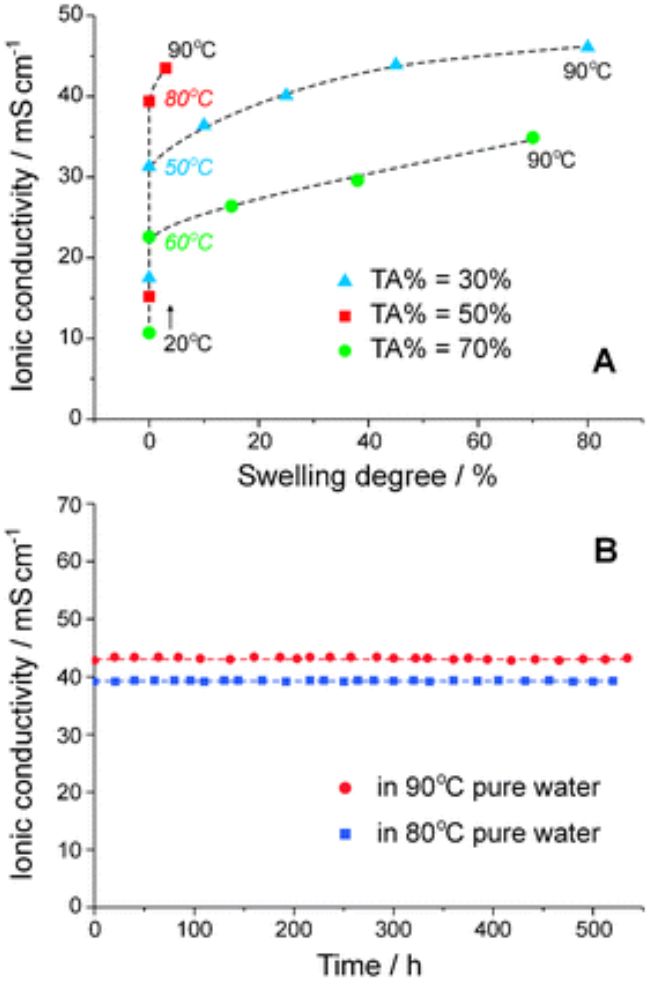

Figure 2.34 (A) the ionic conductivity and swelling degree plot of *x*TQAPS . (B) the stability testing of *x*TQAPS in hot water. © The Royal Society of Chemistry, 2010.[56]

The *x*TQAPS exhibited both high hydroxide conductivity (43 mS/cm) and dimensional stability (Figure 2.34) in deionized water at 90 °C.[56] Besides, both of the ion conductivity and mechanical properties retained the same after immersing in deionized water at 90 °C for 500 h.[56]

2.4 Chemical Degradation of Anion Exchange Membranes

2.4.1 Degradation of AEMs Cations

The long-term stability of AEMs in electrochemical devices is generally of primary concern due to known degradation pathways for tetraalkylammonium ions under strongly alkaline environments, such as β-hydrogen (Hofmann) elimination, direct nucleophilic substitution at the α-carbon, and nitrogen ylide formation.[57-60] The possible degradation mechanism of these membranes based on PPO is shown in Figure 2.35.

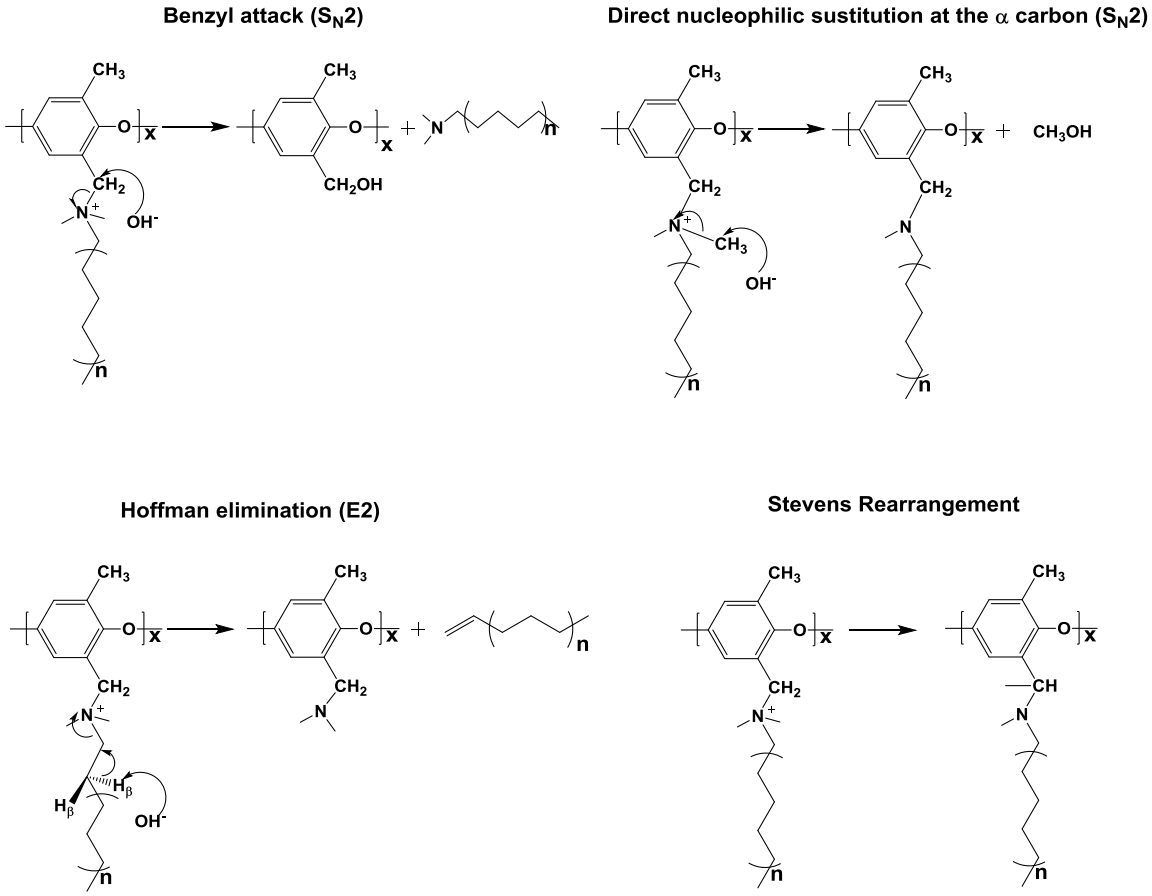

Figure 2.35 Possible degradation pathways of AEMs based on PPO in alkaline environment.

The degradation of the tetraalkylammonium by direct nucleophilic attack (debenzylation) corresponds to S_N2 reaction between OH^- anion and a carbon atom in α-position of the tetraalkylammonium group. The resulting products are polymer containing benzyl alcohol and alkyl amine.[61] The degradation of the tetraalkylammonium by (demethylaztion) involves the S_N2 reaction between OH^- anion and a carbon atom in α-position of the tetraalkylammonium group as well. Two products are generated: a polymer containing an alkyl amine and an alcohol.[61] When the β-position of the nitrogen atom in the quaternary ammonium group bears at least one hydrogen, the alkalized quaternary ammonium group can be cleaved, which is called "Hofmann Elimination" and yields a polymer containing alkyl amine and an olefin.[61] In the case of benzyltrimethylammonium, some products generated by Stevens rearrangement can be observed.[61]

Compared to the $–SO_3H$ cation-exchange groups, the quaternary ammonium groups tethered to the similar polymer backbones are prone to degradation in the presence of the OH^- anion.[61] This backbone degradation is caused by the electrophilic character of the quaternary ammonium group itself.[61] The degradation of the quaternary ammonium group may be further accelerated with the presence of nearby electron-withdrawing groups.[61] Due to the electron-withdrawing effect, the benzyl group can facilitate the nucleophilic attack of OH^-. In addition, its aromatic conjugated system can stabilize radicals and carbanions at the benzylic site, further promoting other degradation pathways.[61] By introducing appropriate substituents to the aromatic ring, the degradation of benzylic quaternary ammonium can be increased or decreased.[61]

Entry	QA	Abbreviation[a]	Half-life [h]
1		TMA	61.9
2	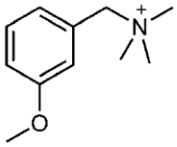	MBTM	16.6
3	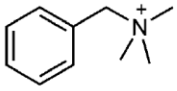	BTM	4.18
4	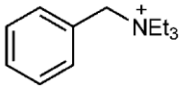	BTE	0.68
5	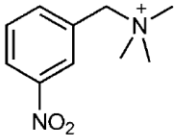	NBTM	0.66
6	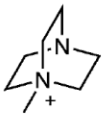	MAABCO	13.5
7	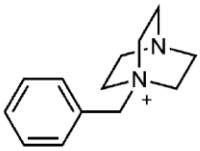	BAABCO	1.4
8	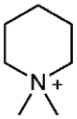	DMP	87.3
9	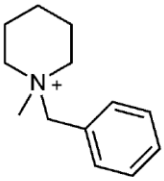	BMP	7.3

Table 2.1 Alkaline stability of various small molecule analogs at 160 °C in 6 M NaOH. © WILEY-VCH Verlag GmbH & Co. KGaA, Weinheim, 2015.[62]

The half-lives of 9 different tetraalkylammonium species in a 6 M NaOH solution at 160 °C studied by Kreuer,[62] *et al*. was listed in Table 1. Although the electron-donating group-functionalized (-OMe, Entry 2) benzyl group counteracts the destabilizing effect of benzylic quaternary ammonium to some extent, the half-life of methyl-functionalized benzyl group still only 27 % of that of TMA.[62] Clearly, the (-NO_2, Entry 5) substituent on the aromatic ring decreased the stability of the benzylic quaternary ammonium.[62]

Recently, it was reported that the addition of an interstitial spacer between the charged group and the aromatic ring obviously enhanced the stability of tetraalkylammonium cations. For example, Lee,[34] *et al.* reported novel fluorene-based AEMs with long alkyl-tethered quaternary ammonium groups on the side chains. The ^{1}H NMR degradation study of the fluorene-based AEMs demonstrated that there was no backbone degradation or ammonium group loss after exposure to 1 M NaOH at 80 °C for 30 days, indicating excellent thermochemical stability under alkaline conditions.[34] Dang,[33] *et al.* reported AEMs based on PPO modified with heptyltrimethylammonium side chains (PPO-7Q), which shown no detectable degradation after exposure to 1 M NaOH at 80 °C for 196 h.

2.4.2 Degradation of AEMs Polymer Backbones

In addition to cation stability, chemical stability of the polymer backbone is of great importance for advanced AEM fuel cell systems, since the polymer backbone and molecular weight impact the mechanical properties of the AEMs.[63] Compared to the intense study of the cation stability, the investigation of the polymer backbone degradation is still rare.

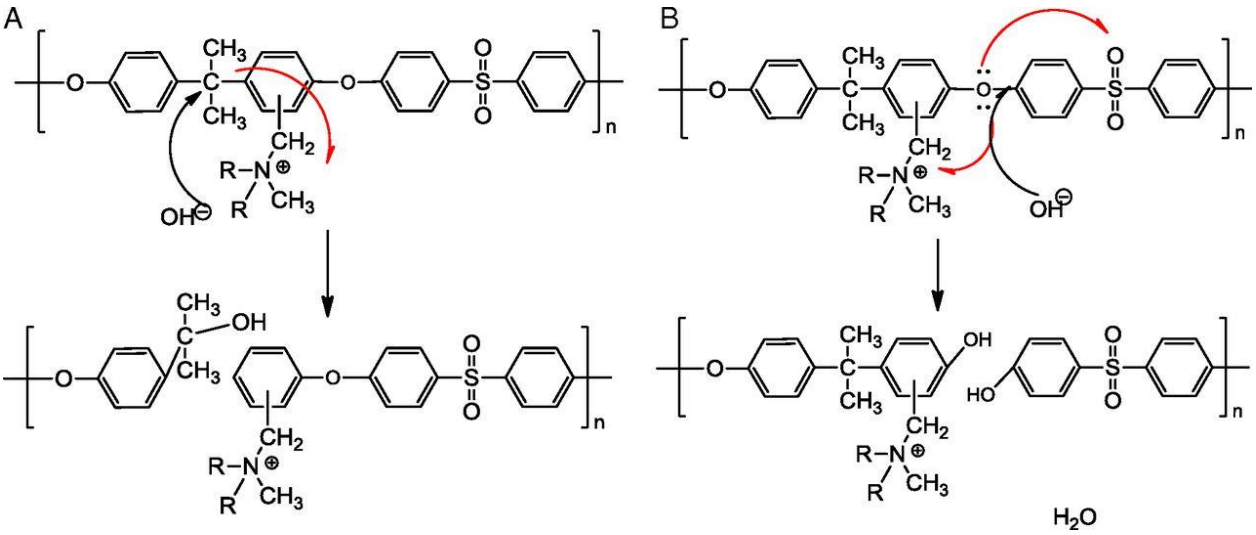

Figure 2.36 Degradation pathways of poly(sulfones) backbone in alkaline media: (A) OH^- attack at quaternary carbon to yield to phenylpropane alcohol, and (B) displacement by OH^- of the aryl ethers to generate phenols. Red lines indicates electron delocalizatioin. ©2013 National Academy of Sciences, 2013.[64]

Arges,[64] *et al.* investigated cation-triggered backbone degradation in polysulfone-based AEMs using two-dimensional NMR spectroscopy. They found that there were two degradation pathways of poly(sulfones) backbone in alkaline media (Figure 2.36): (A) OH^- attack at quaternary carbon to yield to phenylpropane alcohol, and (B) displacement by OH^- of the aryl ethers to generate phenols, as shown in Figure 2.36.[64]

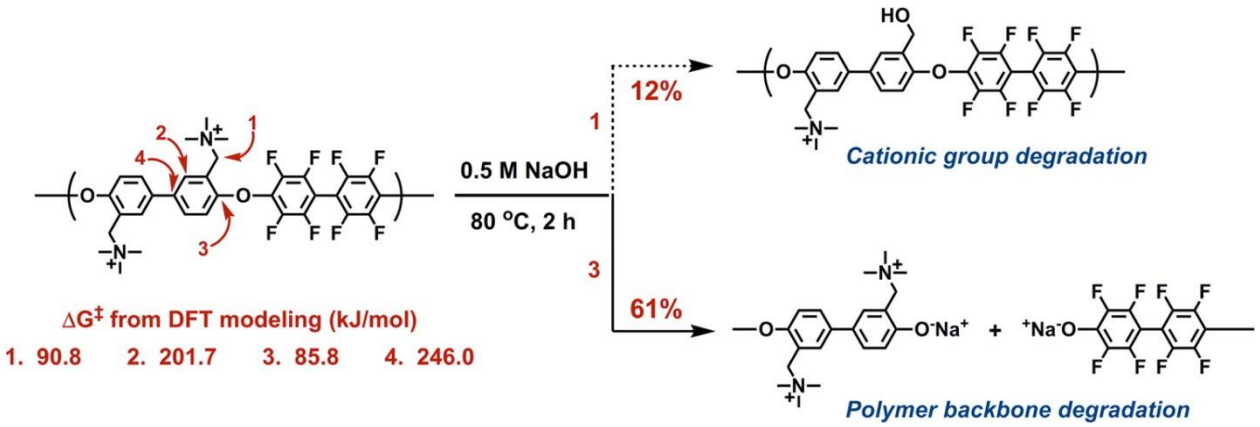

Figure 2.37 Computational and experimental results of alkaline stability of benzyl trimethyl ammonium functionalized polyaromatics. © American Chemical Society, 2014.[65]

Recently, Choe,[65] *et al.* investigated the alkaline stability of benzyl trimethyl ammonium functionalized polyaromatics using both of computational and experimental methods. The barrier height of aryl-ether cleavage initiated by OH^- was calculated to be 85.8 kJ/mol, which was lower than that of nucleophilic substitution of the α-carbons on the benzylic position of the quaternary ammonium groups (90.8 kJ/mol), shown in Figure 2.37.[64] The facile aryl-ether cleavage in the polymer backbone was because of the electron deficiency of the aryl group and low bond dissociation energy caused by ether substituent.[64]

2.5 Summary

To date, there have been many types of AEM structures demonstrated. Some reports in the literature have shown promising conductivity, while others have shown a noteworthy combination of properties including robust mechanical properties, high conductivity, and reasonable hydroxide stability. However, good fuel cell performance is still an elusive goal with many experimental anion exchange membranes. There is currently no consensus in the field on the best way forward to scalable anion exchange membranes that show promising device

performance. These studies are ongoing based on the wealth of structures that have previously been reported.

2.6 Reference

(1) Dragan, E. S.; Avram, E.; Axente, D. Marcu, C. *J. Polym. Sci., Part A: Polym. Chem*. **2004**, *42*, 2451.

(2) Vinodh, R.; Ilakkiya, A.; Elamathi, S.; Sangeetha, D. *MATER SCI ENG B-ADVR*. **2010**, *167*, 43.

(3) Zeng, Q.; Liu, Q.; Broadwell, I.; Zhu, A.; Xiong, Y.; Tu, X. *J. Membr. Sci*. **2010**, *349*, 237.

(4) (a) Yan, J.; Hickner, M. A. *Macromolecules* **2010**, *43*, 2349. (b) Hibbs, M. R.; Fujimoto, C. H.; Cornelius, C. J. *Macromolecules* **2009**, *42*, 8316.

(5) Hibbs, M. R.; Hickner, M. A.; Alam, T. M.; McIntyre, S. K.; Fujimoto, C. Y.; Cornelius, C. *J. Chem. Mater*. **2008**, *20*, 2566.

(6) Zhou, J.; Unlu, M.; Vega, J. A.; Kohl, P. A. *J. Power Sources* **2009**, *190*, 285.

(7) Wang, J.; Li, S.; Zhang, S. *Macromolecules* **2010**, *43*, 3890.

(8) Gu, S.; Cai, R.; Yan, Y. *Chem. Commun.* **2011**, *47*, 2856.

(9) Zhao, Z.; Wang, J.; Li, S.; Zhang, S. *J. Power Sources* **2011**, *196*, 4445.

(10) Varcoe, J. R.; Slade, R. C. T.; Yee, E. L. H.; Poynton, S. D.; Driscoll, D. J.; Apperley, D. C. *Chem. Mater*. **2007**, *19*, 2686.

(11) Wang, G.; Weng, Y.; Chu, D.; Chen, R.; Xie, D. *J. Membr. Sci.* **2009**, *332*, 63.

(12) Mohanty, A. D.; Ryu, C. Y.; Kim, Y. S.; Bae, C. *Macromolecules*, **2015**, *48*, 7085.

(13) Pan, J.; Lu, S.; Li, Y.; Huang, A.; Zhuang, L.; Lu, J. *Adv. Funct. Mater.* **2010**, *20*, 312.

(14) Mohanty, A. D.; Lee, Y.-B.; Zhu, L.; Hickner, M. A.; Bae, C. *Macromolecules* **2014**, *47*, 1973.

(15) Zhang, F.; Zhang, H.; Qu, C. *J. Mater. Chem.* **2012**, *21*, 12744.

(16) Gu, S.; Cai, R.; Luo, T.; Chen, Z.; Sun, M.; Liu, Y.; He, G.; Yan, Y. *Angew. Chem., Int. Ed.* **2009**, *48*, 6499.

(17) Xu, T.; Wu, D.; Wu, L. *Prog. Polym. Sci.* **2008**, *33*, 894.

(18) Yang, Y.; Knauss, D. M. *Macromolecules*, **2015**, *48*, 4471.

(19) Kostalik IV, H. A.; Clark, T. J.; Robertson, N. J.; Mutolo, P. F.; Longo, J. M.; Abruna, H. D.; Coates, G. W. *Macromolecules* **2010**, *43*, 7147.

(20) Noonan, K. J. ; Hugar, K. M. ; Kostalik IV, H. A. ; Lobkovsky, E. B. ; Abruña, H. D. ; Coates, G. W. *J. Am. Chem. Soc.* **2012**, *134*, 18161.

(21) Tanaka, M.; Fukasawa, K.; Nishino, E.; Yamaguchi, S.; Yamada, K.; Tanaka, H.; Bae, B.; Miyatake, K.; Watanabe, M. *J. Am. Chem. Soc*. **2011**, *133*, 10646.

(22) Seo, D. W.; Hossain, M. A.; Lee, D. H.; Lim, Y. D.; Lee, S. H.; Lee, H. C.; Hong, T. W.; Kim, W. G. *Electrochim. Acta*. **2012**, *86*, 360.

(23) Tanaka, M.; Koike, M.; Miyatake, K.; Watanabe, M. *Macromolecules* **2010**, *43*, 2657.

(24) Han, G. L.; Xu, P. Y.; Zhou, K.; Zhang, Q. G.; Zhu, A. M.; Liu, Q. L. *J. Membr. Sci*. **2014**, *457*, 29.

(25) Lin, B.; Qiu, L.; Qiu, B.; Peng, Y.; Yan, F. *Macromolecules* **2011**, *44*, 9642.

(26) Zha, Y.; Disabb-Miller, M. L.; Johnson, Z. D.; Hickner, M. A.; Tew, G. N. *J. Am. Chem. Soc*. **2012**, *134*, 4493.

(27) Thomas, O. D.; Soo, K. J.; Peckham, T. J.; Kulkarni, M. P.; Holdcroft, S. *J. Am. Chem. Soc*. **2012**, *134*, 10753.

(28) Pan, J.; Li, Y.; Han, J.; Li, G.; Tan, L.; Chen, C.; Zhuang, L. *Energy Environ. Sci.* **2013**, *6*, 2912.

(29) Si, J.; Lu, S.; Xu, X.; Peng, S.; Xiu, R.; Xiang, Y. *ChemSusChem*. **2014**, *7*, 3389.

(30) Li, Q.; Liu, L.; Miao, Q.; Jin, B.; Bai, R. *Chem. Commun.* **2014**, *50*, 2791.

(31) Li, N.; Leng, Y.; Hickner, M. A.; Wang, C.-Y. *J. Am. Chem. Soc.* **2013**, *135*, 10124.

(32) Yang, Z.; Zhou, J.; Wang, S.; Hou, J.; Wu, L.; Xu, T. *J. Mater. Chem. A*, **2015**, *3*, 15015.

(33) Dang, H. S.; Weiber, E. A.; Jannasch, P. *J. Mater. Chem. A* **2015**, *3*, 5280.

(34) Lee, W. H.; Mohanty, A. D.; Bae, C. *ACS Macro Lett.* **2015**, *4*, 453.

(35) Lin, B.; Qiu, L.; Qiu, B.; Peng, Y.; Yan, F. *Macromolecules* **2011**, *44*, 9642.

(36) Zhang, M.; Liu, J.; Wang, Y.; An, L.; Guiver, M. D.; Li, N. *J. Mater. Chem. A*, **2015**, *3*, 12284.

(37) Varcoe, J. R.; Atanassov, P.; Dekel, D. R.; Herring, A. M.; Hickner, M. A.; Kohl, P. A.; Kucernak, A. R.; Mustain, W. E.; Nijmeijer, K.; Scott, K.; Xu, T.; Zhuang, L. *Energy Environ. Sci*. **2014**, 7, 3135.

(38) Tsai, T. H.; Ertem, S. P.; Maes, A. M.; Seifert, S.; Herring, A. M.; Coughlin, E. B. *Macromolecules* **2015**, *48*, 655.

(39) Pan, J.; Zhu, L.; Han, J.; Hickner, M. A. *Chem. Mater.* **2015**, *27*, 6689**.**

(40) Zhuo, Y. Z.; Lai, A. N.; Zhang, Q. G.; Zhu, A. M.; Ye, M. L.; Liu, Q. L. *J. Membr. Sci.* **2015**, *491*, 138.

(41) Lin, B.; Chu, F.; Ren, Y.; Jia, B.; Yuan, N.; Shang, H.; Feng, T.; Zhu, Y.; Ding, J. *J. Power Sources* **2014**, *266*, 186.

(42) Li, N.; Wang, L.; Hickner, M. A. *Chem. Commun.* **2014**, *50*, 4092.

(43) Lin, B.; Dong, H.; Li, Y.; Si, Z.; Gu, F.; Yan, F. *Chem. Mater.* **2013**, *25*, 1858.

(44) Lin, X.; Liu, Y.; Poynton, S. D.; Ong, A. L.; Varcoe, J. R.; Wu, L.; Li, Y.; Liang, X.; Li, Q.; Xu, T. *J. Power Sources* **2013**, *233*, 259.

(45) Zhao, Y.; Yu, H.; Yang, D.; Li, J.; Shao, Z.; Yi, B. *J. Power Sources* **2013**, *221*, 247.

(46) Zhou, J. F.; Unlu, M.; Anestis-Richard, I.; Kohl, P. A. *J. Membr. Sci.* **2010**, *350*, 286.

(47) Yang, C. C.; Chiu, S. J.; Chien, W. C.; Chiu, S. S. *J. Power Sources* **2010**, *195*, 2212.

(48) Lin, B.; Qiu, L.; Lu, J.; Yan, F. *Chem. Mater.* **2010**, *22*, 6718.

(49) Xiong, Y.; Fang, J.; Zeng, Q. H.; Liu, Q. L. *J. Membr. Sci.* **2008**, *311*, 319.

(50) Stoica, D.; Ogier, L.; Akrour, L.; Alloin, F.; Fauvarque,J. F. *Electrochim. Acta,* **2007**, *53*, 1596.

(51) Wu, Y. H.; Wu, C. M.; Xu, T. W.; Yu F.; Fu, Y. X. *J. Membr. Sc.*, **2008**, *321*, 299.

(52) Park, J. S.; Park, S. H.; Yim, S. D.; Yoon, Y. G.; Lee, W. Y.; Kim, C. S. *J. Power Sources* **2008**, *178*, 620.

(53) Lin, B.; Qiu, L.; Lu, J.; Yan, F. *Chem. Mater.* **2010**, *22*, 6718.

(54) Robertson, N. J.; Kostalik IV, H. A.; Clark, T. J.; Mutolo, P. F.; Abruña, H. D.; Coates, G. W. *J. Am. Chem. Soc.* **2010**, *132*, 3400.

(55) Li, N.; Wang, L.; Hickner, M. A. *Chem. Commun.* **2014**, *50*, 4092.

(56) Pan, J.; Li, Y.; Zhuang, L.; Lu, J. *Chem. Commun.* **2010**, *46*, 8597.

(57) Varcoe, J. R.; Slade, R. C. T. *Fuel Cells* **2005**, *2*, 187.

(58) Chempath, S.; Einsla, B. R.; Pratt, L. R.; Macomber, C. S.; Boncella,J. M.; Rau, J. A.; Pivovar, B. S. *J. Phys. Chem. C* **2008**, *112*, 3179.

(59) Einsla, B. R.; Chempath, S.; Pratt, L. R.; Boncella, J. M.; Rau, J.; Macomber, C.; Pivovar, B. S. *Electrochem. Soc. Trans.* **2007**, *11*, 1173.

(60) Macomber, C. S.; Boncella, J. M.; Pivovar, B. S.; Rau, J. A. *J. Therm.Anal.Calorim.***2008**, *93*, 225.

(61) Couture, G.; Alaaeddine, A.; Boschet, F.; Ameduri, B. *Prog. Polym. Sci.* **2011**, *36*, 1521.

(62) Kreuer, K. D.; Marino, M. G. *ChemSusChem.* **2015**, *8*, 513.

(63) Fujimoto, C.; Kim, D. S.; Hibbs, M.; Wrobleski, D.; Kim, Y. S. *J. Membr. Sci.* **2012**, *423*, 438.

(64) Arges, C. G.; Ramani, V. *Proc. Natl. Acad. Sci. U.S.A.* **2013**, *110*, 2490.

(65) Choe, Y. K.; Fujimoto, C.; Lee, K. S.; Dalton, L. T.; Ayers, K.; Henson, N. J.; Kim, Y. S. *Chem. Mater.* **2014**, *26*, 5675.

Chapter 3

Experimental Details of Polymer Synthesis, Membrane Preparation and Characterization.

3.1. Introduction

This chapter will introduce general procedures for the synthesis of PPO-based side chain containing copolymers, quaternization of the samples, and membrane preparation used in the dissertation. Additionally, a concise introduction of the characterization methods are included in this chapter. The preparation procedures and characterization methods presented in this chapter are applicable to all PPO copolymer-based AEMs detailed in this dissertation for structure-property elucidation.

3.2 Materials

Poly(2,6-dimethyl-1,4-phenylene oxide) with an average molecular weight of 20,000 g/mol (~ PDI = 1.50) was purchased from Sigma-Aldrich and dried under vacuum at room temperature overnight. *N*,*N*-dimethylhexylamine, *N*,*N*-dimethyldecylamine, *N*,*N*-dimethylhexadecylamine, *N*-bromosuccinimide, 1,8-octanedithiol, and 2,2*'*-azobis(2-methylpropionitrile) were purchased from Sigma-Aldrich and used as received. 2-Bromofluorene, 1,6-dibromohexane, bis(pinacolato)diboron, tetrabutylammonium bromide, potassium acetate, palladium acetate, Sphos, XPhos, [1,1′ bis(diphenylphosphino)ferrocene]dichloropalladium(II), and bromine were obtained from Sigma-Aldrich and used as received. *N,N,N',N'*-tetramethyl-1,6-hexanediamine, 6-bromo-hexane, (5-bromopentyl)trimethylammonium bromide, Jeffamine® ED-600 were obtained from Sigma-Aldrich and used as received.

3.3 Synthesis and Characteriazation of Side Chain Containing PPO Copolymers

This section will introduce the general procedures and characterization techniques used for side chain containing copolymers and quaternization of the copolymer. The techniques used in the characterization of AEMs will be discussed in detail in this section.

3.3.1 Synthesis of Side Chain Containing PPO Copolymer

The detailed procedures for the side chain containing PPO copolymer syntheses in this dissertation will be presented in each section. The side chain, modified PPO and appropriate solvent were added to a round-bottom reaction flask. The vessel was purged with argon to remove oxygen and water from the reaction system and sealed with a rubber septum. The polymerization system was moved into a pre-heated oil bath under the proper temperature to perform the reaction. After the desired reaction time, the reaction was cooled to room temperature under argon atmosphere. The reaction solution was poured into methanol/hexane/toluene to precipitate the polymer. The product was filtered and further washed with methanol/hexane/toluene several times. The polymer was dried in a vacuum oven at 60 °C overnight.

3.4 Characterization of Side Chain Containing PPO Copolymer and Membranes

This section will discuss the typical characterization techniques used for the side chain-containing PPO copolymers. Nuclear magnetic resonance spectroscopy (NMR) was employed to ascertain the chemical structure of the copolymer and calculate the IEC values based on content of quaternary groups. In addition, this section will present the key parameters for evaluation of the AEM performance. Measuring conductivity, water uptake in liquid water techniques, membrane morphology determination, and mechanical properties testing will be discussed.

3.4.1 Nuclear Magnetic Resonance Spectroscopy

^{1}H nuclear magnetic resonance (NMR) spectra were recorded at 300 MHz on a Bruker AV 300 spectrometer and chemical shifts were listed in parts per million (ppm) downfield from tertramethylsilane (TMS). The dried copolymer samples were dissolved in $CDCl_3$/DMSO-d_6 for NMR characterization.

3.4.2 Membrane Preparation

The side chain containing copolymer in bromide form was dissolved in NMP to yield a 5 wt % solution. The solution was then cast onto a leveled glass plate, and dried at 82 °C under ambient pressure for 24 h followed by vacuum drying for another 24 h at 80 °C to give a ~100 μm thick, transparent, tough film.

3.4.3 Conductivity Measurements

Ionic conductivity (σ) was measured using impedance spectroscopy on a Solartron 1260A impedance/gain phase analyzer with a two-point, in-plane geometry at frequencies ranging from 1 MHz to 100 MHz.[1] The membrane resistance was obtained from the real value of the impedance where the imaginary response was zero. The ionic conductivity, σ in mS/cm, of each sample was calculated from $\sigma = L/RA$, where L is the distance between reference electrodes, R is the resistance of the sample, and A is the cross-sectional area of the sample. Bicarbonate conductivities were measured by exchanging the bromide form membranes in 1 M sodium bicarbonate for 24 h followed by rinsing to remove excess salt. Chloride conductivities were measured by exchanging the bromide form membranes in 1 M sodium chloride at room temperature for 24 h followed by extensively rinsing to remove excess salt. Hydroxide

conductivities were measured by exchanging the bromide form membranes in 1 M sodium hydroxide for 24 h followed by rinsing to remove excess salt with degassed and deionized water. The membranes were subsequently placed into conductivity cells and immersed in deionized water that was degassed and blanketed with flowing Argon gas.

3.4.5 Water Uptake

Water uptake was measured after drying the membrane in the desired counterion form at 60 °C under vacuum for 24 h. The dried membrane was immersed in water and periodically weighed on an analytical balance until a constant mass was obtained, giving the mass-based water uptake. Water uptake was calculated by ($WU = (m_{hyd}-m_0)/m_0$), where m_{hyd} is the hydrated sample mass and m_0 is the dry sample mass. The hydration number (λ), or the number of water molecules per ionic group, was calculated from:

$$\lambda = \left(\frac{m_{hyd} - m_0}{m_0} \right) \cdot \left(\frac{1000}{M_{H2O} \cdot IEC} \right) \quad (1)$$

where m_{hyd} is the hydrated membrane mass, m_0 is the mass of the dry membrane, M_{H2O} is the molecular mass of water (18 $g \cdot mol^{-1}$), and IEC is the ion exchange capacity with units of milliequivalents of ions per gram of polymer. The water volume fraction of the sample was calculated from:

$$\phi = \left(\frac{\frac{WU}{\rho_{water}}}{\frac{WU}{\rho_{water}} + \frac{1}{\rho_{membrane}}} \right) \quad (2)$$

where WU is the water uptake of membranes, ρ_{water} is the density of water (1 g·cm^{-3}), $\rho_{membrane}$ is the density of dry membranes. The density of the membranes in the hydroxide form was measured by a buoyancy method.[2]

3.4.6 Titrated Gravimetric IEC Measuring.

To calculate the titrated gravimetric IEC values, membranes in the OH^- form were immersed in 50 mL of 0.01 M HCl standard solution for 24 h. Then, the solutions were titrated with a standardized NaOH (0.01 M) solution to pH = 7. Subsequently, the samples were washed and immersed in deionized water for 24 h to remove the residual HCl, and then dried under vacuum at 50 °C overnight and weighed to calculate the dry masses in the Cl^- form. The IEC of the membranes was calculated via eq 3:

$$IEC = \left(\frac{n_{i(H^+)} - n_{f(H^+)}}{m_{dry(Cl)}} \right) \quad (3)$$

where $m_{dry(Cl)}$ is the mass of dry membranes, $n_{i(H^+)}$ is the initial amount of H^+ in the HCl solution, $n_{f(H^+)}$ is the final amount of H^+ in the HCl solution.

3.4.6 Calculation of the Diffusion Coefficient (D) and Dilute Ion Diffusivity (D_0)

For the membranes, the diffusion coefficients of the mobile ions were calculated from a form of the Nernst-Einstein equation:

$$D = \frac{\sigma \cdot R \cdot T}{c \cdot z^2 \cdot F^2} \quad (4)$$

in which, σ is the measured conductivity, R is the ideal gas constant, T is the absolute temperature (K), c is the concentration of ions in moles per cm^3 calculated by eq. 4, z is valence charge, and F is Faraday's constant.[3] The ion concentration, c, for the membranes was calculated from the volume-based water uptake using:

$$c = 0.001 \cdot \frac{\rho \cdot IEC}{1 + 0.01 X_{v\text{-}H_2O}} \quad (5)$$

where ρ is the polymer density, IEC is the milliequivalents of ion per gram polymer, and $X_{v\,H_2O}$ is the volume-based water uptake.[4]

The dilute ion diffusivity can be calculated from the dilute solution mobilities of the mobile ion using the following equation:

$$D_0 = \frac{\mu \cdot k_B \cdot T}{q} \quad (6)$$

in which k_B is the Boltzmann constant, T is the absolute temperature (K), μ is the dilute solution ion mobility, and q is the ion charge.[5] The dilute solution mobility of bicarbonate ions, chloride ions, and hydroxide ions are 46.4×10^{-5} $cm^2 \cdot V^{-1} \cdot s^{-1}$, 76.3 × 10-5 $cm^2 \cdot V^{-1} \cdot s^{-1}$, and 197.6×10^{-5} $cm^2 \cdot V^{-1} \cdot s^{-1}$, respectively.[6,7]

3.4.7 Mechanical Property Measurements

Tensile measurements were obtained for samples equilibrated in liquid water and ambient air at room temperature. The hydrated membranes were cut into a dumbbell shape (12 mm × 3

mm in the test area), and tensile measurements were performed using an Instron-5866 (Norwood, MA) instrument at a crosshead speed of 5 mm/min at room temperature (25 °C).

3.4.8 Morphological Characterization of the AEMs

Small-angle X-ray scattering curves of unstained dry bromide counterion form membranes were obtained using a Rigaku instrument equipped with a pinhole camera with an Osmic microfocus Cu Kα source and a parallel beam optic. Typical counting times for integration over a multiwire area detector were 45 minutes with typical membrane thicknesses of approximately 100 μm. Measurements were taken under vacuum at room temperature on dry samples. Scattering intensities were normalized for background scattering and beam transmission.

Cast membrane samples were cross-sectioned at -120 °C using a LeicaUltracut UC6 ultramicrotome with an EMFC6 cryo attachment. The sections were supported on carbon/Formvar-coated grids. Transmission electron images were collected on a JEOL JEM 1200 EXII microscope equipped with a tungsten emitter operating at 80 kV. Images were captured on unstained samples recorded on a CCD camera using TCL software.

3.4.9 FTIR Spectra

FTIR spectra were obtained using a Bruker Vertex 70 FTIR spectrometer (Bruker, Billerica, MA) equipped with deuterated triglyceride sulphate (DTGS) detector. ATR measurements were carried out on membranes on a MVP-Pro ATR accessory (Harrick Scientific Products, Inc. NY) with a diamond ATR crystal at a 45° incidence angle. Transmission spectra were collected on KBr pellets prepared by mixing 2.5 mg of polymer with 60 mg of anhydrous KBr (Sigma-Adrich,). The spectra were signal averaged over 100 scans at 4 cm^{-1} resolution with

a 5 mm aperture size and a nitrogen purge at ambient temperature. All spectra were processed using Bruker OPUS 6.5 software.

3.4.10 Gel Fraction for Cross-linked AEMs

After cross-linking, the membranes remained insoluble in all common solvents and gel fraction was used to obtain information on the completeness of the cross-linking reaction. The gel fraction of the cross-linked membranes was calculated from the ratio of the weight of the 2 g polymer after extraction with 50 mL NMP at 80 °C for 1 day and the initial weight of the sample.

3.4.11 Membrane-Electrode Assembly Fabrication and Fuel Cell testing.

Pt/C (60%, Johnson Matthey Co.) was mixed with corresponding ionomer solution, and sprayed onto both sides of the membrane (60 ± 5 μm in thickness), respectively, to prepare the catalyst-coated membranes (CCMs) with the same material in the membrane and in the electrode. The weight percentage of ionomer in both the anode and the cathode was calculated to be 20 wt %. The Pt loading in both anode and cathode was 0.4 mg/cm^2, and the area of the electrodes was 4 cm^2. The resulting CCMs were pressed between two pieces of carbon cloth (CeTech W1S1005) to form the membrane electrode assembly (MEA). The H_2-O_2 fuel cell performance of the MEAs was measured under a galvanic mode using fully humidified H_2 and O_2 gases flowing at a rate of 250 mL/min and at temperature of 60 °C with 0.1 MPa back pressure (850e Multi Range, Scribner Associates Co.).

3.5 References

(1) Fujimoto, C. H.; Hickner, M. A.; Cornelius, C. J.; Loy, D. A. *Macromolecules* **2005**, *38*, 5010.

(2) Xie, W.; Ju, H.; Geise, G. M.; Freeman, B. D.; Mardel, J. I.; Hill, A. J.; McGrath, J. E. *Macromolecules* **2011**, *44*, 4428.

(3) Walls, H. J.; Fedkiw, P. S.; Zawodzinski, T. A.; Khan, S. A. *J. Electrochem. Soc.* **2003**, *150*, E165.

(4) Kim, Y.; Einsla, B.; Sankir, M.; Harrison, W.; Pivovar, B. *Polymer*. **2006**, *47*, 4026.

(5) Muthukumar, M. In *Advances in Chemical Physics*; Rice, S. A., Ed.; 2005; Vol. 131, p. 45.

(6) Voet, D.; Voet, J. G. *Biochemistry*; Fourth.; John Wiley & Sons, 2011; p. 45.

(7) Vanysek, P. In *CRC Handbook of Chemistry and Physics*; Lide, D. R., Ed.; CRC Press: Boca Raton, 2002.

Chapter 4

Cross-linking of Comb-Shaped Polymer Anion Exchange Membranes via Thiol-ene Click Chemistry

This chapter is adapted from the manuscript Zhu, L.; Zimudzi, T. J.; Li, N.; Pan, J.; Lin, B.; Hickner, M. A. published in Polymer Chemistry, DOI: 10.1039/C5PY01911G.

4.1 Introduction

The performance of AEMFCs is extremely dependent on certain key requirements of the polymer membrane materials: high ion conductivity (> 100 mS/cm), dimensional durability, and chemical stability. Higher charge carrier densities in AEMs for fuel cells are required because of the lower mobility of hydroxide ions compared to protons. In order to achieve sufficient ion conductivity for AEM applications, high ion-exchange capacities (IEC) are essential for anion exchange membranes. However, increasing the IEC value is usually accompanied by high water uptake, leading to severe dimensional swelling, or even dissolution.[1,2] This trade-off between dimensional stability and ion conductivity creates a need for methods to enhance dimensional stability without compromising ion conductivity.[3] Cross-linking has been reported as an effective method to enhance the dimensional stability of the membrane and to increase the fuel resistance crossover in the preparation of AEMs.[3-18] Several methods have been employed to fabricate cross-linked AEMs. One method is cross-linking via quaternization by diamines, such as N,N,N',N'-tetramethylhexanediamine.[18] When halomethylated polymers were quaternized with alkyldiamines, AEMs with enhanced dimensional integrities, alkaline stabilities, and acceptable hydroxide ion

conductivities were achieved.[5,10,11,15,16,18] However, cross-linking through quaternization results in a significant reduction in hydroxide ion conductivity due to the introduction of alkyl chains into the ionic domains and reduced water swelling of the material.[5,10,11,15,16,18] Another approach is to introduce a cationic monomer into a network structure. For example, Zha,[19] *et al.* reported norbornenes with attached ruthenium cations to prepare cross-linked AEMs using ring opening metathesis polymerization (ROMP) and dicyclopentadiene (28.6 mS/cm in hydroxide form, at 30 °C). Robertson,[20] *et al*. developed a new cross-linked AEM using cyclooctene cross-linker with quaternary ammonium groups, which showed good mechanical strength and high ion conductivities (111 mS/cm in hydroxide form at 50 °C). Previously, PPO and poly(styrene)-based AEMs have been crosslinked using metathesis of pendant side chain double bonds.[8] While this strategy was effective at producing highly cross-linked material at room temperature, some residual catalyst could remain in the membranes, which is not ideal for application in fuel cells. [8] Additionally, in all of these strategies, the cross-linking of the material occurs as the membrane is cast from solution. Therefore, control of the cross-linking reactions can be difficult and therefore an on-demand cross-linking strategy, such as shown in this work using UV light, may be desirable.

In our previous report, we designed comb-shaped polymers based on poly(2,6-dimethyl-1,4-phenylene oxide) backbones with different lengths of pendant alkyl side chains.[21] These kinds of polymers showed good ion conductivity under alkaline conditions.[21,22] However, due to the increase of ion exchange capacity (IEC), we were unable to obtain membranes with a degree of functionalization (DF) greater than 70 (70 mol % of the polymer repeat units functionalized) in the pursuit of high-conductivity materials. In order to further enhance ion conductivity, increase dimensional stability, and decrease fuel crossover (such as methanol) in the preparation of new AEMs, we here employ a

covalent cross-linking strategy to stabilize comb-shaped AEMs via thiol-ene cross-linking. We introduced side chains with double bonds and used dithiols under UV illumination to accomplish the cross-linking reaction. The advantages of using the thiol-ene click reaction as a strategy for cross-linking are its robustness and efficiency without yielding any harmful byproducts or residue that must be removed from the membrane after the cross-linking reaction has occurred.[23] Also, UV-initiated thiol-ene chemistry was shown to proceed quantitatively with a high degree of specificity within a short time.[23]

4.2 Experimental Section

Materials. Poly(2,6-dimethyl-1,4-phenylene oxide) was purchased from Sigma-Aldrich and dried under vacuum at room temperature overnight. *N*,*N*-Dimethylhexylamine, *N*,*N*-dimethyldecylamine, *N*,*N*-dimethylhexadecylamine, *N*-bromosuccinimide, 1,8-octanedithiol, and 2,2′-azobis(2-methylpropionitrile) were purchased from Sigma-Aldrich and used as received. The brominated PPO polymers with different degrees of bromination (DB) ranging from 60 to 80% were synthesized according to the reported literature.[24]

Synthesis of *N*,*N*-dimethyl-10-undecen-1-amine.[8] 20 mL 11-Bromo-1-undecene was mixed with 200 mL toluene, and 100 mL THF/dimethylamine solution (50 wt % dimethylamine). The resulting mixture was stirred at 60 °C for 2 days. Subsequently, the solution was extracted with satd. $NaHCO_3$ soln. (3 × 60 mL) and distilled water (3 × 60 mL) sequentially. The resulting organic layer was dried with sodium sulfate, filtered, and concentrated by evaporation of the solvent under vacuum.

Finally, the obtained colorless liquid was dried in vacuum at room temperature overnight with a yield of 87 % (mass).

Polymer synthesis. Brominated PPO with a DB of 0.6 (1.7g, 10 mmol) was dissolved in 10 mL of *N*-methyl-pyrrolidone (NMP). Then, *N*,*N*-dimethyl-10-undecen-1-amine (0.6 g, 3.0 mmol) was added slowly. The mixture was stirred for 48 h at room temperature. Subsequently, *N*,*N*-dimethylhexylamine (0.46 g, 3.6 mmol) was added, and the mixture was stirred for another 24 h at room temperature. The solution obtained was poured into 200 mL toluene or hexane to precipitate the polymer. The product was filtered and further washed with hexane and toluene several times. A light yellow powder was obtained and dried under vacuum overnight at room temperature. The resulting product was cross-linkable comb-shaped PPO (X60Y30C6, where the X60 denotes a polymer with 60 mol % DB (total number of PPO repeat units brominated), the Y30 stands for the mol % of cross-linkable alkene groups (out of the total DB of 60 mol %) attached to main chain, and the C6 stands for the length of the alkyl chain) with a yield of 93% (mass) in the bromide form. So, the X60Y30C6 polymer has 30 mol % cross-linking and 30 mol % C6 alkyl amine attachment that remains uncross-linked.

Fabrication of membranes. The X60Y30C6 comb-shaped polymer (0.3 g) in the bromide form was dissolved in NMP (5 mL) to form a 5 wt % solution. Subsequently, 1,8-octanedithiol (45 mg, 0.24 mmol) was added to the polymer solution. The mixture was stirred for several minutes at room temperature. Then, 2-benzyl-2-(dimethylamino)-4*'*-morpholinobutyrophenone (photoinitiator, 30 mg) was added to the mixture. The solution was then cast onto a leveled glass plate, and exposed to UV light (365 nm) for 10 min. The solution was dried at 82 °C under ambient pressure for 24 h followed by vacuum drying for another 24 h at 80 °C to give a thick, transparent, tough film.

4.3 Results and Discussion

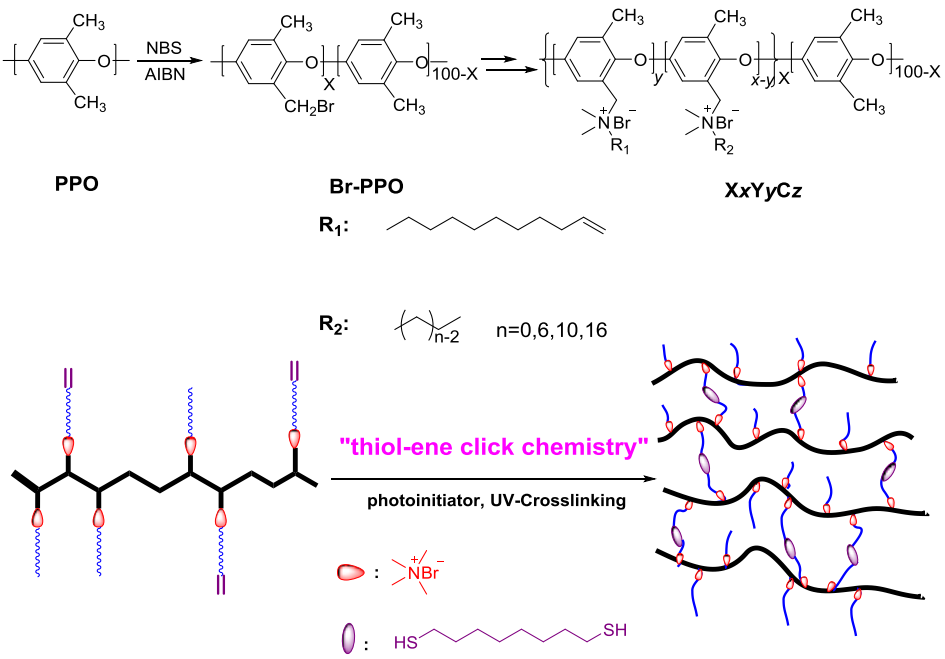

Scheme 4.1 Synthesis of cross-linked comb-shaped AEMs, X*x*Y*y*C*z*, with one alkyl side chain using thiol-ene click chemistry.

***N,N*-dimethyl-10-undecen-1-amine and comb-shaped copolymers synthesis.** The cross-linking reagent *N,N*-dimethyl-10-undecen-1-amine was successfully synthesized from 11-bromo-1-undecene and dimethylamine according to a previous procedure.[8] The chemical structure of this unsaturated dimethyl alkyl amine was confirmed by ^{1}H NMR spectroscopy and shown in Figure 4.1 Br-PPO possessing different degrees of bromination (DB) at the benzyl position were synthesized using *N*-bromosuccinimide and 2, 2*'*-azobis(2-methylpropionitrile) in a refluxing chlorobenzene solution for 3 h according to our previous reports.[8] By altering the usage of *N*-bromosuccinimide and 2, 2*'*-azobis(2-methylpropionitrile), Br-PPOs with DB ranging from 60 to 80 were prepared. Then, a series of cross-linkable comb-shaped ionomers (X*x*Y*y*C*z*) with different side chain length were achieved by the Menshutkin reaction of the olefinic amine with the bromo group of Br-PPO as shown in Scheme 4.1 (where the *x* stands for DB of PPO; *y* refers to the mol % of cross-linkable alkene

groups, *z* indicates side-chain length). The DB of Br-PPO was set at 60 and 80 to obtain samples with calculated IEC_ws ranging from 1.80 to 2.55 mmol/g (Table 4.1). The chemical structures of cross-linkable comb-shaped X80Y*y*C6 cationic copolymers in bromide form were confirmed by ^{1}H NMR spectroscopy.

Table 4.1 Ion exchange capacity, water uptake, swelling and conducting behaviors of cross-linked AEMs.

sample	IEC (mmol/g)[a]	IEC (mmol/g)[b]	WU (%) (OH^-) [d]	WU (%) (HCO_3^-) [c]	WU (%) (Cl^-) [c]	σ (OH^-) [c]	σ (HCO_3^-) [c]	σ (Cl^-) [c]	λ (OH^-)	Swelling ratio (%)[c]	Gel fraction (%)
X60Y15C6	2.51	2.25	90 ± 6	47 ± 3	31 ± 2	33 ± 3	5.3 ± 0.3	8.9 ± 0.4	22.4	23.3 ± 1.4	83
X60Y30C6	2.38	2.06	67 ± 5	41 ± 2	22 ± 2	26 ± 3	4.2 ± 0.2	6.7 ± 0.5	18.2	15.2 ± 0.9	87
X60Y60	2.10	1.83	43 ± 4	34 ± 2	15 ± 3	22 ± 2	3.2 ± 0.2	4.2 ± 0.2	13.5	10.6 ± 0.7	89
X60Y30C10	2.26	2.03	58 ± 5	39 ± 3	21 ± 2	22 ± 2	4.1 ± 0.2	5.4 ± 0.3	16.6	14.5 ± 0.7	89
X60Y30C16	2.07	1.80	46 ± 2	33 ± 2	18 ± 2	17 ± 1	3.3 ± 0.2	4.9 ± 0.2	14.2	13.2± 0.8	90
X80Y20C6	2.94	2.55	193 ± 4	56 ± 3	43 ± 4	60 ± 5	12.2 ±1.1	14.9 ± 1.2	42.5	40.7 ± 3.3	87
X80Y40C6	2.63	2.35	144 ± 4	43 ± 3	30 ± 3	44 ± 2	8.4 ± 0.7	10.9 ± 0.5	34.9	25.0 ± 2.0	92
X80Y80	2.39	2.17	76 ± 3	24 ± 3	13 ± 2	23 ± 3	3.8 ± 0.3	5.8 ± 0.3	21.8	13.3 ± 0.8	95
X80Y40C10	2.52	2.20	49 ± 3	31 ± 3	20 ± 1	21 ± 3	5.1 ± 0.3	7.6 ± 0.4	12.7	15.4 ± 1.1	95
X80Y40C16	2.41	2.08	26 ± 1	20 ± 2	12 ± 1	18 ± 2	3.4 ± 0.2	4.8 ± 0.3	7.3	9.5 ± 0.6	96

[a]Calculated from the polymer composition and the degree of bromination. [b]Titrated values. [c]The membranes in OH^- form were used for measurements of the swelling ratio at room temperature in water.

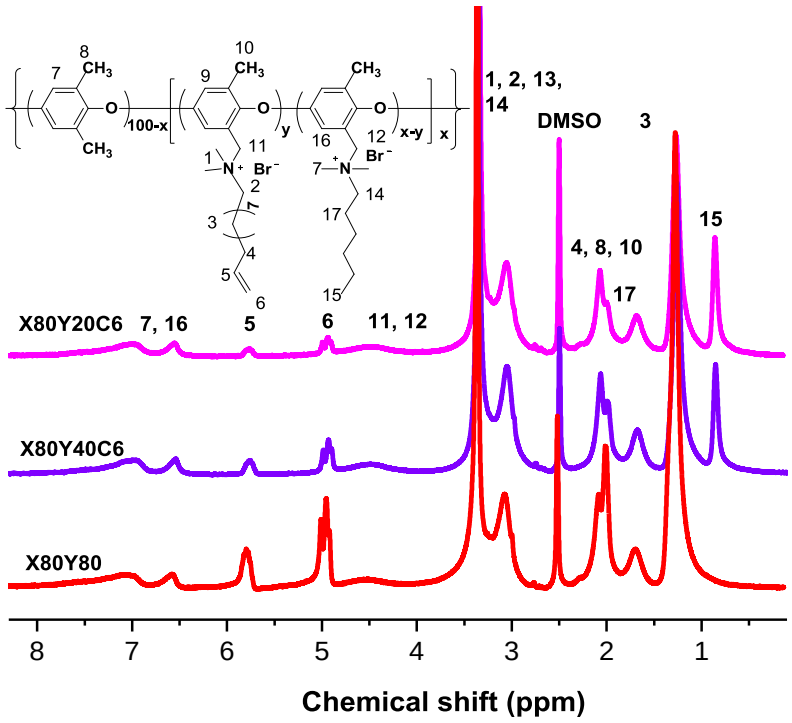

Figure 4.1 ^{1}H NMR of crosslinkable comb-shaped X80Y*y* in bromine salt form in DMSO-d_6.

As is shown in Figure 4.1, the disappearance of the proton resonance arising from the bromobenzyl moiety as a sharp peak at 4.3 ppm along with the appearance of new peaks at 0.5-1.8 ppm and 3.0 ppm assigned to alkyl chains indicated that the quaternary ammonium groups were formed. Probably, due to the deshielding effect of the quaternary ammonium groups, a broad resonance from 4.3 to 4.5 ppm was detected, which could be assigned to benzylic protons (H11, H12 in Figure 1).[8] The appearance of peaks 5 and 6 in Figure 1 indicated the presence of end alkene groups in the copolymers. Also, the intensity of peaks 5 and 6 increased as the number of cross-linkable alkyne groups was increased. The integral ratio of alkyne protons, H5 and H6 at 5.8, 5.1 ppm to aromatic peaks at 6.6-7.1 ppm indicated the quaternization reaction was

quantitative. The IEC_w of the cross-linkable comb-shaped X80Y*y*C6 membranes calculated from the integrals ratios were consistent with the theoretical values, further suggesting the complete and reliable quaternization of the bromomethyl groups.

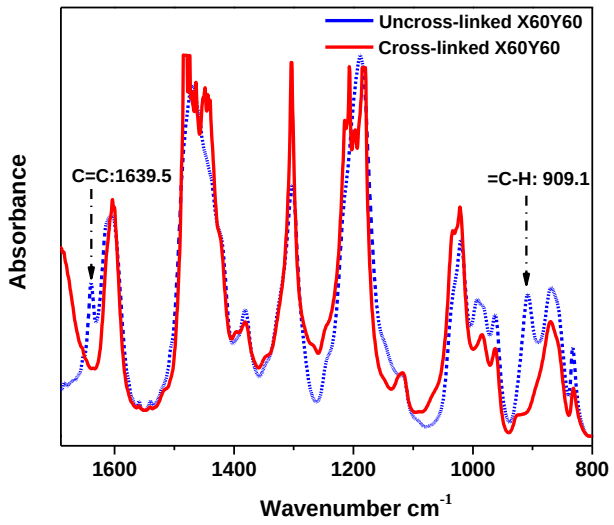

Figure 4.2 FTIR spectra of uncross-linked and cross-linked membranes.

FTIR was used to confirm the reaction of the alkene double bonds with the thiols to form the cross-linked network. As shown in Figure 4.2, there was a distinct *v* (C=C) peak at 1639 cm^{-1} for the uncross-linked X60Y60 membrane, which disappeared after cross-linking along with the v (=C-H) peak at 909 cm^{-1}.[25] Considering all the evidence and results, a strong covalent cross-linking network was formed by the thiol-ene click cross-linking reaction which was further confirmed by the gel fraction (>80%) in NMP, Table 4.1. In order to test the reliability and stability of UV-initiated thiol-ene cross-linking method, each experimental condition was repeated three times to prepare three membrane samples, suggesting UV cross-linking was a reliable strategy for cross-linking these copolymers.

Swelling behavior. To demonstrate the effect of the degree of cross-linking (DC) on the swelling behavior of the AEM samples, we compared the water uptakes and swelling ratios of X60Y*y*C6 and X80Y*y*C6 membranes with different degrees of cross-linking (DC).

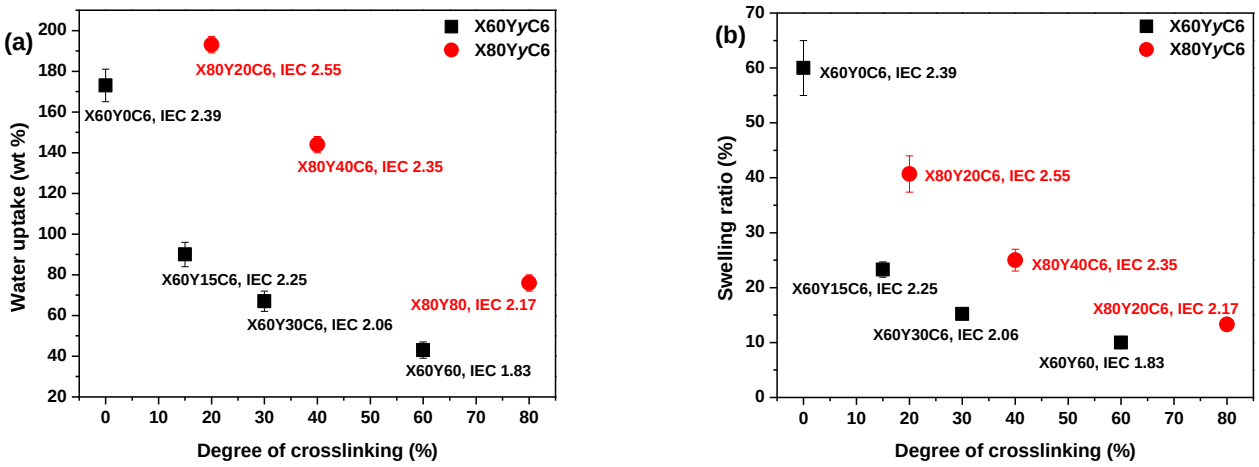

Figure 4.3 Liquid water uptake (a) and swelling ratio (b) of membranes in OH^- form as a function of degree of cross-linking at room temperature.

As shown in Figure 4.3, the thiol-ene cross-linking drastically lowered the water uptake and thus the swelling ratio. Specifically, the cross-linked X80Y40C6 membrane had a water uptake of 144 % and swelling ratio of 25 % at room temperature while the uncross-linked X80Y0C6 sample could be dissolved in water. In addition, the water uptake and swelling ratio of the samples generally decreased with increasing DCs. For example, X60Y15C6 and X60Y60 water uptakes were 90 wt % and 43 wt %, and the swelling ratios were 23 % and 10 % at room temperature, respectively. In contrast, the uncross-linked X60Y0C6 showed showed greater water uptake (173 wt %) and swelling ratio (60 wt %) compared to either of the cross-linked samples.

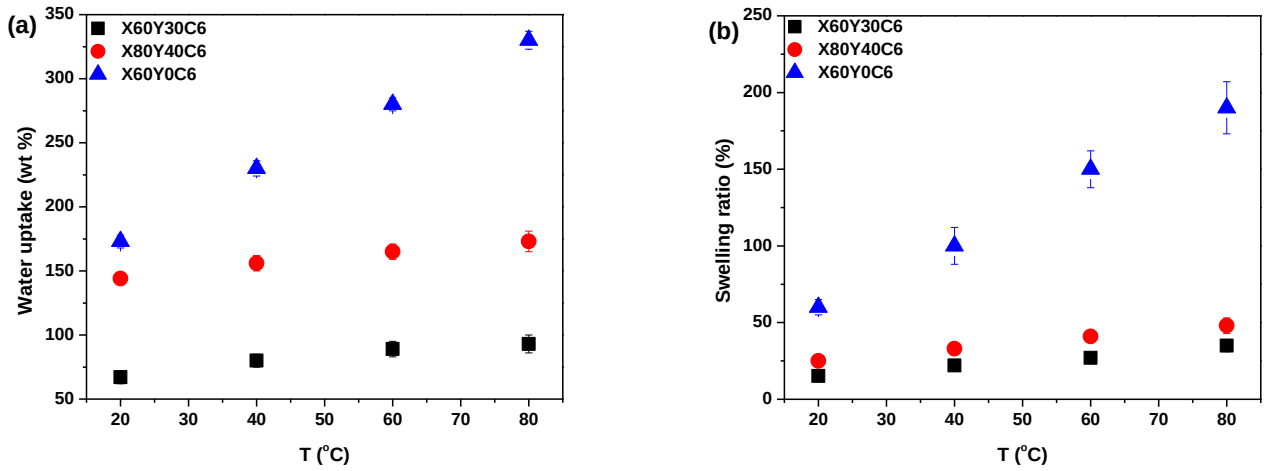

Figure 4.4 Liquid water uptake (a) and swelling ratio (b) of membranes in OH^- form as a function of temperature.

Figure 4.4 compares the swelling behaviors at elevated temperatures of membranes with different DCs. Although the water uptakes and swelling ratios for all the samples increased with elevated temperatures, increasing the DCs significantly enhanced the dimensional stability of the AEMs. For X60Y30C6 and X80Y40C6, the water uptakes were 67 wt % and 144 wt %, and the swelling ratios were 15 % and 25 % at room temperature, respectively. When the temperature was increased to 80 °C, the water uptake of the samples increased to 93 wt % and 173 wt %, and their swelling ratios went up to 35 % and 48 %, respectively. In comparison, large increases of water uptake and swelling ratio were observed for the uncross-linked X60Y0C6 sample when the temperature was increased from 20 to 80 °C (increases of 157 % for water uptake increment and 130 % for swelling ratio increment). Considering the remarkable agreement between the high solvent resistance and low swelling ratio, a strong covalent cross-linking network was likely formed by the thiol-ene cross-linking.

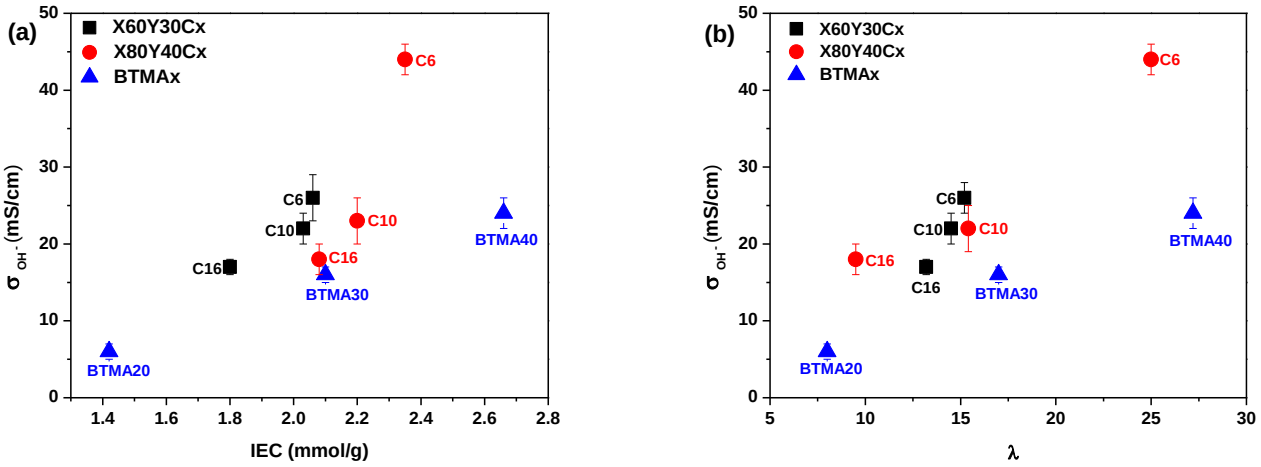

Figure 4.5 Hydroxide conductivity of cross-linked and BTMA membranes as a function of (a) IEC (ion exchange capacity) and (b) hydration number λ.

In addition, it was shown in Figure 4.5 that longer alkyl side chain restricted the water absorption of AEMs, resulting in lower ion conductivity.[21]

Ionic conductivity. High ionic conductivity is one of the most important properties for the application of AEMs in devices.

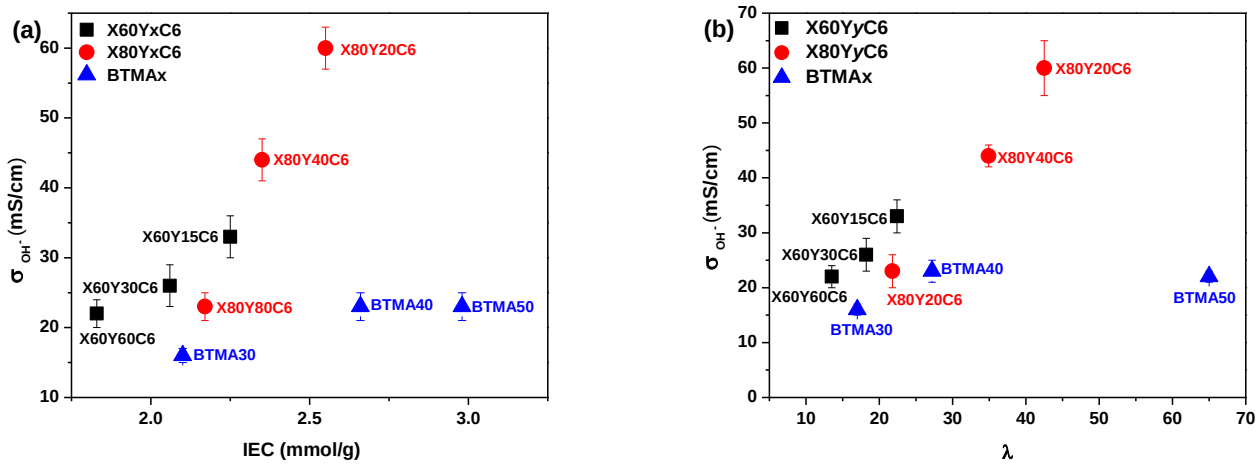

Figure 4.6 Hydroxide conductivity of membranes as a function of (a) IEC (ion exchange capacity) and (b) hydration number λ (moles of water per mole of quaternary ammonium group) in water at room temperature. Conductivities were measured with samples exposed to liquid water.

Shown in Figure 4.6a, the hydroxide conductivity of the cross-linked membranes increased with increasing IEC because of the increase in the water content. When comparing the hydroxide conductivity of the cross-linked and BTMA (benzyltrimethyl ammonium) membranes, the cross-linked membranes demonstrated much higher hydroxide conductivity under the same conditions. For example, the X80Y20C6 membrane with IEC= 2.65 mmol/g showed a conductivity of 60 mS/cm, which was almost three times higher than that of the BTMA40 membrane (23 mS/cm) with an IEC of 2.66 mmol/g. It should also be pointed out that the cross-linked membranes showed much larger hydroxide conductivity than the BTMA*x* membranes under a given hydration number (λ), Figure 4.6b.

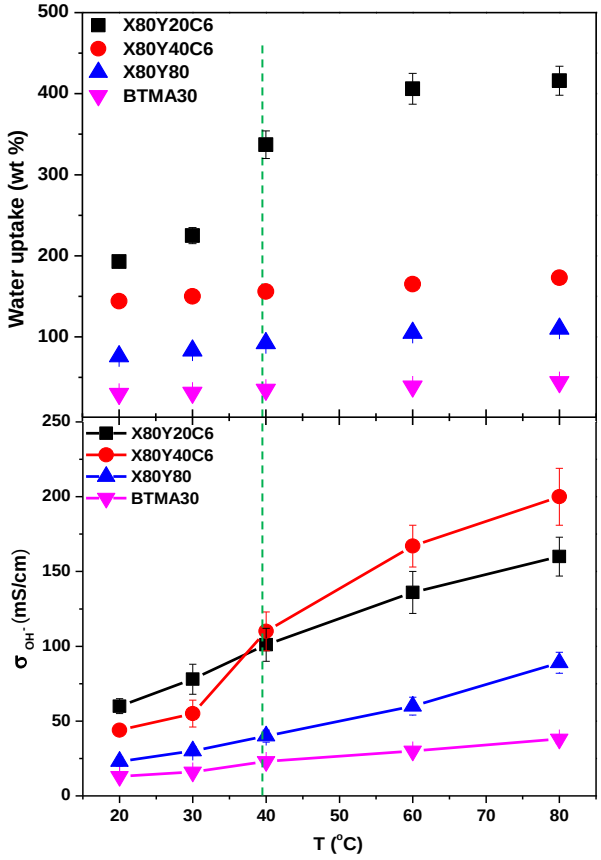

Figure 4.7 Hydroxide conductivity of X80Y*x*C6 and BTMA30 membranes as a function of temperature. Conductivities were measured with samples exposed to liquid water.

The hydroxide conductivity of the X60Y*x*C6 and BTMA30 membranes as a function of temperature is shown in Figure 4.7. The hydroxide conductivity steadily increased with increasing temperature and displayed values of 89-200 mS/cm for X80Y*x*C6 membranes at 80 °C, which are greater than the previous reported values. [3-12, 26, 27] For example, Yan,[28] *et al.* reported SCL-TPQPOH with an IEC = 1.23 mmol/g exhibiting hydroxide conductivity of 32.7 mS/cm in water at room temperature. The cross-linked PP-AEMs synthesized by Zhang,[5] *et al.* exhibited hydroxide conductivity of 56.5 mS/cm in deionized water at 80 °C. The cross-linked,

epoxy-based AEMs reported by Kohl,[12] *et al*. exhibited hydroxide conductivity of 14 mS/cm and 78 mS/cm at 30 and 80 °C, respectively. The X80Y40C6 sample exhibited the highest OH^- conductivity (200 mS/cm) at 80 °C, which was nearly six times greater than that of BTMA30 under the same conditions. The X80Y40C6 membranes exhibited the highest hydroxide conductivity above 40 °C due to a trade-off between water uptake, ionic content and conductivity and did not swell greatly like the less cross-linked X80Y20C6 membranes that showed promising conductivity at lower temperatures.

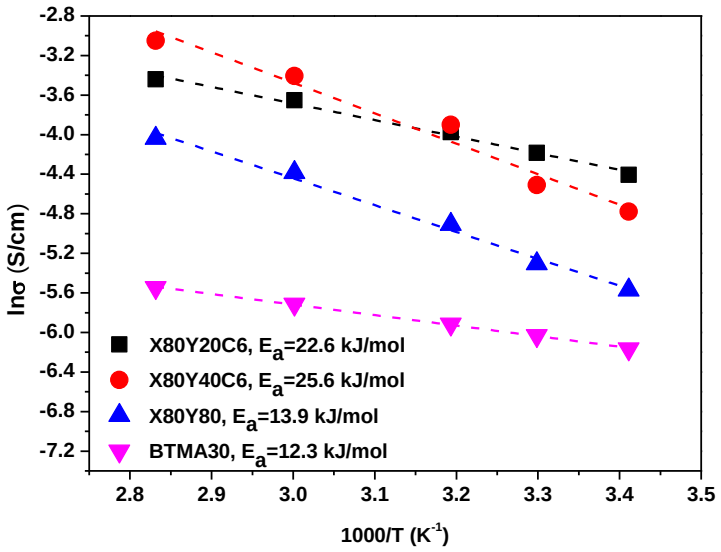

Figure 4.8 Bicarbonate conductivity of AEMs as a function of temperature and the computed Arrhenius activation energies.

As shown in Figure 4.8, the HCO_3^- conductivities of the membranes showed an approximate Arrhenius-type temperature dependence promoted by the thermal activation of water motion.[29] The apparent activation energy estimated from the slopes of the ln(σ) vs 1000/T curves was ~ 12.2 - 22.5 kJ/mol across the measured samples. The apparent activation energies of the tested membranes was comparable to or somewhat lower than those of other reported AEMs (10-

23 kJ/mol), indicating that these membranes have a water-facilitated OH^- conduction mechanism similar to other hydrated AEMs.[29]

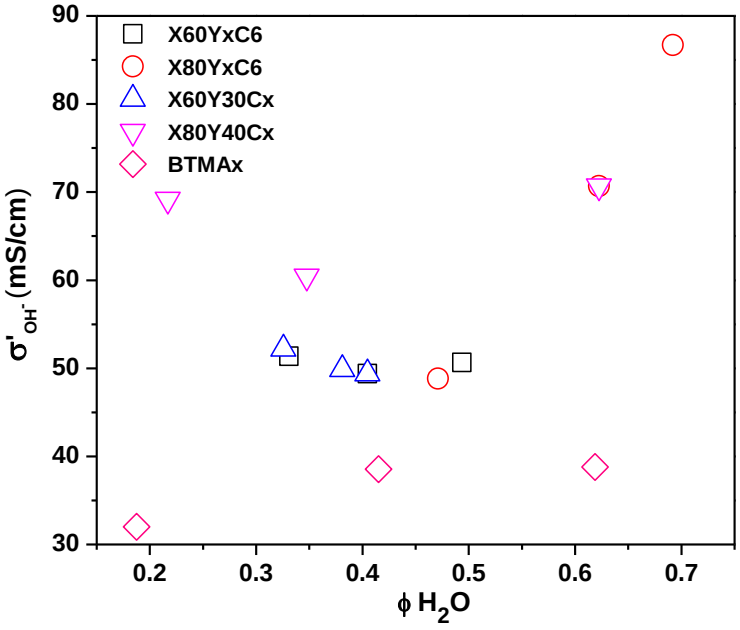

Figure 4.9 Water volume fraction dependence of the effective hydroxide conductivity in the water channels (σ') in water at room temperature.

After normalizing the samples' hydroxide conductivity on the basis of water volume fraction, the effective hydroxide conductivity in the water channels, σ', which demonstrates efficiency of the water molecules inside the membranes for transport of hydroxide ions was obtained.[21] All of the cross-linked membranes showed higher σ' than the corresponding BTMA*x* samples, as shown in Figure 4.9. These results indicated that the well-developed micro-phase separation of the cross-linked samples, as discussed in the next section, could efficiently enhance the transport of hydroxide ions.

Morphological characterization. More efficient ion transport in anion exchange membranes usually results from better OH^- transport pathways as the material is hydrated. Generally, for the different AEMs with similar IECs and water uptakes, it is desirable to develop ionic domain aggregation, which ensures ionic channels for transport. To investigate the microphase separated morphologies of the materials in this study, small-angle x-ray scattering (SAXS) was used to investigate the X60Y60, X60Y30C6, and uncross-linked X60Y60 samples.

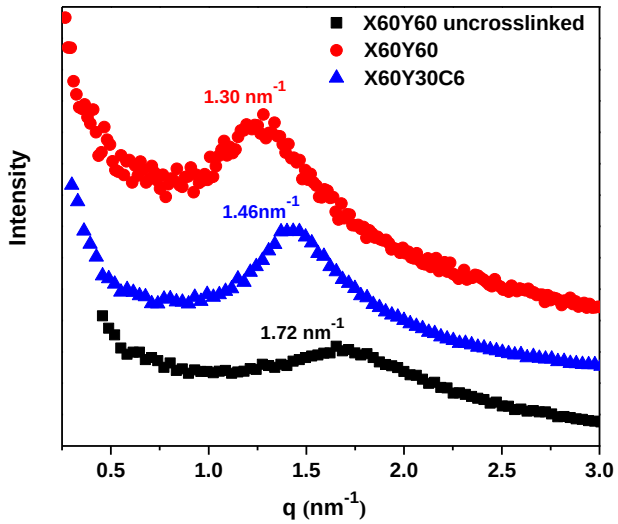

Figure 4.10 SAXS profiles of dry polymer membranes in the bromide form.

SAXS profiles, Figure 4.10, revealed clear peaks for all samples. These results were indicative of nanophase separation between the polar PPO backbone with attached ionic groups and the hydrophobic alkyl side chains. The lack of a second order scattering peak for all the cross-linked membranes demonstrated that no long range ordered structures were formed in these membranes, but only locally correlated arrangement of phase separated domains existed in these samples. Generally, the characteristic separation length or interdomain spacing, d, between the ion-rich domains in ionomers can be calculated by the values of q_{max} through the equation d =

$2\pi/q_{max}$. The corresponding interdomain spacing values fall into the range of 3.6 - 4.8 nm, which roughly corresponds to double the length of the extended aliphatic side chains.[21] As shown in Figure 4.10, the ionic domain peak of the highly cross-linked membrane X60Y60 shifted to lower q (higher d value) upon cross-linking likely indicating extension of the ionic domains with the addition of the cross-linking reagent.

In our previous report,[30] we developed a method for analyzing the mobility of ions in PEMs and AEMs via calculating the ion diffusion coefficients (D) which included information obtained from conductivity, ion concentration, and water uptake of the polymer membranes. For different ions, we determined the barrier to ion transport via the ratio of the diffusion coefficient to the dilute ion diffusivity (D/D_0), where D_0 is the maximum diffusivity of an ion in water.[31]

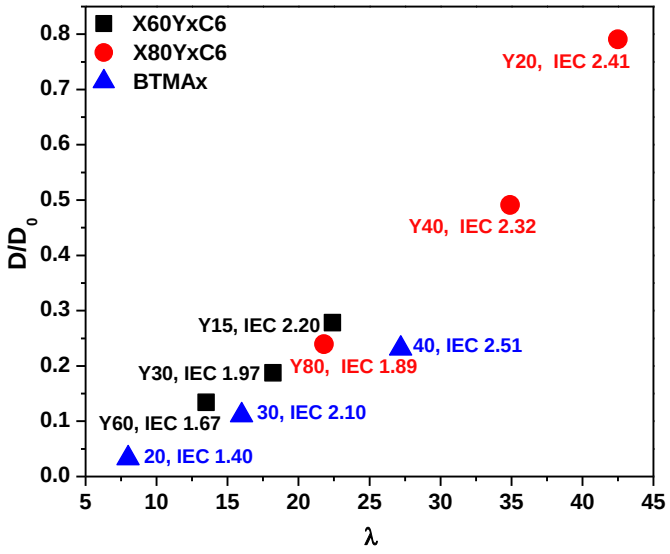

Figure 4.11 Ratio of the diffusion coefficient, D, to the dilute solution diffusivity, D_0, as a function of hydration number for membranes in the hydroxide form.

As shown in Figure 4.11, the D/D_0 ratio increased with increasing hydration for membranes in the hydroxide form, the highest D/D_0 ratio obtained was 0.79 at $\lambda = 43$ with IEC = 2.41 meq/g for the X80Y20C6 sample. The cross-linked membranes showed relatively higher D/D_0 values than the BTMA membranes at the same λ, suggesting more facile transport of hydroxide in the phase-separated systems as demonstrated by SAXS.

Membrane Stability. The long-term stability of AEMs is generally of concern due to known degradation pathways for tetraalkylammonium ions under alkaline conditions, such as β-hydrogen (Hofmann) elimination, direct nucleophilic substitution at the α-carbon, and benzyl attack.[32-36]

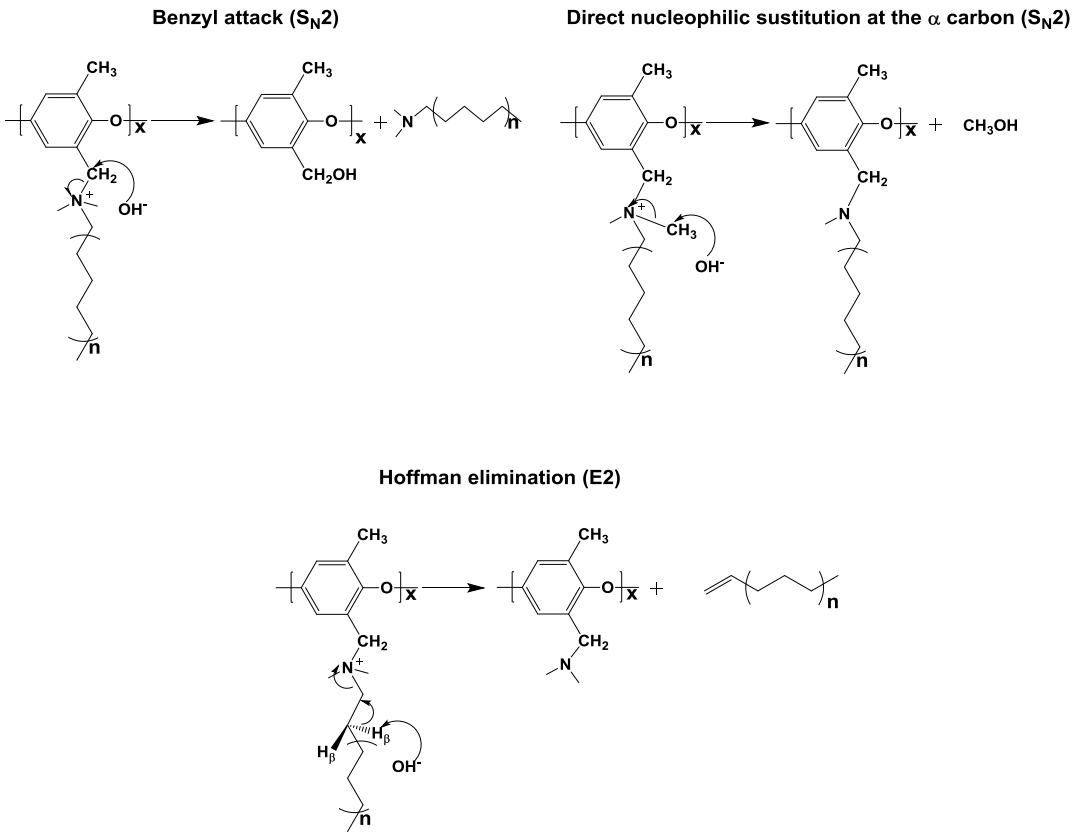

Scheme 4.2 Possible degradation pathways of the quaternary ammonium cations in the membranes.

The possible degradation mechanism of these membranes is shown in Scheme 4.2. The products of the different degradation pathways may help to unravel the most prominent degradation mechanisms of the materials. For example, the formation of an alkene accompanies Hofmann elimination while debenzylation results in the appearance of benzyl alcohol. While the signatures of degradation (such as the formation of a tertiary amine during debenzylation and demethylation) maybe convoluted, careful examination of the degradation byproducts will lead to better understanding of the most vulnerable sites for hydroxide attack on these materials and provide a basis for improvement of next-generation membranes.

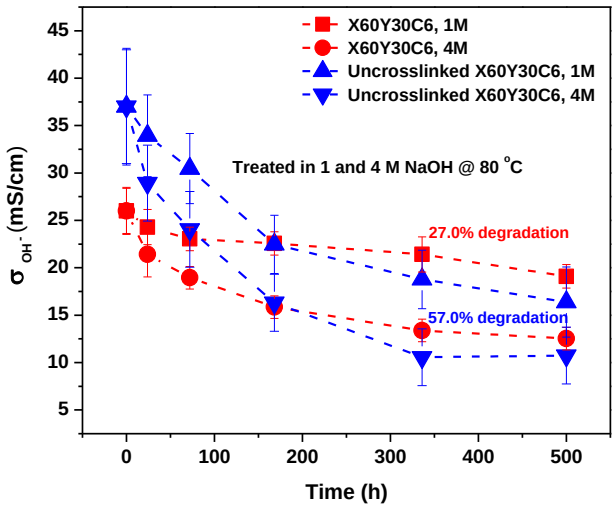

Figure 4.12 Chemical stability of the quaternary ammonium cation of X60Y30C6 and uncross-linked X60Y30C6 in 1 M and 4 M NaOH solution at 80 °C, and OH^- conductivity as a function of duration time measured at 20 °C.

To evaluate the long-term alkaline stability of the AEMs, X60Y30C6 and uncross-linked X60Y30C6 samples were immersed in argon-saturated 1 M NaOH solution at 80 °C for 500 hours, with replacement of the 1 M NaOH every 3 days during the testing period. Figure 4.12 illustrates the changes in OH^- conductivity during stability testing of the samples. During the 500

h test, X60Y30C6 exhibited significantly greater cation stability than that of uncross-linked X60Y30C6. The OH^- conductivity of X60Y30C6 decreased by 27.0 % and 52.0 %, in 1 M and 4 M NaOH solution, respectively. In contrast, the OH^- conductivity of uncross-linked X60Y30C6 film decreased by 57.0% and 73.1%, in 1 M and 4 M NaOH solution, respectively. Better stability of the cross-linked AEMs was demonstrated due to the cross-linking of alkyl side chains.[12]

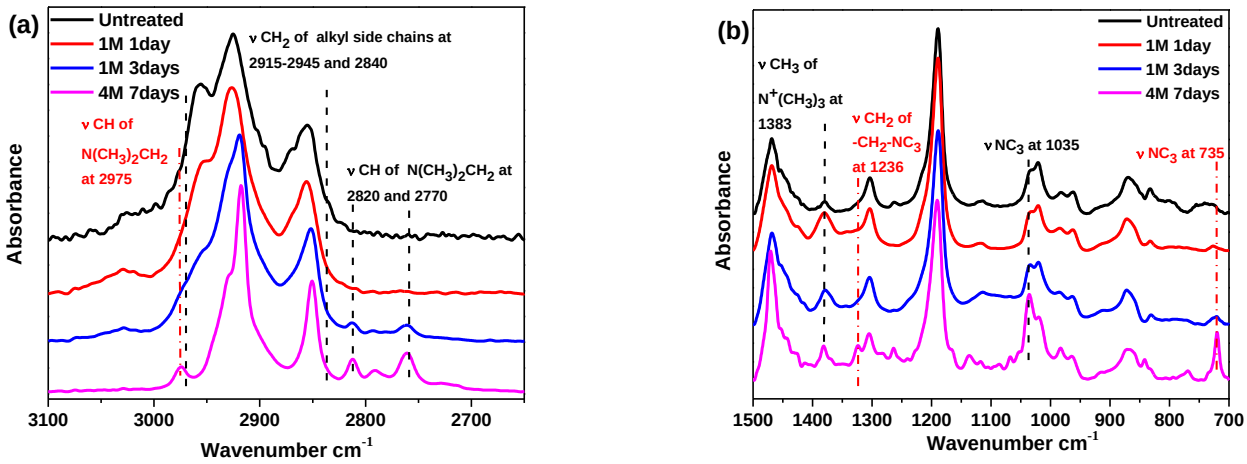

Figure 4.13 ATR spectra of treated X60Y15C6 membrane (a) ATR spectra of functional group region (b) fingerprint region.

In order to further study the degradation pathways and mechanism, ATR-FTIR spectroscopy was employed to characterize the membranes after being treated in 1 M sodium hydroxide at 80°C. As stated previously, in the AEMs, the major degradation pathways are benzyl attack, direct nucleophilic substitution at the α-carbon, or β-hydrogen (Hofmann) elimination.[32-36] Analysis of the ATR spectrum of membranes under degradation conditions provided a method to differentiate between the three mechanisms. Notably, the intensity ν (CH_2) peak of long alkyl side chains at 2915-2945 and 2840 cm^{-1} decreased as the degradation time

increased which was shown in Figure 4.13a, indicating that the β-hydrogen (Hofmann) elimination and/or benzyl attack occurred during the testing period.[37] The characteristic benzyl alcohol peaks between 3625 cm^{-1} and 3180 cm^{-1} were not readily evident in the spectra, indicating that benzyl attack may be a minor pathway in solid membranes, while the β-hydrogen (Hofmann) elimination is a major pathway for degradation. In addition, the new peaks in Figure 4.13a, assigned to ν (CH) of $(NCH_3)_2CH_2$ appeared at 2975, 2820 and 2770 cm^{-1}, demonstrating the formation of the NC_3 group.[38] This observation further confirmed the β-hydrogen (Hofmann) elimination could be the major pathway for degradation in membranes. As shown in Figure 4.13b, two new peaks assigned to ν (NC_3) at 735 and 1035 cm^{-1} became apparent in the fingerprint region for the degraded membranes.[38] In addition, another new peak assigned to ν (CH_2) of -CH_2-NC_3 appeared at 1236 cm^{-1} supporting the formation of the NC_3 group.[38] The intensity of the peak assigned to ν (CH_3) of $N^+(CH_3)_3$ at 1383 cm^{-1} weakened as the degradation time increased.[39,40] All the degradation information in the ATR-FTIR spectra demonstrated that β-hydrogen (Hofmann) elimination was a major pathway for degradation in these membranes.

4.4 Conclusions

In summary, we have designed and synthesized a new class of cross-linkable, comb-shaped copolymers for stable anion exchange membrane applications. The cross-linked comb-shaped membranes were achieved by thiol-ene click chemistry and the degree of cross-linking was readily controlled by tuning the amount of alkene-containing side chains pendant to the polymer backbone. The obtained cross-linked AEMs displayed a nanoscale phase-separated morphology, which was responsible for the higher ion conductivity of these materials compared to conventional BTMA AEMs. The cross-linking of the membranes enhanced both the chemical and dimensional stability of the membranes. After 500 h immersion in 1 M and 4 M NaOH at 80

°C, the cross-linked membranes maintained significantly higher hydroxide conductivity than those of uncross-linked AEMs. The ATR-FTIR spectra clearly demonstrated that the major degradation pathway of the quaternary ammonium functionalized poly(2,6-dimethyl-1,4-phenylene oxide)s under alkaline conditions was β-hydrogen (Hofmann) elimination. The combination of the good solubility of the precursor and the highly efficient thiol-ene click chemistry enables this cross-linking strategy as a promising technology for preparing attractive AEM materials for fuel cells applications.

4.5 References

(1) Varcoe, J. R.; Atanassov, P.; Dekel, D. R.; Herring, A. M.; Hickner, M. A.; Kohl, P. A.; Kucernak, A. R.; Mustain, W. E.; Nijmeijer, K.; Scott, K.; Xu, T.; Zhuang, L. *Energy Environ. Sci*. **2014**, 7, 3135.

(2) Pan, J.; Lu, S.; Li, Y.; Huang, A.; Zhuang, L.; Lu, J. *Adv. Funct. Mater.* **2009**, *19*, 1.

(3) Tsai, T. H.; Ertem, S. P.; Maes, A. M.; Seifert, S.; Herring, A. M.; Coughlin, E. B. *Macromolecules* **2015**, *48*, 655.

(4) Pan, J.; Zhu, L.; Han, J.; Hickner, M. A. *Chem. Mater.* **2015**, *27*, 6689.

(5) Zhang, M.; Liu, J.; Wang, Y.; An, L.; Guiver, M. D.; Li, N. *J. Mater. Chem. A* **2015**, *3*, 12284.

(6) Zhuo, Y. Z.; Lai, A. N.; Zhang, Q. G.; Zhu, A. M.; Ye, M. L.; Liu, Q. L. *J. Membr. Sci.* **2015**, *491*, 138.

(7) Lin, B.; Chu, F.; Ren, Y.; Jia, B.; Yuan, N.; Shang, H.; Feng, T.; Zhu, Y.; Ding, J. *J. Power Sources* **2014**, *266*, 186.

(8) Li, N.; Wang, L.; Hickner, M. A. *Chem. Commun.* **2014**, *50*, 4092.

(9) Lin, B.; Dong, H.; Li, Y.; Si, Z.; Gu, F.; Yan, F. *Chem. Mater.* **2013**, *25*, 1858.

(10) Lin, X.; Liu, Y.; Poynton, S. D.; Ong, A. L.; Varcoe, J. R.; Wu, L.; Li, Y.; Liang, X.; Li, Q.; Xu, T. *J. Power Sources* **2013**, *233*, 259.

(11) Zhao, Y.; Yu, H.; Yang, D.; Li, J.; Shao, Z.; Yi, B. *J. Power Sources* **2013**, *221*, 247.

(12) Zhou, J. F.; Unlu, M.; Anestis-Richard, I.; Kohl, P. A. *J. Membr. Sci.* **2010**, *350*, 286.

(13) Yang, C. C.; Chiu, S. J.; Chien, W. C.; Chiu, S. S. *J. Power Sources* **2010**, *195*, 2212.

(14) Lin, B.; Qiu, L.; Lu, J.; Yan, F. *Chem. Mater.* **2010**, *22*, 6718.

(15) Xiong, Y.; Fang, J.; Zeng, Q. H.; Liu, Q. L. *J. Membr. Sci.* **2008**, *311*, 319.

(16) Stoica, D.; Ogier, L.; Akrour, L.; Alloin, F.; Fauvarque,J. F. *Electrochim. Acta* **2007**, *53*, 1596.

(17) Wu, Y. H.; Wu, C. M.; Xu, T. W.; Yu F.; Fu, Y. X. *J. Membr. Sci.* **2008**, *321*, 299.

(18) Park, J. S.; Park, S. H.; Yim, S. D.; Yoon, Y. G.; Lee, W. Y.; Kim, C. S. *J. Power Sources* **2008**, *178*, 620.

(19) Zha, Y.; Disabb-Miller, M. L.; Johnson, Z. D.; Hickner, M. A.; Tew, G. N. *J. Am. Chem. Soc*. **2012**, 134, 4493.

(20) Robertson, N. J.; Kostalik IV, H. A.; Clark, T. J.; Mutolo, P. F.; Abruña, H. D.; Coates, G. W. *J. Am. Chem. Soc.* **2010**, *132*, 3400.

(21) Li, N. W.; Leng, Y. J.; Hickner, M. A.; Wang, C. Y. *J. Am. Chem. Soc*. **2013**, *135*, 10124.

(22) Amel, A.; Zhu, L.; Hickner, M.; Ein-Eli, Y. *J. Electrochem. Soc*. **2014**, *161*, F615.

(23) Killops, K. L.; Campos, L. M.; Hawker, C. J. *J. Am. Chem. Soc.* **2008**, *130*, 5062.

(24) Li, N.; Yan, T.; Li, Z.; Thurn-Albrecht, T.; Binder, W. H. *Energy Environ. Sci.* **2012**, *5*, 7888.

(25) Sclavons, M.; Laurent, M.; Devaux, J.; Carlier, V. *Polymer* **2005**, *46*, 8062.

(26) Yan, J.; Hickner, M. A. *Macromolecules* **2010**, *43*, 2349.

(27) Noonan, K. J.; Hugar, K. M.; Kostalik IV, H. A.; Lobkovsky, E. B.; Abruña, H. D.; Coates, G. W. *J. Am. Chem. Soc.* **2012**, *134*, 18161.

(28) Gu, S.; Cai., R.; Yan, Y. *Chem. Commun.* **2011**, *47*, 2856.

(29) Chen, D.; Hickner, M. A. *Macromolecules* **2013**, *46*, 9270.

(30) Disabb-Miller, M. L.; Zha, Y.; DeCarlo, A. J.; Pawar, M.; Tew, G. N.; Hickner, M. A. *Macromolecules*, **2013**, *46*, 9279.

(31) Disabb-Miller, M. L.; Johnson, Z. D.; Hickner, M. A. *Macromolcules* **2013**, *46*, 949.

(32) Varcoe, J. R.; Slade, R. C. T. *Fuel Cells* **2005**, *2*, 187.

(33) Nuñez, S. A.; Hickner, M. A. *ACS Macro Lett*. **2013**, *2*, 49.

(34) Chempath, S.; Einsla, B. R.; Pratt, L. R.; Macomber, C. S.; Boncella,J. M.; Rau, J. A.; Pivovar, B. S. *J. Phys. Chem. C* **2008**, *112*, 3179.

(35) Einsla, B. R.; Chempath, S.; Pratt, L. R.; Boncella, J. M.; Rau, J.; Macomber, C.; Pivovar, B. S. *Electrochem. Soc. Trans.* **2007**, *11*, 1173.

(36) Macomber, C. S.; Boncella, J. M.; Pivovar, B. S.; Rau, J. A. *J. Therm.Anal.Calorim.* **2008**, *93*, 225.

(37) Zhou, W.; Yao, N.; Yao, G.; Deng, C.; Zhang, X.; Yang, P. *Chem. Commun.* **2008**, *43*, 5577.

(38) Gayles, J. N. *Spectrochim. Acta* **1967**, *23*, 1521.

(39) Christe, K. O.; Wilson, W. W.; Wilson, R. D.; Bau, R.; Feng, J. A. *J. Am. Chem. Soc.* **1990**, *112*, 7619.

(40) Ebsworth, E. A. V.; Sheppard N. *Spectrochim. Acta* **1959**, *13*, 261.

Chapter 5

Multication Side Chain Anion Exchange Membranes

This chapter is adapted from the manuscript "Multication Side Chain Anion Exchange Membranes" Zhu, L.; Pan, J.; Wang, Y.; Han, J.; Zhuang, L.; Hickner, M. A. published in Macromolecules, DOI: 10.1021/acs.macromol.5b02671

5.1 Introduction

In the past decade much effort has been placed on developing materials and cell operational technologies for AEMFCs. Among them, studies on high-performance polymeric AEMs have garnered increased attention to improve the lifetime and performance of AEMFCs. AEMs should show high ionic conductivity, low degrees of swelling, have excellent mechanical properties, and possess demonstrated chemical and thermal stabilities. There are indeed more than 100 different AEM compositions available in the literature, however, high-performance AEMs which can meet all the requirements of practical fuel cells and other electrochemical devices are rare.[1-8]

For common AEMs, high ionic conductivity frequently requires a material with high IEC. However, high IEC, which usually necessitates a higher grafting degree of the cationic group on the polymer backbone, leads to more water uptake in the material and generally poor mechanical properties.[9-11] AEMs with high IECs and high degrees of functionalization usually exhibit low chemical stability. An increase in the number of tethered cationic groups along the backbone not only exposes more active sites on the polymer backbone to OH^- attack, but also the increased degree of functionalization does not allow the formation of hydrophobic domains, which can resist swelling and alleviate degradation by resisting hydroxide intrusion into the material. [9-11]

Reducing the degree of functionalization while increasing the charge number of the cationic groups was reported as a method to balance the ionic conductivity and the other required properties of AEMs.[9-11] Zhuang,[9] *et al*. investigated a polysulfone (PSF)-based AEM with double quaternary ammonium groups (DQAPS). Compared to common AEMs, *i.e.*, quaternary ammonium polysulfone (QAPS), DQAPS enabled higher IECs without increasing the DF, and exhibited higher ionic conductivity as well as a lower swelling degree and higher chemical stability.[9] Although the DQAPS showed promising properties, the previous report did not detail systematic studies to demonstrate the effect of the arrangement of the charges on the performance of the AEMs.

In the current approach, we synthesized a series of poly(phenylene oxide) (PPO)-based AEMs with different kinds of cationic side chains to study the relationship between the degree of functionalization (DF), the structure of the side chain (charge number and charge arrangement), and the AEM performance in terms of ionic conductivity, swelling degree, and chemical stability of the material.

5.2 Experimental Section

Materials. Poly(2,6-dimethyl phenylene oxide) was purchased from Sigma-Aldrich and dried under vacuum at room temperature overnight. *N,N,N',N'*-tetramethyl-1,6-hexanediamine, *N,N,N',N'*-tetramethyl-1,3-propanediamine, (5-bromopentyl)trimethylammonium bromide, (3-bromopropyl)trimethylammonium bromide, 6-bromo-hexane, *N*-bromosuccinimide, and 2, 2'-azobis(2-methylpropionitrile) were obtained from Sigma-Aldrich and used as received. The brominated PPO polymers with different degrees of functionalization (DF) ranging from 15 to 40

mol % of the repeat units on the backbone with one benzyl bromide group were synthesized according to the reported literature.[12]

Synthesis of 1-(*N', N'*-dimethylamino)-6-(*N,N,N*-trimethylammonium) dodecane bromide (1a). To 300 mL chloroform, 150 mmol of *N, N, N', N'*-tetramethyl-1,6-hexanediamine and 15 mmol of 6-bromo-hexane were dissolved and heated at 60 °C for 12 h.[13,14] After evaporation of the chloroform, the residual liquid reagent was removed under vacuum. The crude product was further purified through recrystallization in methanol. The recrystallized product was dried in a vacuum oven at room temperature with a yield of 89 %. The chemical structure and purity of the product was characterized by ^{1}H NMR in $CDCl_3$.

Synthesis of 1-(*N',N'*-dimethylamino)-3-(*N,N,N*-trimethylammonium) nonane bromine and 1-(*N',N'*-dimethylamino)-2-(*N,N,N*-trimethylammonium) octane bromide (1b). The syntheses of 1-(*N',N'*-dimethylamino)-3-(*N,N,N*-trimethylammonium) nonane bromide were similar to the procedure described above. To 300 mL chloroform, 150 mmol of *N,N,N',N'*-tetramethyl-1,3-propanediamine and 15 mmol of 6-bromo-hexane were dissolved, and heated at 60 °C for 12 h. The crude product was purified using the same method described above. The final product was dried in a vacuum oven at room temperature with a yield of 85 %. The chemical structure and purity of the product was characterized by ^{1}H NMR dissolved in $CDCl_3$.

Synthesis of 1-(*N',N'*-dimethylamino)-6,11-(*N,N,N*-trimethylammonium) undecane bromide (2a). To 200 mL of chloroform, 100 mmol of *N,N,N',N'*-tetramethyl-1,6-hexanediamine and 10 mmol of (5-bromopentyl)trimethylammonium bromide were dissolved, and heated at 60 °C for 12 h. After evaporation of the chloroform, the residual liquid reagent was removed under vacuum at elevated temperature. The crude product was further purified through recrystallization in methanol. The recrystallized product was dried in a vacuum oven at room temperature with a

yield of 90 %. The chemical structure and purity of the product was characterized by ^{1}H NMR in DMSO-d_6.

Synthesis of 1-(*N′,N′*-dimethylamino)-6,9-(*N,N,N*-trimethylammonium) nonane bromide (2b). The synthesis of 1-(*N′,N′*-dimethylamino)-6,9-(*N,N,N*-trimethylammonium) nonane bromide was similar to the procedure described above. To 200 mL chloroform, 100 mmol of *N,N,N′,N′*-tetramethyl-1,3-propanediamine and 10 mmol of (3-bromopropyl) trimethylammonium bromide were dissolved, and heated at 60 °C for 12 h. The crude product was purified using the same method described above. The final product was dried in a vacuum oven at room temperature with a yield of 87 %. The chemical structure and purity of the product was characterized by ^{1}H NMR dissolved in DMSO-d_6.

Polymer synthesis. Brominated PPO with a DF of 40 (1 g, 6.62 mmol) was dissolved in 10 mL of *N*-methyl-pyrrolidone (NMP). Then, 1-(*N',N'*-dimethylamino)-6-(*N,N,N*-trimethylammonium) dodecane bromide (1.1 g, 3.26 mmol) was added slowly. The mixture was stirred at 50 °C for 72 h. The obtained solution was poured into 100 mL toluene or hexane to precipitate the polymer. The product was filtered and further washed with hexane and toluene several times. A dark yellow powder was obtained and dried at 50 °C under vacuum overnight. The resulting product was double-cation side chain PPO (D40NC6NC6, where the D stands for double-cation; the 40 refers to the degree of functionalization as 40 mol %; the first N means the first quaternary ammonium group ($N^{+}C_4$) in the side chain; the first C6 indicates that the spacer is 6 methylenes; the second N represents the second $N^{+}C_4$; the second C6 stands for a terminal hexyl from the pendant cation) with a yield of 90% in the bromide form. For the synthesis of triple-cation side chain PPO, brominated PPO with a DB of 25 (1 g, 7.14 mmol) was dissolved in 20 mL of NMP. Then, 1-(*N',N'*-dimethylamino)-6,11-(*N,N,N*-trimethylammonium) undecane bromide (1.0 g, 2.30 mmol) was added slowly. The mixture was stirred at 50 °C for five days.

The obtained solution was poured into 200 mL toluene or hexane to precipitate the polymer. The crude product was purified using the same method described above. A light yellow powder was obtained and dried at 50 °C under vacuum overnight. The resulting product was triple-cation side chain PPO (T25NC6NC5N, where the T stands for triple-cation; the 25 refers to the degree of functionalization as 25 mol %; the first N means the first N^+C_4 in the side chain; the C6 indicates that the spacer between the first N^+C_4 and the second N^+C_4 is 6 methylenes; the second N represents the second N^+C_4 in the side chain; C5 means the spacer between the second and third ammonium group is 5 methylenes; the third N represents the third N^+C_4 with a CH_3 terminal group from the cation) with a yield of 90% in the bromide form.

Fabrication of membranes. The D40NC6NC6 double-cation side chain polymer (0.25 g) in bromide form was dissolved in NMP (5 mL) to yield a 5 wt % solution. The solution was then cast onto a leveled glass plate, and dried at 82 °C under ambient pressure for 24 h followed by vacuum drying for another 24 h at 80 °C to give a ~100 μm thick, transparent, tough film. The T25NC6NC5N triple-cation side chain membrane was prepared via the same method described above.

Membrane-electrode assembly fabrication and fuel cell testing. Pt/C (60%, Johnson Matthey Co.) was mixed with D30NC6NC6 (IEC = 2.47 mmol/g), T20NC6NC5N (IEC = 2.52 mmol/g), or S60NC6 (IEC = 2.60 mmol/g) ionomer solution,[15] and sprayed onto both sides of D30NC6NC6 (IEC = 2.47 mmol/g), T20NC6NC5N (IEC = 2.52 mmol/g), or S60NC6 (IEC = 2.60 mmol/g) membrane (60 ± 5 μm in thickness), respectively, to prepare the catalyst-coated membranes (CCMs) with the same material in the membrane and in the electrode. The weight percentage of ionomer in both the anode and the cathode was calculated to be 20 wt %. The Pt loading in both anode and cathode was 0.4 mg/cm^2, and the area of the electrodes was 4 cm^2. The resulting CCMs were pressed between two pieces of carbon cloth (CeTech W1S1005) to form the

membrane electrode assembly (MEA). The H_2-O_2 fuel cell performance of the MEAs was measured under a galvanic mode using fully humidified H_2 and O_2 gases flowing at a rate of 250 mL/min and at temperature of 60 °C with 0.1 MPa back pressure (850e Multi Range, Scribner Associates Co.).

5.3 Results and Discussion

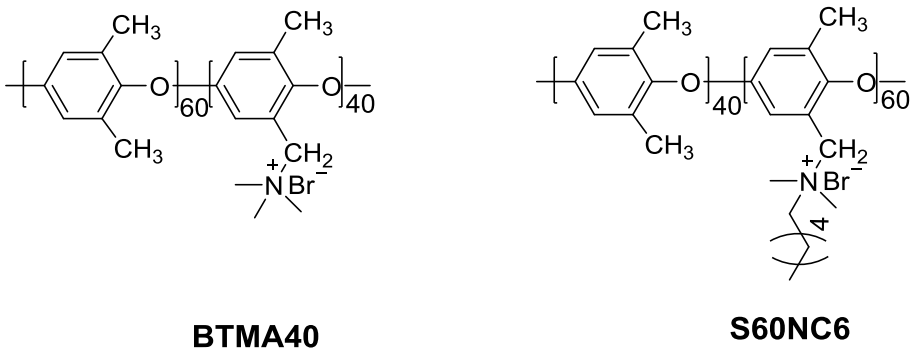

Scheme 5.1 Chemical structures of BTMA40 and S60NC6.

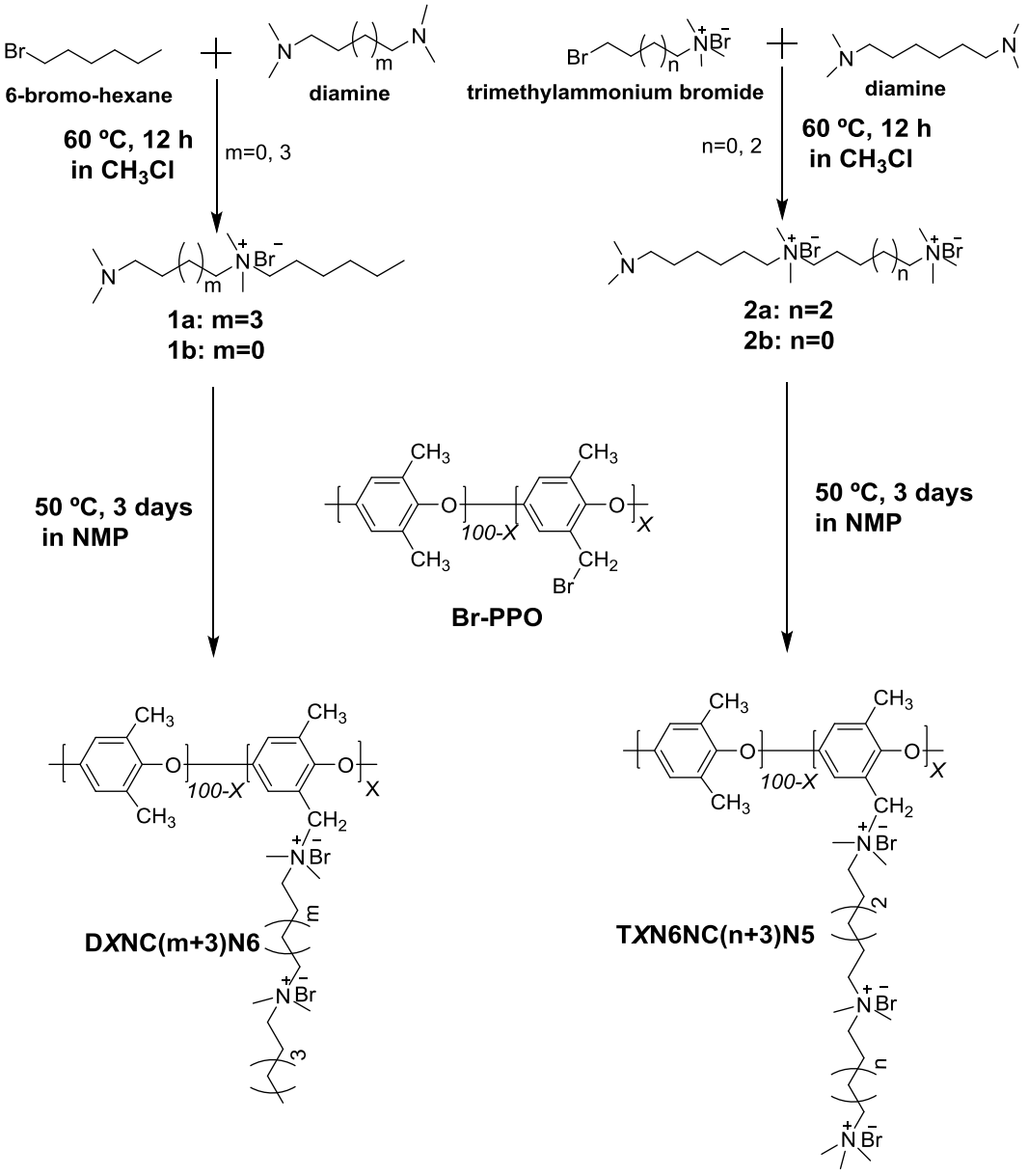

Scheme 5.2 Synthetic route for multication sidechain AEMs.

Synthesis. The synthesis of the PPO-based AEMs included three steps, namely; preparation of brominated PPO (Br-PPO), synthesis of cation side-chain precursors, and finally the Menshukin reaction between Br-PPO and cation precursors. Br-PPOs possessing a degree of functionalization (DF) from 20 to 40 mol % of the monomer units on the backbone functionalized

with benzyl bromide groups were synthesized according to our previous reports.[16] Precursor Br-PPOs with different DFs and side chains with varying cation number allowed the production of a wide range of quaternary ammonium functionalized PPOs with different IECs.

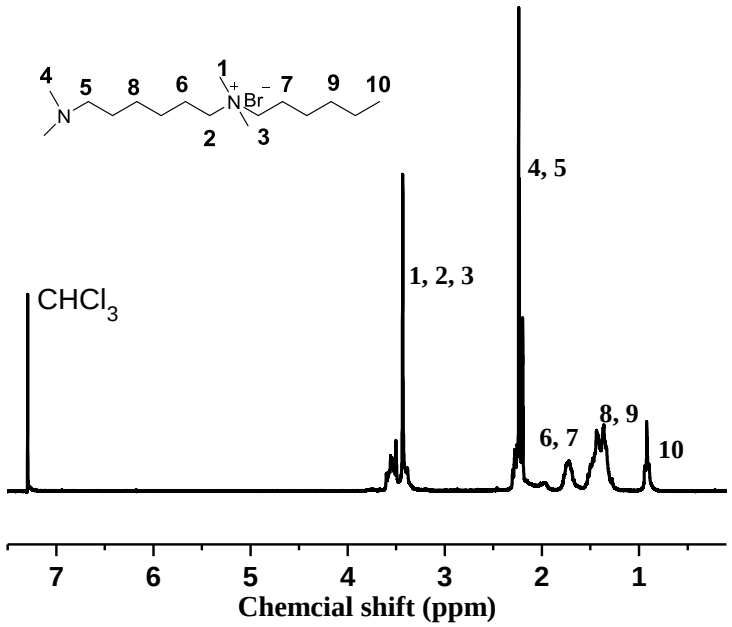

Figure 5.1 ^{1}H NMR of 1-(*N',N'*-dimethylamino)-6-(*N,N,N*-trimethylammonium) dodecane bromide in $CHCl_3$-d_1.

The cation precursor, 1-(*N',N'*-dimethylamino)-6-(*N,N,N*-trimethylammonium) dodecane bromide and 1-(*N',N'*-dimethylamino)-3-(*N,N,N*-trimethylammonium) nonane bromide, for synthesizing the double-cation AEMs were successfully synthesized according to the reported method.[13,14] The ^{1}H NMR spectra of the double-cation monomers are shown in Figure 5.1. The appearance of the peaks at 3.30-3.49 ppm indicated that the quaternary ammonium groups were formed in compound **1a (**1-(*N',N'*-dimethylamino)-6-(*N,N,N*-trimethylammonium) dodecane

bromide), the peaks at 2.0-2.5 ppm demonstrated the presence of the tertiary amine groups. Additionally, the peaks at 0.9 to 2.0 ppm corresponded to the protons in end alkyl chain, which demonstrated the successful reaction between *N,N,N',N'*-tetramethyl-1, 6-hexanediamine and n-alkyl bromide.

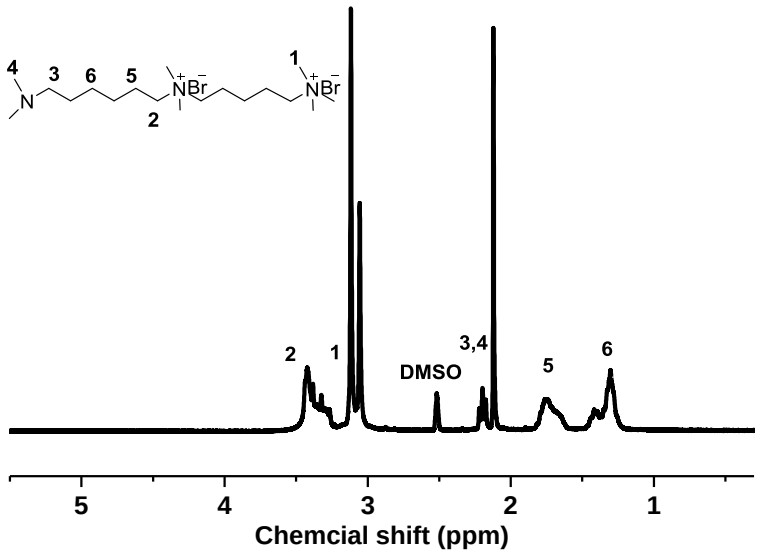

Figure 5.2 ^{1}H NMR of 1-(*N',N'* - dimethylamino)-6,11-(*N,N,N*-trimethylammonium) undecane bromide in $CHCl_3$-d_1.

The triple-cation precursor, 1-(*N',N'*-dimethylamino)-6,11-(*N,N,N*-trimethylammonium) undecane bromide and 1-(*N',N'*-dimethylamino)-6,9-(*N,N,N*-trimethylammonium) nonane bromine, were prepared from *N,N,N',N'*-tetramethyl-1,6 hexanediamine, (5-bromopentyl)trimethylammonium bromide and and (3-bromopropyl) trimethylammonium bromide via the Menshutkin reaction. As is shown in Figure 5.2, the quaternary ammonium groups located in the middle of the monomers, which were produced from the reaction of (5-

bromopentyl) trimethylammonium bromide with *N,N,N',N'*-tetramethyl-1,6-hexanediamine (Scheme 5.2) showed peaks at 3.30-3.49 ppm in ^{1}H NMR spectra. The peaks located at 3.11-3.22 ppm corresponded to the end quaternary ammonium groups contributed from the (5-bromopentyl) trimethylammonium bromide. Furthermore, as in the double-cation monomers, the protons which belonged to the tertiary amine groups and alkyl chains in the triple-cation monomers can be identified in the ^{1}H NMR spectra.

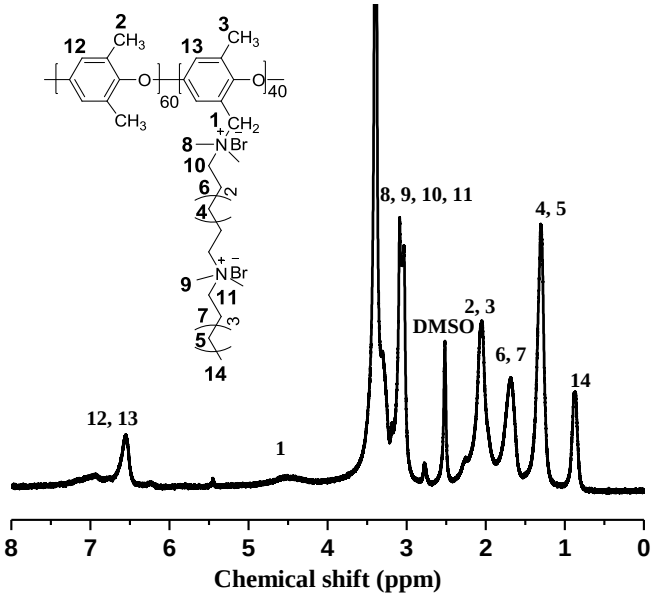

Figure 5.3. ^{1}H NMR of D40NC6NC6 in bromide salt form in DMSO-d_6.

The reactions for synthesizing different AEM samples were conducted between Br-PPOs and different cation precursors (Scheme 5.2). The double-cation AEM, D40NC6NC6, which employed a 6 methylene spacer between the two cations was achieved by the Menshutkin reaction of the double cation precursor with Br-PPOs. As shown in Figure 5.3, the disappearance of the proton resonance arising from the bromobenzyl moiety as a sharp peak at 4.3 ppm along with the appearance of new peaks at 0.7-1.8 ppm and 3.1-3.3 ppm assigned to the alkyl chains of

the cationic side chains demonstrated that quaternary ammonium groups were formed. Probably due to the deshielding effect of the quaternary ammonium group, a broad resonance from 4.3 to 4.5 ppm was detected, which could be assigned to the benzylic protons (H1 in Figure 5.3).[31] The integral ratio of benzylic protons (H1 in Figure 5.3) at 4.3 to 4.5 ppm to the aromatic peaks at 6.6-7.1 ppm indicated the quaternization reaction was quantitative. The IEC_w of the two-cation side chain PPO membranes calculated from the integral ratios was consistent with the theoretically calculated values, further suggesting the complete and reliable quaternization of the bromomethyl groups. Using Br-PPOs with different DFs (20, 30, 35 and 40 mol %), double cation AEMs showed the IECs ranging from 1.94 to 2.93 mmol/g (Table 1).

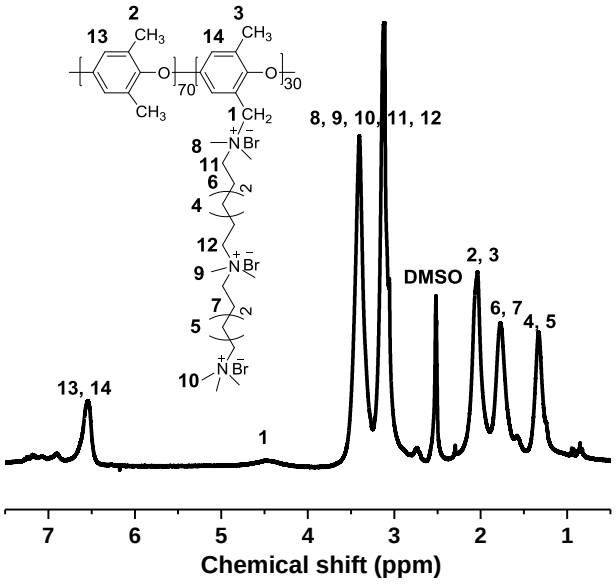

Figure 5.4 ^{1}H NMR of T30NC6NC5N in bromide salt form in DMSO-d_6.

Similar to that of the double cation AEMs, triple cation AEMs were synthesized and characterized by ^{1}H NMR. As shown in Figure 5.4, all of the peaks in the spectrum can be

attributed to the protons located in the backbone and side chain of the triple cation AEMs. The IECs of such AEMs ranged from 2.10 to 3.10 mmol/g (Table 1).

Table 5.1 Properties of the multication side chain PPO membranes.

sample	IEC (mmol/g)[a]	IEC (mmol/g)[b]	WU (wt%) (OH^-)[c]	WU (wt%) (HCO_3^-)[c]	WU (wt%) (Cl^-)[c]	σ (mS/cm) (OH^-)[c]	σ (mS/cm) (HCO_3^-)[c]	σ (mS/cm) (Cl^-)[c]	λ (OH^-)	in-plane swelling(%)[c]
D20NC6NC6	2.15	1.94	61 ± 2	29 ± 1	24 ± 1	30 ± 2	6 ± 1	10 ± 1	16	14
D30NC6NC6	2.74	2.47	130 ± 3	61 ± 2	53 ± 2	52 ± 3	11 ± 1	18 ± 2	26	25
D35NC6NC6	2.97	2.71	187 ± 5	80 ± 3	71 ± 3	58 ± 3	14 ± 1	20 ± 2	35	40
D40NC6NC6	3.18	2.93	257 ± 10	97 ± 3	90 ± 3	53 ± 2	12 ± 1	18 ± 2	45	61
T15NC6NC5N	2.31	2.10	65 ± 2	43 ± 1	38 ± 1	53 ± 2	9 ± 1	14 ± 1	16	10
T20NC6NC5N	2.74	2.52	135 ± 5	76 ± 3	56 ± 2	72 ± 3	16 ± 1	23 ± 2	27	18
T25NC6NC5N	3.07	2.87	189 ± 5	89 ± 3	72 ± 3	97 ± 5	21 ± 1	34 ± 3	34	31
T30NC6NC5N	3.35	3.10	310 ± 10	150 ± 3	130 ± 3	77 ± 3	16 ± 1	26 ± 2	51	89

[a]Calculated from the polymer composition and the degree of functionalization. [b]Titrated values. [c]Measured at room temperature in water.

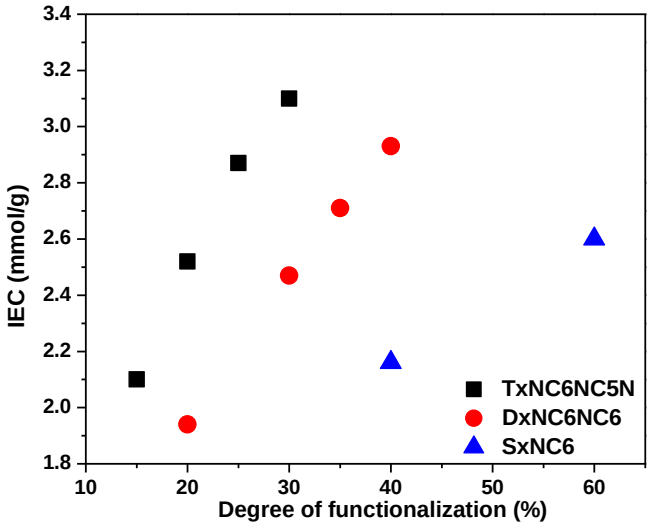

Figure 5.5 IEC values as a function of the degree of polymer backbone functionalization and side chain type.

Increasing the charge number of the cation ensured high IEC AEMs with low DFs. As shown in Figure 5.5, for example, with the same DF of 30%, the IEC of the triple-cation AEM, i.e., T30NC6NC5N, was 3.1 mmol/g, which was 1.3 and 1.8 times higher than that of D30NC6NC6 (double-cation AEM), S30NC6 (single-cation AEM), respectively. AEMs with low DFs and high IECs were expected to exhibit excellent physical properties and to facilitate the stability of the PPO backbone.[9]

Swelling behavior. To demonstrate the effect of the backbone DF and the charge number of the side chain on the swelling behavior of the AEM samples, we compared the water uptakes and swelling ratios of BTMAx, SxNC6, DxNC6NC6, and TxNC6NC5N membranes with

different DFs. In this study, the long spacers attached to the cationic groups in DxNC6NC6 and TxNC6NC5N were chosen to be 5 or 6 methylene units.

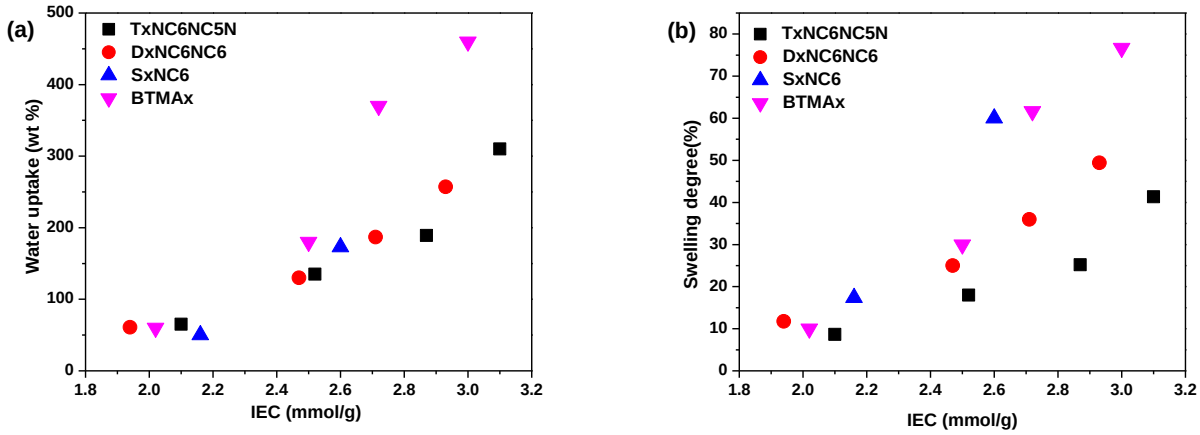

Figure 5.6 Liquid water uptake (a) and swelling ratio (b) of membranes in OH^- form as a function of IEC at room temperature.

As shown in Figure 5.6a, the water uptake of the samples generally increased with increasing IEC. Among these samples, SxNC6, DxNC6NC6, and TxNC6NC5N exhibited similar swelling behaviors, while BTMA membranes showed greater water uptake than the other AEMs with the same IECs. The presence of hydrophilic/hydrophobic micro-phase separation is likely the reason for the lower water uptake in the AEMs with long spacers. The lower water uptakes of these samples guaranteed lower swelling degrees (Figure 5.6b), and higher mechanical strength.[9,16,17]

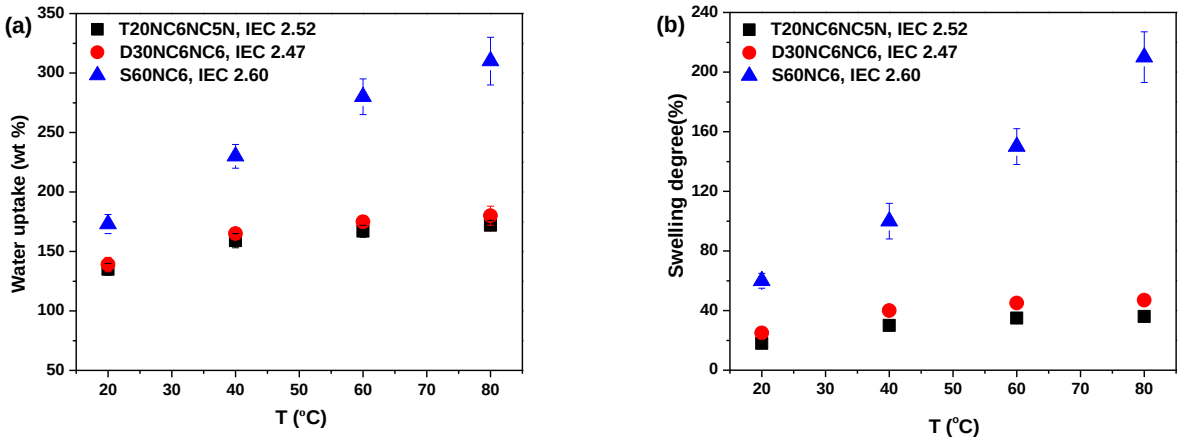

Figure 5.7 Liquid water uptake (a) and swelling ratio (b) of membranes in OH^- form as a function temperature.

Figure 5.7 compares the swelling behaviors at elevated temperatures of different AEMs with similar IECs and long cation spacers. Although the water uptakes and swelling ratios for all the samples increased with elevated temperatures, increasing the charge number in the cation side chain can improve the dimensional stability of the AEMs. For the double- and triple-cation AEMs, D30NC6NC6 and T20NC6NC5N, the water uptakes were 139 wt % and 135 wt %, and the swelling ratios were 25 % and 18 % at room temperature, respectively. When the temperature was increased to 80 °C, the water uptakes of the samples increased to 180 wt % and 172 wt %, and their swelling ratios went up to 47% and 36%, respectively. In comparison, large increases of water uptake and swelling ratio were observed for the single cation S60NC6 sample when the temperature was increased from 20 to 80 °C (increases of 140% for water uptake increment and 137% for swelling ratio increment). Since the AEMs which possessed similar IECs had the same polymer backbone and similar cation structure, the differences in the dimensional stabilities between the samples could be attributed to the arrangement of cations on the backbone of the

materials. The increased charge density of the side chain and low DF of the backbone enhanced the intermolecular interactions of the hydrophobic segments of the backbone to prevent swelling.[9]

Ionic conductivity in multication side chain AEMs. High ionic conductivity is one of the most important properties for the application of AEMs in devices. To study how the charge number of the cation side chain affected the ion transport, OH^- conductivities of the AEMs with different IECs were measured.

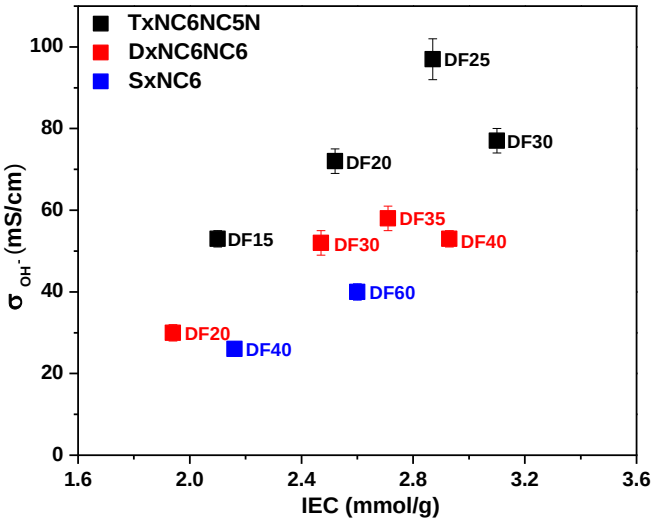

Figure 5.8 Hydroxide conductivity of multication and single-cation AEMs in liquid water at 20 °C as a function of IEC.

Generally, the hydroxide conductivity of the AEMs increased with increasing IEC due to an increase in the water content which enhanced the local mobility of water and induced long-range ionic domain percolation.[16] As expected, for the same type of AEM, the ionic conductivity first increased and then decreased with increasing IEC (Figure 5.8). Generally, higher IECs, which yield increasing water uptake, show lower conductivity where the membrane is too water

swollen and ionic dilution occurs. As shown in Figure 5.8, the T25NC6NC5N membrane displayed a maximum OH^- conductivity of 99 mS/cm at room temperature with an IEC of 2.87 mmol/g, compared to 58 and 40 mS/cm for D35NC6NC6 (IEC = 2.71 mmol/g) and S60NC6 (IEC = 2.6 mmol/g, data for SxNC6 with IEC > 2.6 mmol/g cannot be obtained since the high IEC samples dissolved in pure water) under the same testing conditions.

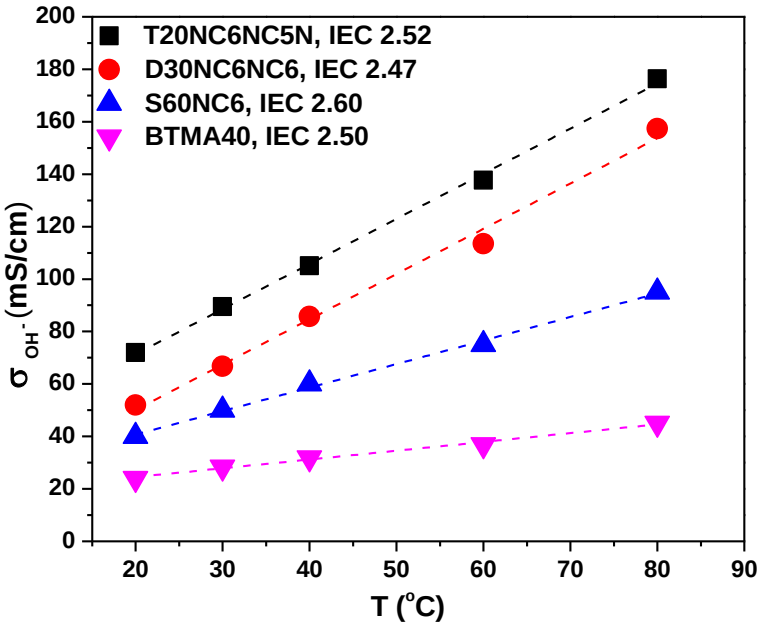

Figure 5.9 Hydroxide conductivity of AEMs as a function of temperature.

The temperature dependence of the OH^- conductivities in liquid water of the multication side chain, S60NC6, and BTMA40 membranes with similar IEC is illustrated in Figure 5.9. The T20NC6NC5N sample exhibited the highest OH^- conductivity (176 mS/cm) at 80 °C, which was nearly four times higher than that of BTMA40 under the same conditions. More importantly, the OH^- conductivity showed a regular increase when the number of cations in the side chain increased from one to three. These results suggest the rational arrangement of multiple cations in

the side chain, which enhance the micro-phase formation, can greatly facilitate ion transport in the materials, thus enhancing their OH^- conductivity.

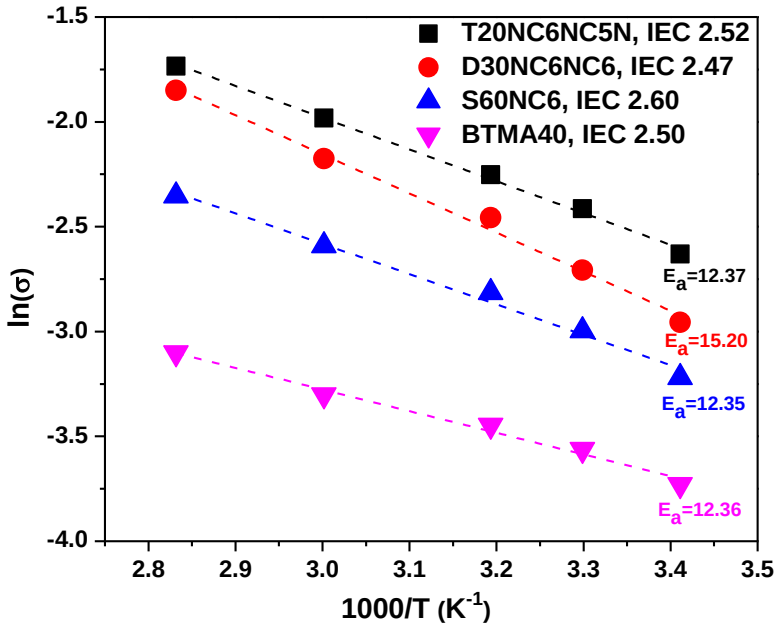

Figure 5.10 Hydroxide conductivity of AEMs in an Arrhenius-type temperature plot showing activation energies in kJ/mol.

As shown in Figure 5.10, the OH^- conductivities of the membranes with a similar IEC showed an approximate Arrhenius-type temperature dependence promoted by the thermal activation of water motion.[18] The apparent activation energy estimated from the slopes of the ln(σ) vs 1000/T curves was ~ 12-15 kJ/mol and similar among the measured samples. The apparent activation energies of the tested membranes was comparable to or somewhat lower than those of other reported AEMs (10-23 kJ/mol), indicating that these membranes have a water-facilitated OH^- conduction mechanism similar to other hydrated AEMs.

Morphological characterization. More efficient ion transport in fuel cell membranes usually results from better OH^- transport pathways as the material is hydrated. Generally, for the different AEMs with similar IECs and water uptakes, obvious ion aggregation, which ensures ionic channels for transport, is desirable. To investigate the micro-phase morphologies of the materials in this study, SAXS patterns and TEM images were taken for the D30NC6NC6 (IEC = 2.47 mmol/g), T20NC6NC5N (IEC = 2.52 mmol/g), and BTMA40 (IEC = 2.50 mmol/g) samples.

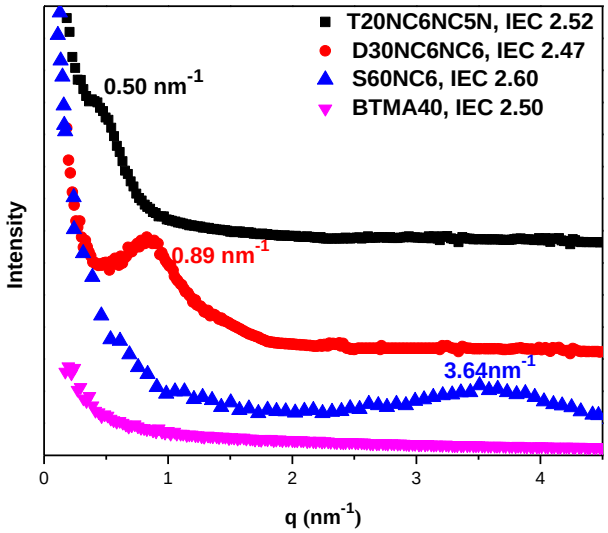

Figure 5.11 SAXS profiles of dry membranes in the bromide form.

SAXS profiles, Figure 5.11, revealed different morphologies in the three membranes. Ionic peaks for the S40NC6, D30NC6NC6, and T20NC6NC5N emerged at 3.64,[16] 0.89 and 0.50 nm^{-1}, corresponding to Bragg spacings of approximately 1.8, 7.0 and 12.6 nm.

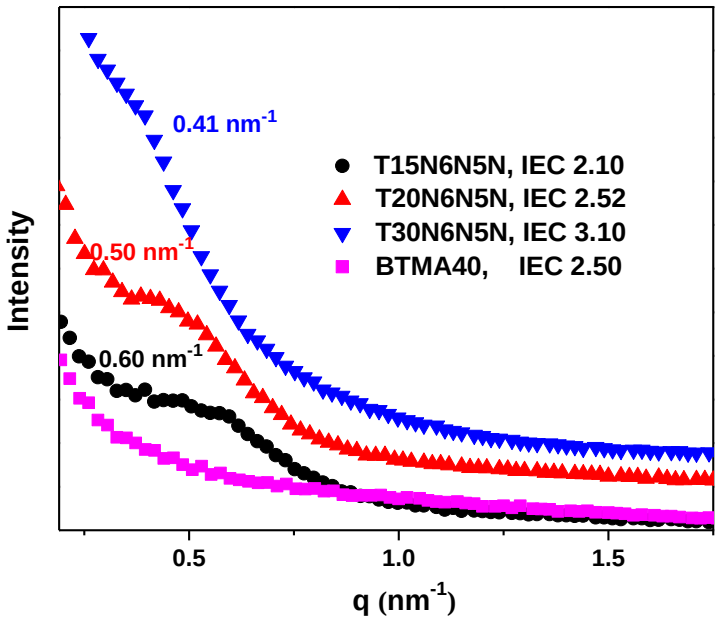

Figure 5.12. SAXS profiles of triple-cation and BTMA40 AEMs in the bromide form.

The SAXS peaks (Figure 5.12) of the TxNC6NC5N membranes shifted to lower q as the IEC increased, indicating that the size of the ionic clusters grew with increasing IEC.

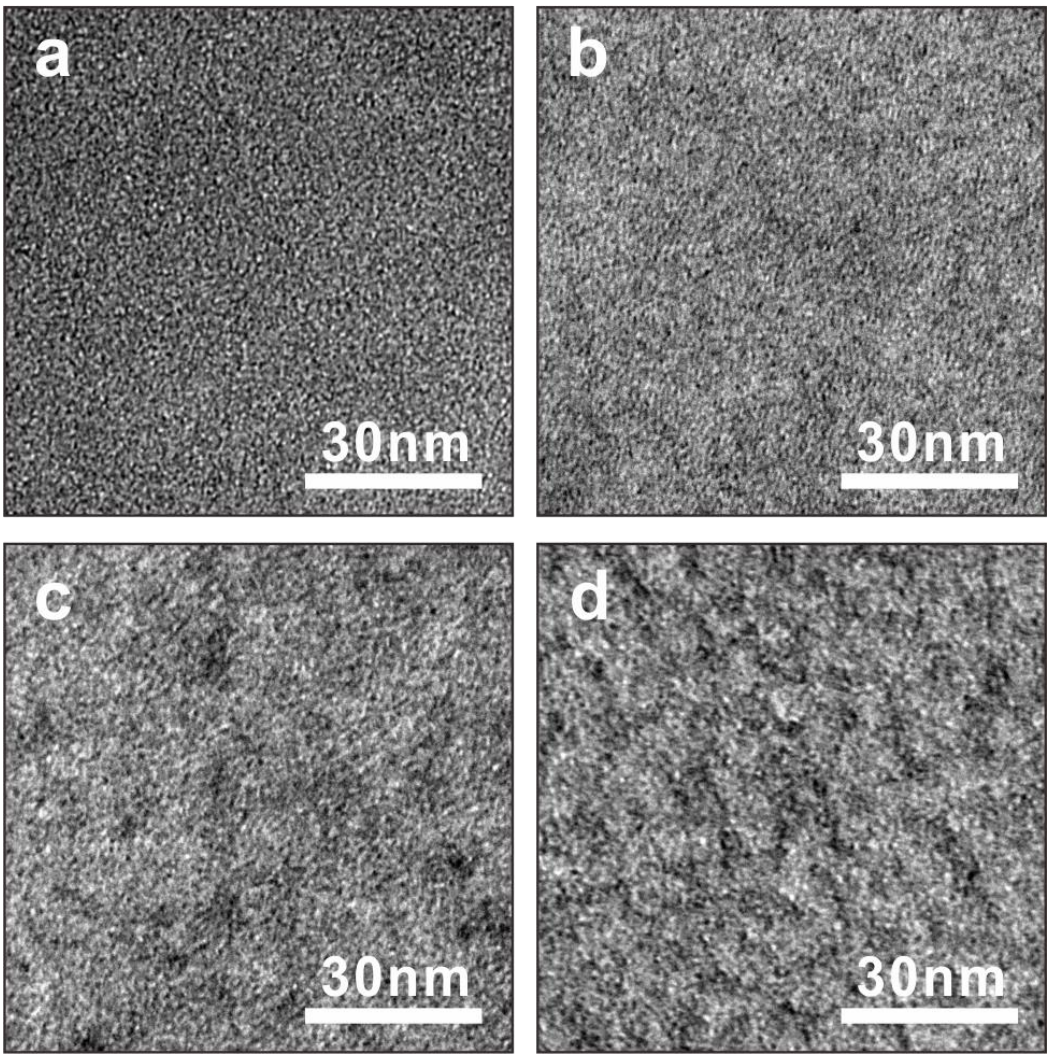

Figure 5.13TEM images of dry membranes in the bromide form (a) BTMA40; (b) S60NC6; (c) D30NC6NC6; (d) T20NC6NC5N.

From the SAXS data, it is difficult to determine the extent of phase separation for the T20NC6NC5N sample since the peak is close to the beam stop. However, as shown in the transmission electron micrographs in Figure 6, the phase separation is clearly well-developed in the T20NC6NC5N sample. The dark areas represent the ionic domains stained by ruthenium tetroxide, while the bright areas represent the non-ionic domains. For the S60NC6 membrane, some ion aggregation was observed in the TEM image. For the double- and triple-cation AEMs,

more obvious hydrophilic/hydrophobic phase separation was observed tying the increased conductivity of these samples to their better-developed morphologies.

Ion transport. In order to further investigate the relationship between the OH^- conductivity and water volume fraction inside the membranes, we normalized the OH^- conductivity on the basis of water volume fraction to obtain the effective hydroxide conductivity in the water channels, σ', which demonstrates the efficiency of the water molecules inside the membranes for transport.[16]

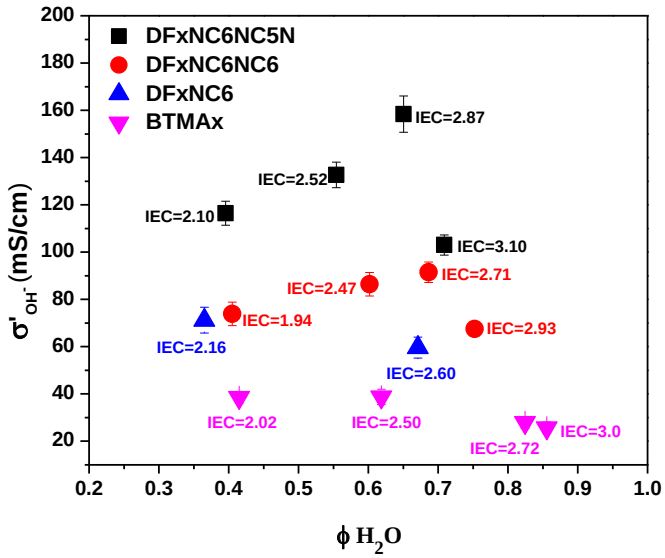

Figure 5.14 Water volume fraction dependence of the effective hydroxide conductivity in the water channels (σ') in liquid water at room temperature.

As shown in Figure 5.14, the multication side chain membranes show much higher σ' values at the same water volume fraction, compared to the BTMA membranes. The results demonstrated that the formation of continuous nanoscale ionic domains could enhance the ion transport because of the phase separation.[16,18] The more important point is that the TxNC6NC5N show significantly higher σ' (Figure 5.14) values than those of DxNC6NC6 and SxNC6 under the

same conditions, which is attributed to the arrangement of the cations in the side chains. As expected, all of the membranes displayed an inflection point at high water volume fraction due to the decline of ion concentration with increased swelling. However, the triple-cation side chain membranes showed the inflection point at much higher hydroxide conductivity and IEC than those of the other samples. These results suggest that the strategy of attaching a multication on each side chain to boost the ionic conductivity was effective for the PPO-based AEMs.

In our previous report,[19] we demonstrated the utility of comparing the calculated diffusion coefficient of ions in the membrane (D) with the dilute solution diffusion coefficient. For different ions, the barrier to ion transport could be determined via the ratio of the diffusion coefficient to the dilute ion diffusivity (D/D_0), in which D_0 is the maximum diffusivity of an ion in pure water.[20]

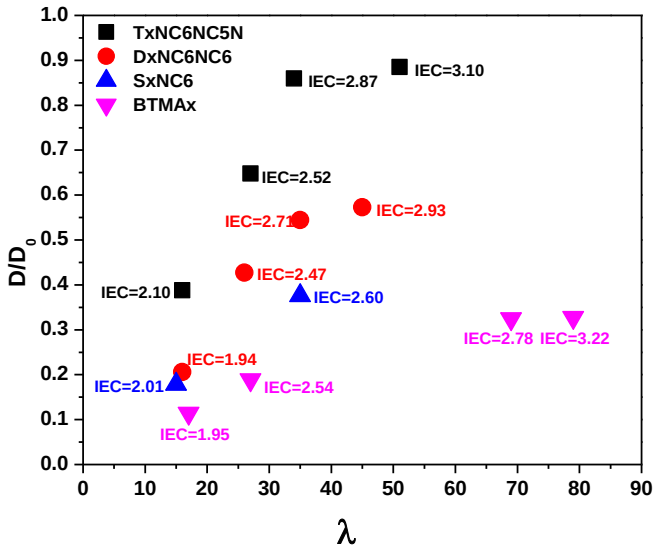

Figure 5.15 Ratio of the diffusion coefficient, D, to the dilute solution diffusivity, D_0, as a function of hydration number for membranes in the hydroxide form.

Similar to the ionic conductivity, the D/D_0 ratio increased with increasing hydration for membranes in the hydroxide form due to the increase in IEC values. As shown in Figure 5.15, the multication side chain membranes showed relatively higher D/D_0 values than the BTMA membranes at the same λ, demonstrating more facile mobility for the hydroxide ions in these membranes. It is important to point out that the highest D/D_0 ratio obtained was 0.88 at $\lambda = 51$ with IEC = 3.10 meq/g for the T30N6N5N sample. These results indicated that the mobility of the anions in the multication side chain membranes were greater than in the BTMA samples. We hypothesized that these results might be ascribed to the formation of nanoscale ionic domains because of the immiscibility of the arylene ether polymer backbone (PPO) with the aliphatic grafted side chain. These nanoscale ionic domains should be able to facilitate and enhance the mobility of the ions in the membranes with the help of water molecules.

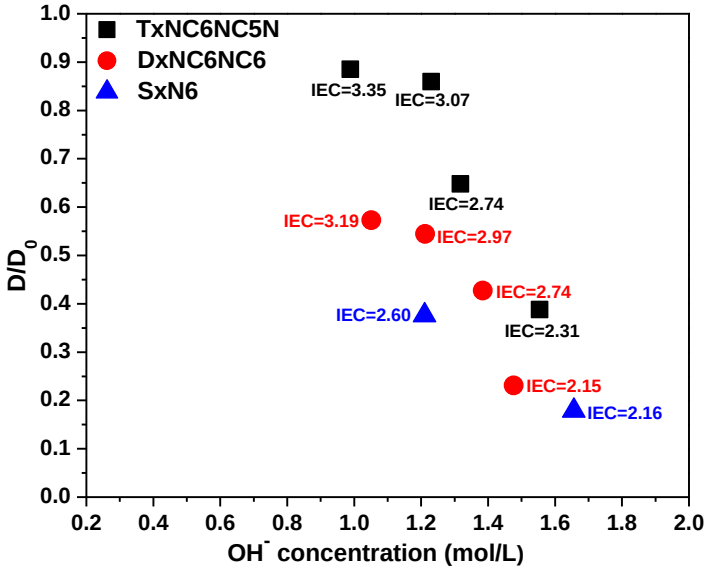

Figure 5.16 OH^- mobility ratios (D/D_0) of multication and single-cation AEMs as a function of OH^- concentrations in liquid water at 20 °C.

Figure 5.16 shows the relationship between the D/D_0 and the OH^- concentration. The D/D_0 generally decreases with increased OH^- concentration which could be a sign of counterion condensation in these materials since the calculation of D assumes full dissociation of the tethered ions.

Alkaline **stability.** AEMs with quaternary ammonium groups are known to degrade under alkaline conditions. The degradation mechanisms for the cations with long alkyl spacers included β-hydrogen (Hofmann) elimination, direct nucleophilic substitution at the α-carbon, benzyl attack, and nitrogen ylide formation.[21-25] To evaluate the long-term alkaline stability of the AEMs, T20NC6NC5N (IEC = 2.52 mmol/g), D30NC6NC6 (IEC = 2.47 mmol/g), S60NC6 (IEC = 2.60 mmol/g) and BTMA40 (IEC = 2.50 mmol/g) samples were immersed in argon-saturated 1 M NaOH solution at 80 °C for 500 hours, with replacement of the 1 M NaOH every 3 days during the testing period.

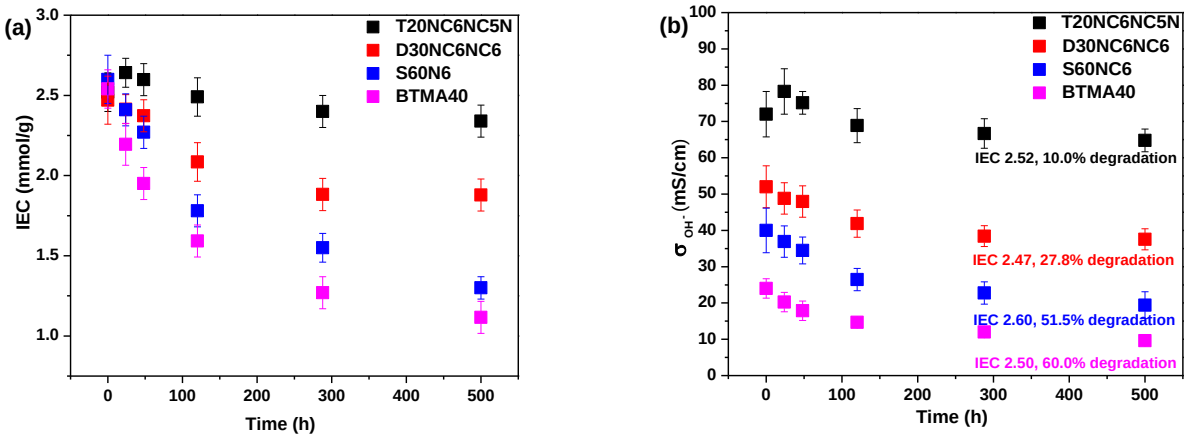

Figure 5.17 Stability of the T20NC6NC5N, D30NC6NC6, S60NC6 and BTMA40 samples in 1 M NaOH solution at 80 °C; (a) IEC and (b) OH^- conductivity as a function of duration time measured at 20 °C.

Figure 5.17 illustrates the changes in IEC and OH^- conductivity during stability testing of the samples. During the 500 h test, T20NC6NC5N exhibited the greatest cation stability. The IEC and OH^- conductivity of this membrane decreased by 7.1 % and 10.0 %, respectively. The D30NC6NC6 demonstrated moderately enhanced cation stability compared to single cation membranes where the IEC and OH^- conductivity of D30NC6NC6 decreased by 24.2 % and 27.8 %, respectively. We propose that D30NC6NC6 is not as stable as T20NC6NC5N because of the increased functionalization of the D30NC6NC6 backbone. In contrast, the IECs of S60NC6 and BTMA40 films decreased to 1.30 and 1.12 mmol/g and the OH^- conductivities decreased to 19.4 and 9.6 mS/cm at 20°C, which were 51.5 and 60 % lower than the values measured for the sample before the stability test.

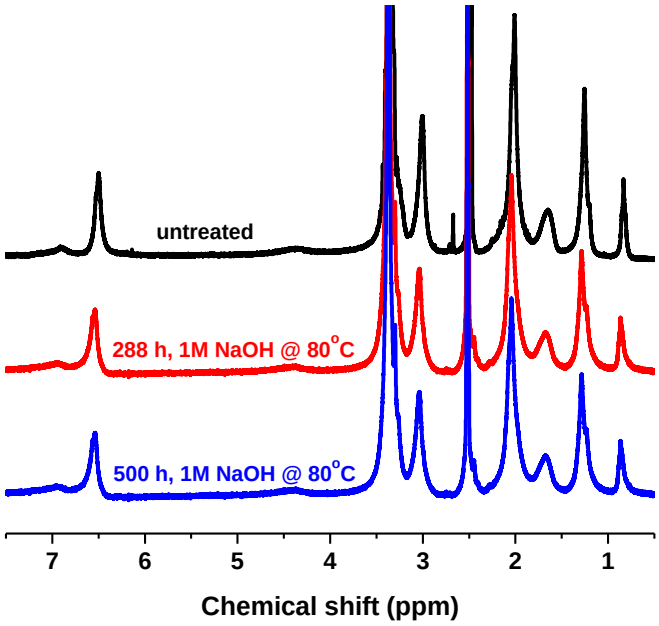

Figure 5.18. ^1H NMR spectra of D30NC6NC6 before and after stability tests in 1 M NaOH solution at 80 °C.

In order to further study the alkaline stability of the membranes, ^1H NMR spectra (Figure 5.18) were employed to characterize the changes in chemical AEM structures. Due to the complex of the

structure of these AEMs, it was difficult to determine the detailed degradation pathways of the membranes via the ^{1}H NMR spectra. In order to obtain degradation information from the ^{1}H NMR spectra, we calculated the integration ratio of the methyl groups on the quaternary ammonium substituent. The IEC of the D30NC6NC6 membranes calculated from the peak ratios decreased by 23.3 % and 23.7 % after exposure to 1 M NaOH solution at 80 °C for 288 and 500 h, respectively.

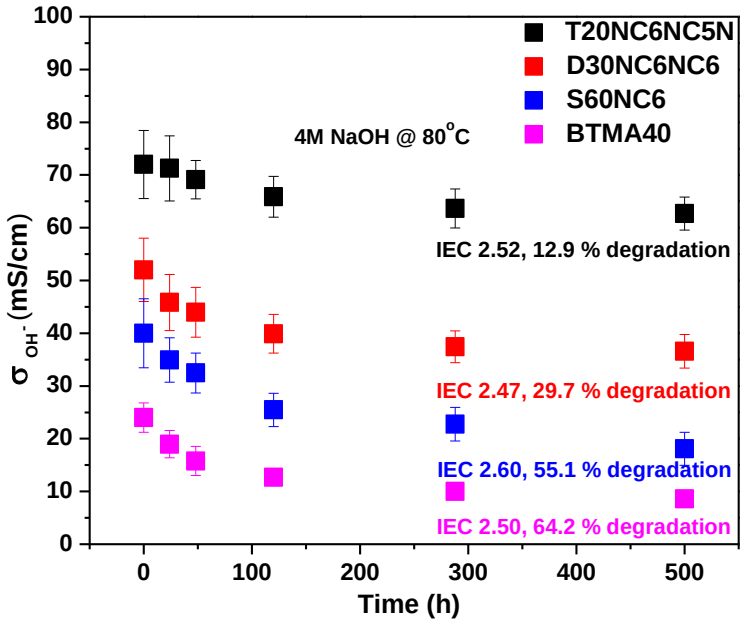

Figure 5.19 OH^- conductivity measured at 20 °C for the T20NC6NC5N, D30NC6NC6, S60NC6 and BTMA40 samples in 4 M NaOH solution at 80 °C as a function of degradation time.

In addition to testing the chemical stability in 1 M NaOH solution, we evaluated the alkaline stability of the samples in 4 M NaOH at 80 °C (Figure 5.19). Increasing the concentration of alkaline solution from 1 M to 4 M showed no obvious influence on the chemical stability of the AEM samples, therefore increasing the base concentration did not lead to more severe degradation of the AEM materials.[27] Since all the alkaline stability tests were conducted in 250 mL of NaOH solution, there was a large excess of OH^- during the tests. Increasing the concentration to 4 M may not cause a significant change of

the environment surrounding the AEMs, and thus similar degradation rates were observed in these two solutions.[26] Better stability of the multication AEMs was demonstrated due to the low DF polymer backbones and an increase in the microphase separation of hydrophilic and hydrophobic domains, which is in good agreement with other reported results.[9]

Multication side chain AEMs with different spacers. The studies above revealed that more charges in the cation side-chains ensured the multication AEMs had higher IECs under lower DFs, and the DxNC6NC6 and TxNC6NC5N membranes with hexyl and/or amyl chain as spacers showed higher conductive performance and chemical stability than that of the single-cation AEM. For the multication side chain groups, in addition to the charge numbers, the length of the spacers was also an important factor for determining the cation structure.[27-35] To establish the relationship between cation structures and AEM performances, a series of multication side chain membranes with different spacer lengths among cations were designed.

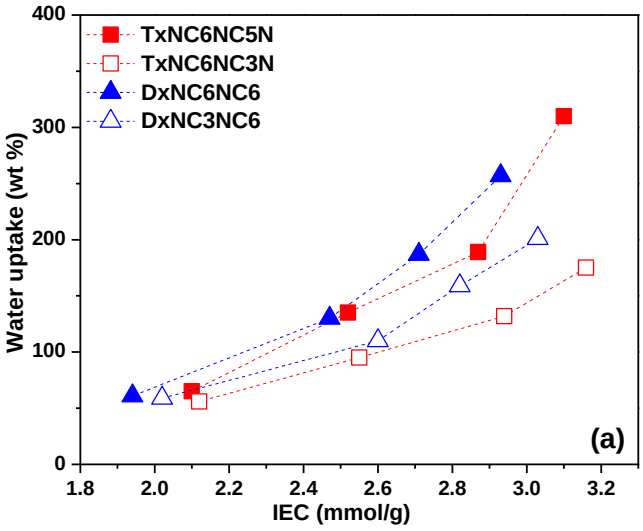

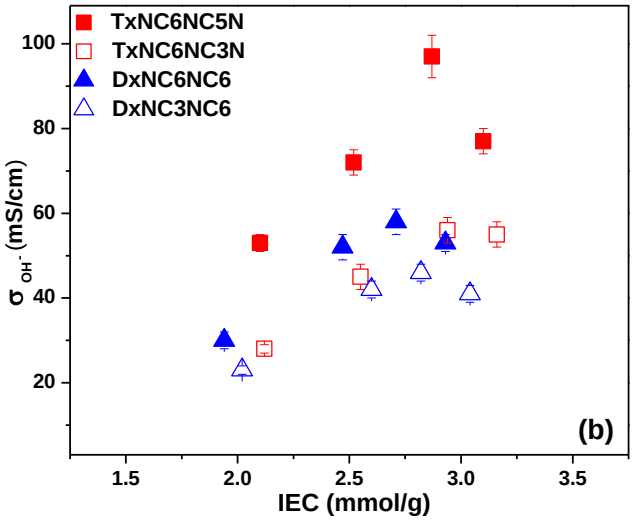

Figure 5.20 Water uptake (a) and Hydroxide conductivity (b) of multication AEMs with different length of spacers at 20 °C as a function of IEC.

As is shown in Figure 5.20a, when some of the linkages between the charges in the multication were shorten than hexyl or amyl to propyl groups, the water uptakes were decreased. Shortening the linkages led to increasing charge densities in cation side chains, which may bring about stronger interactions between AEM chains, thus lowering water uptakes in such materials. Specifically, D35NC3NC6 (IEC = 2.82 mmol/g) and T25NC6NC3N (IEC = 2.94 mmol/g) showed the highest conductivities of 46 and 56 mS/cm when the water uptakes were 159 and 132 wt%, respectively, which were significantly lower than that of the D35NC6NC6 (IEC = 2.71 mmol/g) and T25NC6NC5N (IEC = 2.87 mmol/g) under the same testing conditions (the conductivity for 35N6N6 (IEC = 2.71 mmol/g) and 25N6N5N (IEC = 2.87 mmol/g) were 58 and 97 mS/cm when the water uptake were 187 and 189 wt%, respectively).

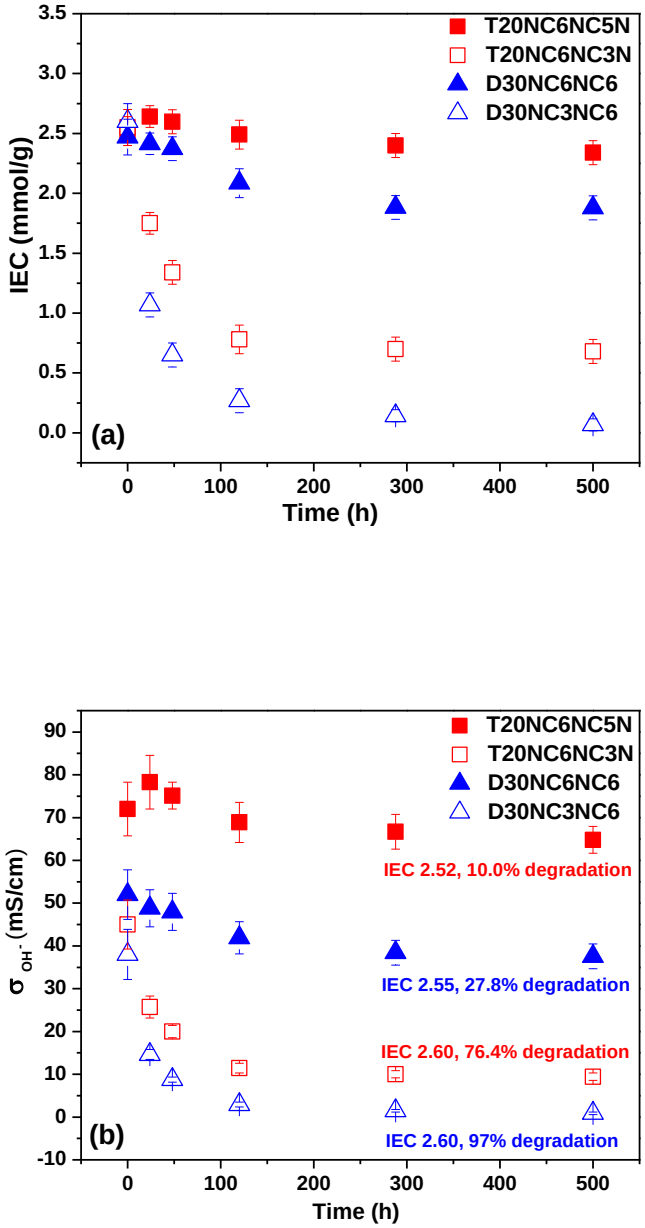

Figure 5.21 Stability of the T20NC6NC5N, T20NC6NC5N, D30NC6NC6, and D30NC3NC6 samples in 1 M NaOH solution at 80 °C; (a) IEC and (b) OH^- conductivity as a function of duration time measured at 20 °C.

In addition to poorer conductivities, shorten the spacers would lead to poorer chemical stability in multication AEMs. The IEC and OH^- conductivity of the triple-cation T20NC6NC5N (IEC = 2.52

mmol/g) remained 93 and 90% of their initials value after the testing of 500 h, while the 20N6N3N (IEC = 2.55 mmol/g) with the similar IEC decreased to 24% of the original value. Similar trend was observed for the double-cation AEMs, which were further proved by the degradation curves showed in Figure 21. Longer spacers for cations resulted larger steric for cations, which helped to keep the cations in T20NC6NC5N and D30NC6NC6 from severe degradations.[36-39] Lower conductivity and poorer stability observed in the multication AEMs with shorter spacers suggested that proper spacers (hexyl or amyl group) were necessary between the cations in the side chains for the rational design of the AEMs.

Fuel cell performance. Selected AEMs, T20NC6NC5N (IEC = 2.52 mmol/g), D30NC6NC6 (IEC = 2.47 mmol/g), and S60NC6 (IEC = 2.60 mmol/g), were evaluated in fuel cells to ascertain the suitability of the materials in real devices.

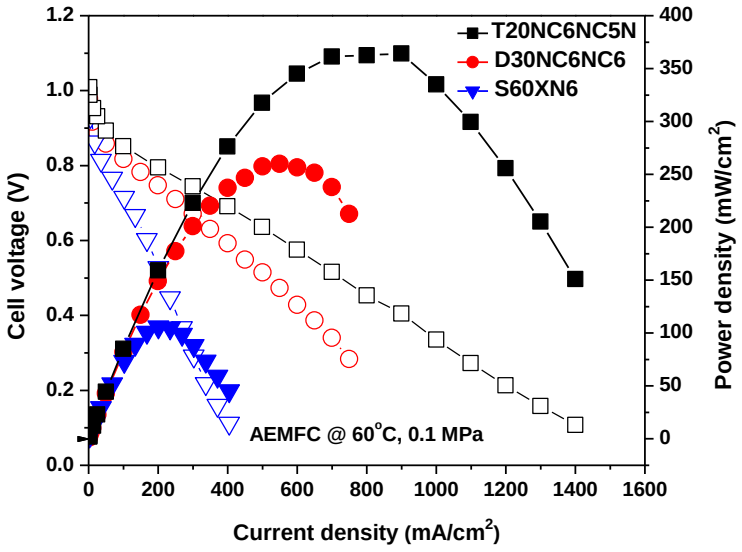

Figure 5.22 Fuel cell performance of the AEM samples under H_2/O_2 conditions.

As is displayed in Figure 5.22, with similar membrane thickness (55 ± 5 μm) and Pt catalyst loading (0.4 mgPt/cm^2 on the anode and cathode), the assembled H_2-O_2 single cells with the same material in the electrode and the membrane show that the AEM influenced the cell performance. Specifically, at a cell operating temperature of 60 °C and gas flow rates of 250 mL/min with back pressure of 0.1 MPa, the

peak power densities for the single-, double-, and triple-cation AEMs were 105.8, 260.1, and 364.2 mW/cm^2 under current densities of 200, 550, and 900 mA/cm^2, respectively. This data demonstrates that the triple-cation AEMs with the highest conductivity were the best performer in fuel cell devices as could be predicted from the ex-situ membrane data.

5.4 Conclusions

In summary, we have designed and synthesized side-chain containing AEMs with one, two or three cations per side chain, enabling a study of how the degree of polymer backbone functionalization and arrangement of cations on the side chain impact AEM properties. Compared with typical AEMs based on the benzyltrimethyl ammonium motif and pendant benzyldimethylhexyl ammonium single cationic group, the muti-cation side chain membranes exhibited much higher ionic conductivity but lower water uptake, due to the phase separation of the hydrophobic domains at low DF and larger ionic clusters induced by the presence of the side chains. When compared with the S60NC6 and BTMA40 single cation membranes, the triple cation T20NC6N5N membrane with a similar IEC showed greater stability and was stable up to 500 h in 1 M NaOH at 80 °C, due to the low backbone DF. More importantly, the TxNC6NC5N membranes with three cations in the side chain showed better properties including lower water uptake, higher ionic conductivity and better alkaline stability compared to DxNC6NC6 membranes with two cations in the side chain.

5.5 References

(1) Noonan, K. J. ; Hugar, K. M. ; Kostalik IV, H. A. ; Lobkovsky, E. B. ; Abruña, H. D. ; Coates, G. W. (2012). *J. Am. Chem. Soc.* **2012**, *134*, 18161.

(2) Hinksman, P.; Isaac, D. H.; Morrissey, P. *Polym. Degrad. Stab*. **2000**, *68*, 299.

(3) Zha, Y.; Disabb-Miller, M. L.; Johnson, Z. D.; Hickner, M. A.; Tew, G. N. *J. Am. Chem. Soc*. **2012**, *134*, 4493.

(4) Thomas, O. D.; Soo, K. J. W. Y.; Peckham, T. J.; Kulkarni, M. P.; Holdcroft, S. *J. Am. Chem. Soc*. **2012**, *134*, 10753.

(5) Deavin, O. I.; Murphy, S.; Ong, A. L.; Poynton, S. D.; Zeng, R.; Herman, H.; Varcoe, J. R. *Energy Environ. Sci*. **2012**, *5*, 8584.

(6) Arges, C. G.; Ramani, V. *Proc. Natl. Acad. Sci. U.S.A.* **2013**, *110*, 2490.

(7) Fujimoto, C.; Kim, D. S.; Hibbs, M.; Wrobleski, D.; Kim, Y. S. *J. Membr. Sci*. **2012**, *423*, 438.

(8) Chempath, S.; Boncella, J. M.; Pratt, L. R.; Henson, N.; Pivovar, B. S. *J. Phys. Chem. C* **2010**, *114*, 11977.

(9) Pan, J.; Li, Y.; Han, J.; Li, G.; Tan, L.; Chen, C.; Zhuang, L. *Energy Environ. Sci.* **2013**, *6*, 2912.

(10) Si, J.; Lu, S.; Xu, X.; Peng, S.; Xiu, R.; Xiang, Y. *ChemSusChem*. **2014**, *7*, 3389.

(11) Li, Q.; Liu, L.; Miao, Q.; Jin, B.; Bai, R. *Chem. Commun.* **2014**, *50*, 2791.

(12) Li, N.; Yan, T.; Li, Z.; Thurn-Albrecht, T.; Binder, W. H. *Energy Environ. Sci.* **2012**, *5*, 7888.

(13) Li, J.; Wang, L.; Shi, F.; Liu, S.; He, Y.; Lu, L.; Ma, X.; Deng, Y. *Catal. Lett*., **2011**, *141*, 339.

(14) Jo, C.; Jung, J.; Shin, H. S.; Kim, J.; Ryoo, R. Angew. *Chem., Int. Ed*. **2013**, *125*, 10198.

(15) Pan, J.; Chen, C.; Li, Y.; Wang, L.; Tan, L.; Li, G.; Tang, X.; Xiao, L.; Lu, J.; Zhuang, L. *Energy Environ. Sci*. **2014**, *7*, 354.

(16) Li, N.; Leng, Y.; Hickner, M. A.; Wang, C.-Y. *J. Am. Chem. Soc.* **2013**, *135*, 10124.

(17) Tanaka, M.; Fukasawa, K.; Nishino, E.; Yamaguchi, S.; Yamada, K.; Tanaka, H.; Bae, B.; Miyatake, K.; Watanabe, M. *J. Am. Chem. Soc*. **2011**, *133*, 10646.

(18) Chen, D.; Hickner, M. A. *Macromolecules* **2013**, *46*, 9270.

(19) Disabb-Miller, M. L.; Zha, Y.; DeCarlo, A. J.; Pawar, M.; Tew, G. N.; Hickner, M. A. *Macromolecules*, **2013**, *46*, 9279.

(20) Disabb-Miller, M. L.; Johnson, Z. D.; Hickner, M. A. *Macromolcules* **2013**, *46*, 949.

(21) Varcoe, J. R.; Slade, R. C. T. *Fuel Cells* 2005, *2*, 187.

(22) Merle, G.; Wessling, M.; Nijmeijer, K. *J. Membr. Sci.* **2011**, *377*, 1.

(23) Chempath, S.; Einsla, B. R.; Pratt, L. R.; Macomber, C. S.; Boncella,J. M.; Rau, J. A.; Pivovar, B. S. *J. Phys. Chem. C* **2008**, *112*, 3179.

(24) Einsla, B. R.; Chempath, S.; Pratt, L. R.; Boncella, J. M.; Rau, J.; Macomber, C.; Pivovar, B. S. *Electrochem. Soc. Trans.* **2007**, *11*, 1173.

(25) Macomber, C. S.; Boncella, J. M.; Pivovar, B. S.; Rau, J. A. *J. Therm.Anal.Calorim.***2008**, *93*, 225.

(26) Pan, J.; Zhu, L.; Han, J.; Hickner, M. A. *Chem. Mater.* **2015**, *27*, 6689**.**

(27) Sata, T.; Tsujimoto, M.; Yamaguchi, T.; Matsusaki, K. *J. Membr. Sci*. **1996**, *112*, 161.

(28) Li, C.; Wang, S.; Wang, W.; Xie, X.; Lv, Y.; Deng, C. *Int. J. Hydrogen Energy*, **2013**, *38*, 11038.

(29) Tomoi, M.; Yamaguchi, K.; Ando, R.; Kantake, Y.; Aosaki, Y.; Kubota, H. *J. Appl. Polym. Sci*. **1997**, *64*, 1161.

(30) Komkova, E. N.; Stamatialis, D. F.; Strathmann, H.; Wessling, M. *J. Membr. Sci*. **2004**, *244*, 25.

(31) Park, J. S.; Park, G. G.; Park, S. H.; Yoon, Y. G.; Kim, C. S.; Lee, W. Y. *Macromol. Symp*., **2007**, 249−250, 174.

(32) Park, J. S.; Park, S. H.; Yim, S. D.; Yoon, Y. G.; Lee, W. Y.; Kim, C. S. *J. Power Sources* **2008**, *178*, 620.

(33) Zeng, L.; Zhao, T. S. *Electrochem. Commun***. 2013**, *34*, 278.

(34) Zhang, Z.; Wu, L.; Varcoe, J.; Li, C.; Ong, A.; Poynton, S.; Xu, T. *J. Mater. Chem. A* **2013**, *1*, 2595.

(35) Hibbs, M. R. *J. Polym. Sci. Polym. Phys*. **2013**, *51*, 1736.

(36) Park, J. S.; Park, G. G.; Park, S. H.; Yoon, Y. G.; Kim, C. S.; Lee, W. Y. *Macromol. Symp*. **2007**, *249*, 174.

(37) Park, J. S.; Park, S. H.; Yim, S. D.; Yoon, Y. G.; Lee, W. Y.; Kim, C. S. *J. Power Sources* **2008**, *178*, 620.

(38) Komkova, E. N.; Stamatialis, D. F.; Strathmann, H.; Wessling, M. *J. Membr. Sci*. **2004**, *244*, 25.

(39) Zeng, L.; Zhao, T. S. *Electrochem. Commun*. **2013**, *34*, 278.

Chapter 6

Poly(2,6-dimethyl-1,4-phenylene oxide)s With Fluorene Side Chains for Anion Exchange Membranes

This chapter is adapted from the manuscript Zhu, L.; Pan, J.; Christensen, *C. M.; Lin Bencai.; Hickner, M. A. submitted to Macromolecules.*

6.1 Introduction

Despite the great importance of robust AEMs to alkaline fuel cell technology, the development of high-performance and long-durability AEMs remains a research challenge.[1] The poor chemical stability of AEMs is still the crucial issue that hinders the practical application of AEMs in fuel cells operating at high pH and elevated temperature.[1] Currently, there are only a few reports where AEMs containing quaternary ammonium (QA) cationic groups are stable under long-term alkaline conditions above 80 °C.[1,2]

Recently, AEMs containing fluorenly groups have been proven to not only have good chemical, thermal and chemical stability, but these types of AEMs have also been shown to have high hydroxide ion conductivity.[3-8] For example, Miyatake,[3] *et al.* found that quaternized multiblock copolymers containing fluorene units demonstrated good hydroxide ion conductivities and stability at 80 °C. The fluorene-based hydroxide ion conducting AEMs synthesized by Bae,[4] *et al.* exhibited excellent chemical stability after treatment in 1 M NaOH solution at 80 °C for 30 days. Although enhanced ionic conductivity and chemical stability was observed, the cost of the fluorene monomer and the need to custom-synthesize these polymers may hinder these AEMs in wide-spread applications. Recently, it was reported that the addition of an interstitial spacer between the charged group and the aromatic ring obviously enhanced the stability of

tetraalkylammonium cations.[4,9-12] Additionally, a study of polymer degradation of AEM backbones demonstrated that poly(phenylene oxide) provided a more stable polymer backbone than poly(sulfone) architectures at elevated temperature.[13] Thus, it is desirable to obtain a poly(2,6-dimethyl-1,4-phenylene oxide) (PPO) based n-alkyl interstitial spacers tetraalkylammonium cations AEMs, which can demonstrate both high hydroxide ion conductivity and excellent chemical stability.

Suzuki-Miyaura coupling is arguably the most important and powerful transformation for construction of carbon-carbon bonds in modern organic chemistry.[47] Moreover, it is now possible to couple hindered substrates by using efficacious supporting ligands and an appropriate catalytic/ligand system.[14] For example, Buchwald,[14] *et al.* reported a Suzuki-Miyaura coupling of aryl and heteroaryl halides with aryl-, heteroaryl-boronic acids that proceeded in good yield with the use of 2-(2',6'-dimethoxybiphenyl)-dicyclohexylphosphine. This ligand facilitated the preparation of extremely hindered biaryls in a good yield with low catalyst levels. Herein, we present a facile synthetic strategy for synthesis of fluorene side chain PPO AEMs containing QA cationic groups via the Suzuki-Miyaura coupling reaction.

6.2 Experimental Section

Materials. Poly(2,6-dimethyl-1,4-phenylene oxide) was purchased from Sigma-Aldrich and dried under vacuum at room temperature overnight. 2-Bromofluorene, 1,6-dibromohexane, bis(pinacolato)diboron, tetrabutylammonium bromide, potassium acetate, palladium acetate, SPhos, XPhos, [1,1′ bis(diphenylphosphino)ferrocene]dichloropalladium(II), and bromine were obtained from Sigma-Aldrich and used as received. The aromatic brominated PPO polymers with

different degrees of bromination (DB) ranging from 30 to 60% were synthesized according to the reported literature.[15]

Synthesis of 2-Bromo-9, 9-bis(6'-bromohexyl) fluorene.[16] 1,6-dibromohexane (47.6 g, 187 mmol, 30 mL) was added to a mixture of 2-bromofluorene (5 g, 15 mmol) and tetrabutylammonium bromide (0.1 g, 0.3 mmol). Subsequently, 50% (wt %) sodium hydroxide aqueous solution (30 mL) was added to the mixture. The reaction mixture was stirred at 65 °C for 7 h. An excess of dichloromethane was added, the organic layer was washed with water and brine, and dried over magnesium sulfate. After evaporation of the dichloromethane, the residual liquid reagent was removed under vacuum. The crude product was purified by column chromatography over silica gel with hexane as the eluent to give a colorless liquid (yield 80%). ^{1}H NMR (300 MHz, $CHCl_3$-d_1, δ in ppm): 7.26-7.70 (m, 6H, Ar-*H*), 3.25-3.32 (t, 4H, -C*H*$_2$Br), 1.90-2.02 (t, 4H, Ar-C*H*$_2$), 0.61-1.73 (m, 16H, -CH_2-C*H*$_2$-CH_2-).

Synthesis of 2-dioxaborolane-9, 9-bis(6'-bromohexyl) flurorene.[16] Under an argon atmosphere, bis(pinacolato)diboron (5.91 g, 23.27 mmol), 2-bromo-9, 9-bis(6'-bromohexyl) fluorene (8.86 g, 15.51 mmol), KOAc (3.81 g, 38.78 mmol), and Pd(dppf)Cl_2 (0.126 g, 0.155 mmol) were dissolved in dioxane (100 mL) and heated to 75 °C for 12 h. After the reaction solution was cooled to room temperature, the reaction mixture was poured into water. The aqueous phase was extracted with dichloromethane, and the combined organic layers were dried over magnesium sulfate. The solvent was removed under vacuum. The crude product was purified by column chromatography over silica gel with hexane/dichloromethane as the eluent to give a light white solid (yield 78%). ^{1}H NMR (300MHz, $CHCl_2CHCl_2$-d_2, δ in ppm): 7.26-7.70 (m, 6H, Ar-*H*), 3.25-3.32 (t, 4H, -C*H*$_2$Br), 1.92-2.03 (t, 4H, Ar-C*H*$_2$), 1.25-1.36 (s, 12H, -C(C*H*$_3$)$_2$-), 0.58-1.67 (m, 16H, -CH_2-C*H*$_2$-CH_2-).

Polymer synthesis.[15] Aromatic brominated PPO (0.2 g, 1.32 mmol) with a degree of bromination (DB, the mol % of brominated repeat units on the PPO backbone) of 40 was dissolved in a mixture of 8 mL toluene and 0.8 mL water under an argon atmosphere at room temperature. Then, 2-dioxaborolane-9,9-bis(6'-bromohexyl) fluorene (0.48 g, 0.78 mmol), K_3PO_4 (0.22 g, 1.00 mmol), $Pd(OAc)_2$ (6 mg, mmol), and XPhos (20.0 mg, 0.04 mmol) were added under an argon atmosphere. The mixture was stirred at 100 °C for 24 h under argon. The reaction solution was poured into 50 mL methanol to precipitate the polymer. The product was filtered and further washed with methanol several times. A light white powder (PPO-fluorene) was obtained and dried at 50 °C under vacuum overnight. The PPO-fluorene with a DB of 0.4 (0.48 g, 1.56 mmol) was dissolved in 10 mL of *N*-methyl-pyrrolidone (NMP). Then, 0.67 mL trimethylamine (2.50 mmol) solution (31-35 wt %) in ethanol was added slowly. The mixture was stirred at 50 °C for 24 h. The obtained solution was poured into 100 mL toluene or hexane to precipitate the polymer. The product was filtered and further washed with hexane and toluene several times. A light yellow powder was collected and dried at 60 °C under vacuum overnight. The resulting product was fluorene side chain PPO (40PPOFC6N, where the 40 refers to the degree of aromatic bromination where 40 mol % of the PPO repeat units are brominated; the F stands for the fluorene side chain; the C6 indicates that the cation spacer is six carbons; and the N represents quaternary ammonium group (N^+C_4) in the side chains) with a yield of 87% in the bromide counterion form. For the synthesis of 40PPOFC6NC6 (where the 40 refers to the degree of bromination; the F stands for the fluorene side chain; the C6 indicates that the cation spacer is six carbons; the N represents quaternary ammonium group (N^+C_4) in the side chains, the second C6 represents a pendant C6 alkyl chain from the cation), the PPO-fluorene with a DB of 40 (0.48 g, 1.56 mmol) was dissolved in 10 mL of *N*-methyl-pyrrolidone (NMP). Then, *N*, *N*-dimethylhexylamine (0.24 g, 1.87 mmol) was added slowly. The mixture was stirred at 60 °C for

48 h. The obtained solution was poured into 100 mL toluene or hexane to precipitate the polymer. The polymer was further purified prepared via the methods described above.

Fabrication of membranes. The 40PPOFC6N polymer (0.20 g) in the bromide form was dissolved in NMP (5 mL) to yield a 4 wt % solution. The solution was then cast onto a leveled PTFE mold and dried at 82 °C under ambient pressure for 24 h followed by vacuum drying for another 24 h at 80 °C to give a transparent, tough film (60 ± 5 μm in thickness). The 40PPOFC6NC6 membrane was prepared as described above.

6.3 Results and Discussion

Herein we present a facile strategy for the synthesis of fluorene side chain containing AEMs with quaternary ammonium cationic groups and poly(2,6-dimethyl-1,4-phenylene oxide) backbones, Scheme 6.1.

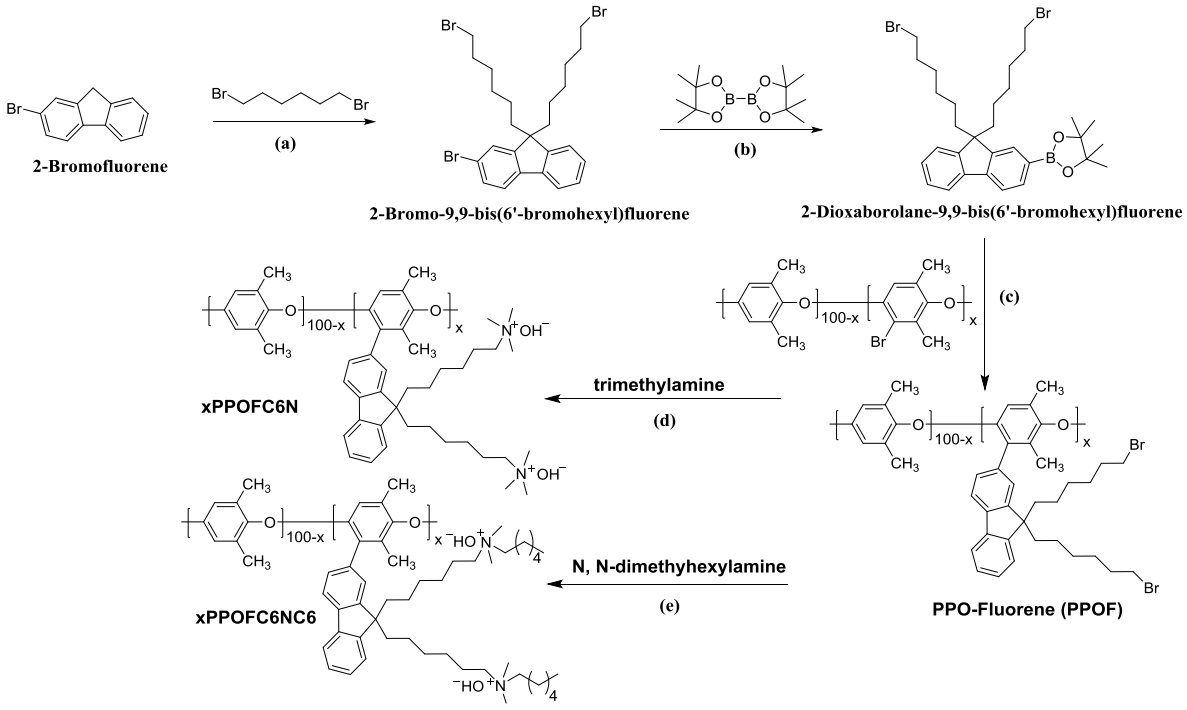

Scheme 6.1 Synthetic route for fluorene side chain ionomers. (a) 50 wt % NaOH, tetrabutylammonium, 65 °C, 7 h; (b) Pd(dppf)Cl_2, KOAc, dioxane, 75 °C, 12 h; (c) Pd$(OAc)_2$, K_3PO_4, XPhos, toluene/water, 100 °C, 24 h; (d) 50 °C, 24 h; (e) 60 °C, 72 h.

We developed a novel PPO derivative (PPOF) with a pendant fluorene-based side-chain via Suzuki coupling. The brominated poly(2,6-dimethyl-1,4-phenylene oxide)s possessing different degrees of bromination (DB) at the aromatic ring were synthesized using bromine according to literature procedures.[15] The PPOFs were successfully obtained by reaction of aryl bromine and boronated fluorene with excellent yield (≥95%). The fluorene side-chain containing AEMs were realized by the Menshutkin reaction of the olefinic amine with the alkyl bromide group of the PPOF residue.[2] Brominated PPOs with the bromine functionality residing on the aromatic ring (Ar-BrPPOs) with DBs ranging from 30 to 60 (30 to 60 mol % of the PPO repeat units functionalized) were prepared to obtain samples with calculated IECs ranging from 1.77 to 2.26 mmol/g (Table 6. 3).

Table 6.1 Suzuki-Miyaura couplings of aryl bromide of PPO with boronic acid.

Entry[a]	Catalyst	Ligand	Mol% Pd	Condition	NMR Conv.(%)
1	$Pd(OAc)_2$	-	0.9	24 h	30
2	$Pd(OAc)_2$	-	2.7	24 h	35
3	$Pd(OAc)_2$	-	0.9	48 h	33
4	$Pd(OAc)_2$	SPhos	0.9	24 h	93
5	$Pd(OAc)_2$	XPhos	0.9	24 h	96

[a]Reaction conditions:1equiv of aryl bromide, 1.5 equiv of boronic acid, 2 equiv of K_3PO_4, 0.07 equiv of ligand, 100 °C.

Table 6.2 Mechanical properties of hydrated PPOF and BTMA30 AEMs.

Sample	Tensile strength (MPa)	Elongation at break (%)
50PPOFC6N	14	18.4
50PPOFC6NC6	16	21.7
BTMA30	24	51.7

Table 6.3 Ion exchange capacity, water uptake, swelling and ionic conductivity of PPOF AEMs.

sample	IEC (mmol/g)[a]	IEC (mmol/g)[b]	WU (wt%) (OH^-)[c]	WU (wt%) (HCO_3^-)[c]	WU (wt%) (Cl^-)[c]	σ (mS/cm) (OH^-)[c]	σ (mS/cm) (HCO_3^-)[c]	σ (mS/cm) (Cl^-)[c]	λ (OH^-)	in-plane swelling (%)[c]
30PPOFC6N	1.97	1.84	63 ± 3	32 ± 2	28 ± 1	25 ± 3	7 ± 1	10 ± 1	19	15
40PPOFC6N	2.19	2.05	85 ± 5	62 ± 3	44 ± 3	32 ± 2	8 ± 1	12 ± 1	23	21
50PPOFC6N	2.34	2.16	102 ± 6	77 ± 5	59 ± 4	37 ± 3	9 ± 1	13 ± 2	26	24
60PPOFC6N	2.46	2.26	123 ± 9	98 ± 6	73 ± 5	40 ± 3	10 ± 1	14 ± 2	30	29
30PPOFC6NC6	1.77	1.60	57 ± 3	28 ± 2	25 ± 2	31 ± 1	8 ± 1	12 ± 1	20	16
40PPOFC6NC6	1.94	1.77	76 ± 8	54 ± 5	40 ± 3	36 ± 3	10 ± 1	13 ± 2	24	20
50PPOFC6NC6	2.06	1.89	97 ± 9	65 ± 4	51 ± 3	42 ± 2	12 ± 1	15 ± 2	28	23
60PPOFC6NC6	2.11	1.93	116 ± 8	83 ± 5	66 ± 4	46 ± 4	13 ± 1	16 ± 1	33	27

[a]Calculated from the polymer composition and the degree of bromination. [b]Titrated values. [c]Measured at room temperature in liquid water.

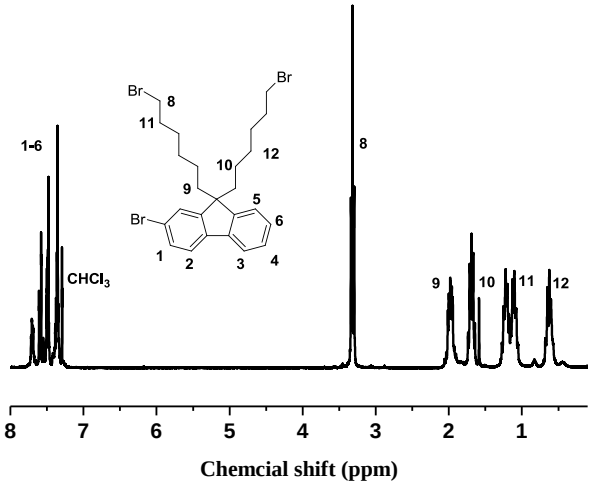

Figure 6.1 ^{1}H NMR of 2-bromo-9, 9-bis(6'-bromohexyl) fluorene in $CHCl_3$-d_1.

The purity and chemical structures of 2-bromo-9, 9-bis(6'-bromohexyl) fluorene and 2-dioxaborolane-9, 9-bis(6'-bromohexyl) fluorene were confirmed by ^{1}H NMR spectroscopy. Figure 6.1 shows the expected chemical shifts and intensities for the pure 2-bromo-9, 9-bis(6'-bromohexyl) fluorene. The appearance of the proton resonance arising from the bromoalkyl moiety at 3.3 ppm along with the appearance of new peaks at 0.7-1.8 ppm assigned to alkyl chains indicated that 2-bromofluorene were successfully alkylated with 1,6-dibromohexane to give the desired product.

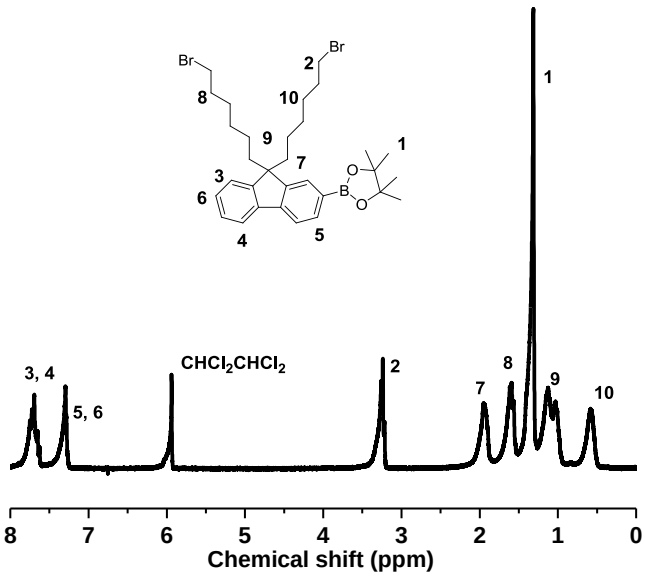

Figure 6.2 ^{1}H NMR of 2-dioxaboralane-9, 9-bis(6'-bromohexyl)fluorene in $CHCl_2CHCl_2$-d_2.

The 2-bromo-9, 9-bis(6'-bromohexyl) fluorene was transformed into the 2-dioxaborolane-9, 9-bis(6'-bromohexyl) fluorene using the Miyaura reaction. The chemical structure of the 2-dioxaborolane-9, 9-bis(6'-bromohexyl) fluorene is shown in Figure 6.2. The chemical shift of the methyl groups were observed at 1.4 ppm, which demonstrates the formation of the boronic ester. Suzuki-Miyaura cross-coupling has been a powerful tool for biaryl formation and with the use of proper ligands and this reaction for hindered biaryls can proceed in excellent yield. Using proper ligands, as shown in Table 1 (entry 4 and 5), efficient coupling reactions with small amounts of palladium can be achieved between the hindered fluorene unites and brominated PPO. For example, the coupling of 2-dioxaborolane-9, 9-bis(6'-bromohexyl) fluorene with brominated PPO using XPhos as ligand at 100 °C for 24 h provided a 96 % isolated yield of product (Table 1, entry 5). In contrast, only 30 % isolated yield was observed (Table 1, entry 1) under similar conditions without ligands. Additionally, only 3 and 5 % increased isolated yield were observed,

when the reaction time extended from 24 to 48 h and the loading of palladium was increased from 0.9 to 2.7 mol %, respectively (Table 1, entry 3 and 2).

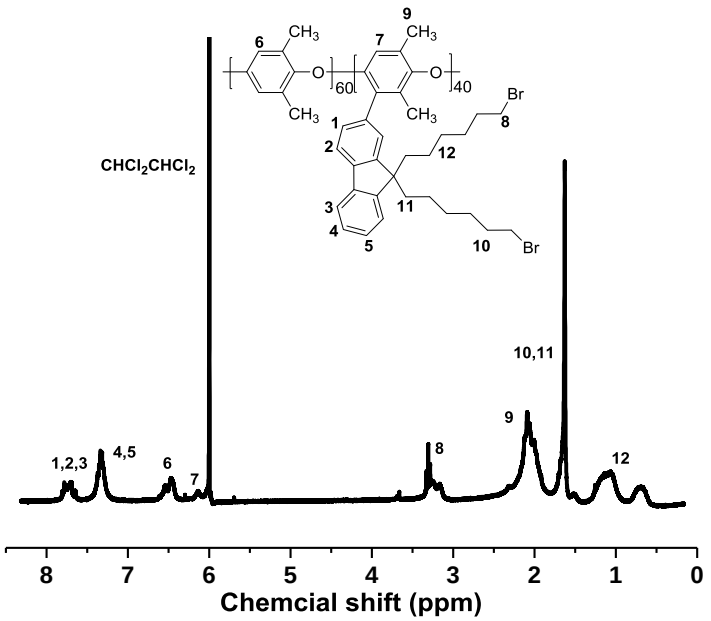

Figure 6.3 ^{1}H NMR of 40PPO-flurorene (PPOF) in $CHCl_2CHCl_2$-d_2.

The chemical structure of the PPOF was characterized and confirmed by ^{1}H NMR spectroscopy (Figure 6.3). The disappearance of the sharp peak at 1.4 ppm assigned to the methyl protons of boronic ester demonstrated a successful cross-coupling reaction. The integral value of peaks (6.0-6.5 ppm) assignable to the aromatic protons of PPO backbone was proportional to the integrated value of the peaks at 7.3-7.7 ppm assigned to the aromatic protons of fluorene, suggesting the complete grafting of fluorene side chains to the PPO backbones.

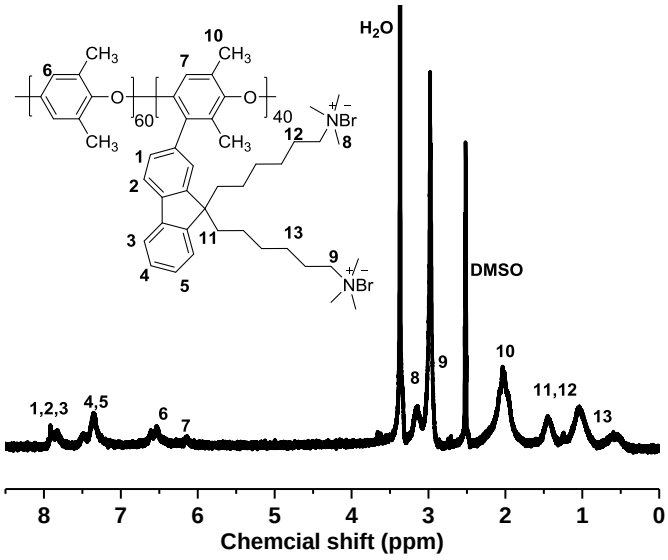

Figure 6.4 ^{1}H NMR of 40PPOFC6N in DMSO-d_6.

Figure 6.4 illustrates the ^{1}H NMR spectrum for the 40PPOFC6N sample containing pendant ammonium groups. Chemical shifts of the fluorene side chain units were observed at 7.3-7.7 ppm. The peaks assigned to methyl protons of quaternary ammonium groups appeared at 3.1-3.4 ppm, which were absent in the ^{1}H NMR spectra of the precursor 40PPOF, suggesting the successful Menshutkin reaction of the olefinic amine with bromide group of PPOF.

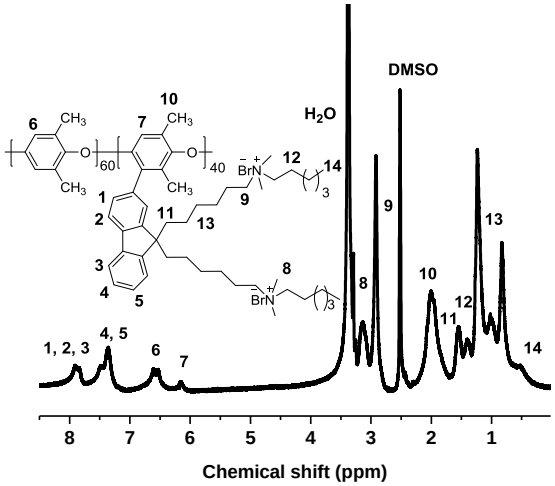

Figure 6.5. ^{1}H NMR of 40PPOFC6NC6 in DMSO-d_6.

The purity and chemical structures of 40PPOFC6NC6 was confirmed by ^{1}H NMR spectroscopy in a similar manner as shown in Figure 6.5.

Mechanical properties. The comparison of mechanical properties between AEMs with different structures and compositions are shown in Table 6.2. The tensile strength of 50PPOFC6N and 50PPOFC6NC6 in hydroxide form are 14 and 16 MPa, respectively, with elongation at breaks of 18.4 % and 21.7 %. Compared to BTMA30, AEMs in this study showed lower tensile strength and elongation at break due to the rigid fluorene side chain of PPOF membranes. However, the mechanical properties are likely to be sufficient for fuel cell applications. [17]

Water uptake. Table 6.3 lists the water uptake and swelling ratio of the PPOF membranes in hydroxide form at 20 °C in liquid water. As expected, the PPOF samples absorbed more water with increasing IEC due to the higher ionic content of the membranes.

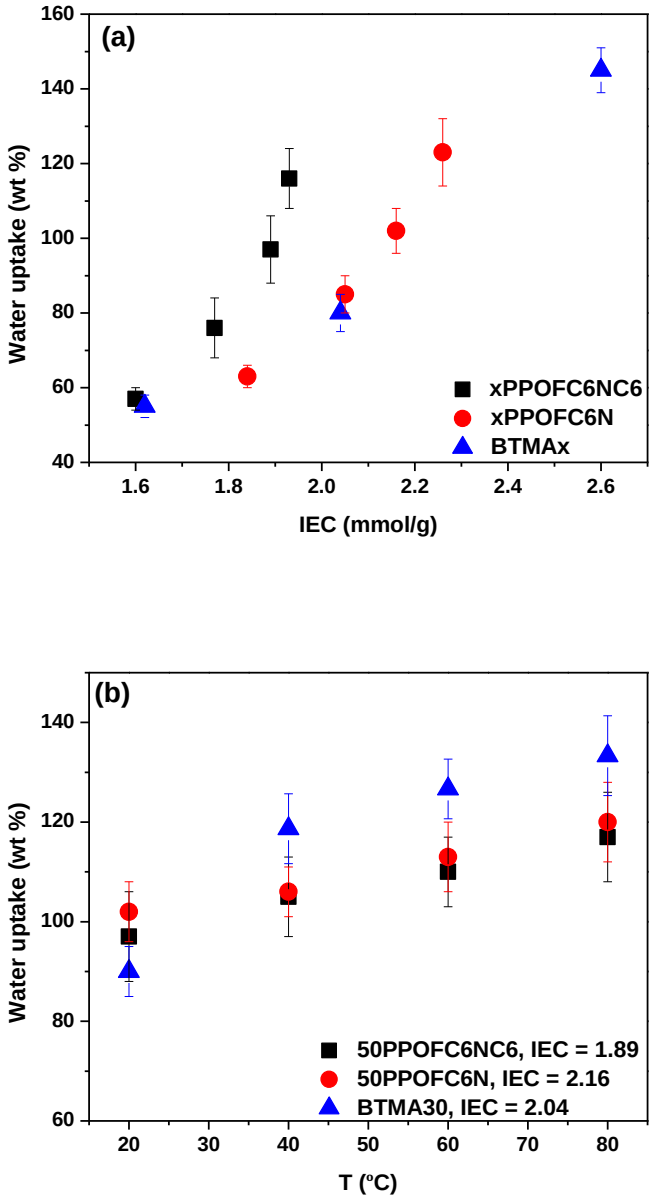

Figure 6.6 Liquid water uptake of membranes in OH^- form as a function of (a) IEC and (b) temperature.

The water uptake of the PPOF membranes was plotted as function of IEC and temperature in Figure 6.6. Compared with the BTMAx membranes (AEMs based on the benzyltrimethyl ammonium motif), the water uptake of PPOF membranes had a similar trend

with increasing water content with increasing IEC. Although all of the samples with a similar IEC showed an increase in water uptake upon elevating the temperature, PPOF membranes exhibited a much lower increase in water uptake with increasing temperature. For example, 50PPOFC6N had water uptake of 102 wt % at room temperature, and the water uptake rose to 120 wt % at 80 °C. However, a large water uptake increment, 43%, from 90 wt % to 133 wt %, was observed for the BTMA30 sample when the temperature was increased from 20 to 80 °C. These results indicated that the PPOF membranes have much more dimensional stability than that of BTMA membranes at elevated temperature due to the presence of rigid fluorene side chains.[4]

Ionic transport. Similar to the water uptake, the hydroxide ion conductivity of the PPOF membranes increased with greater IEC due to the higher water content which facilitated the ionic transport.

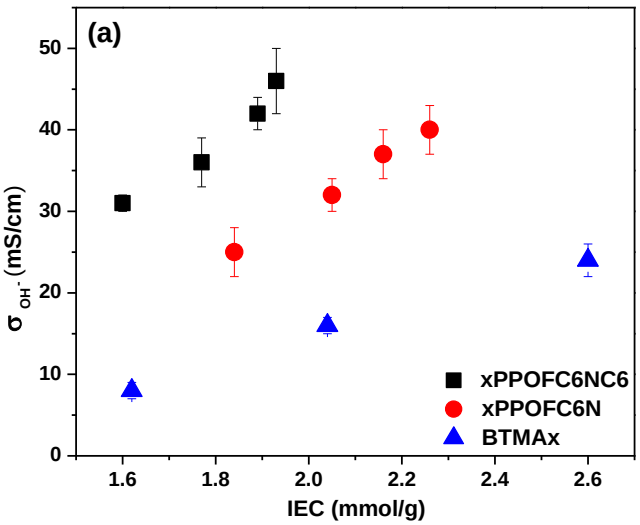

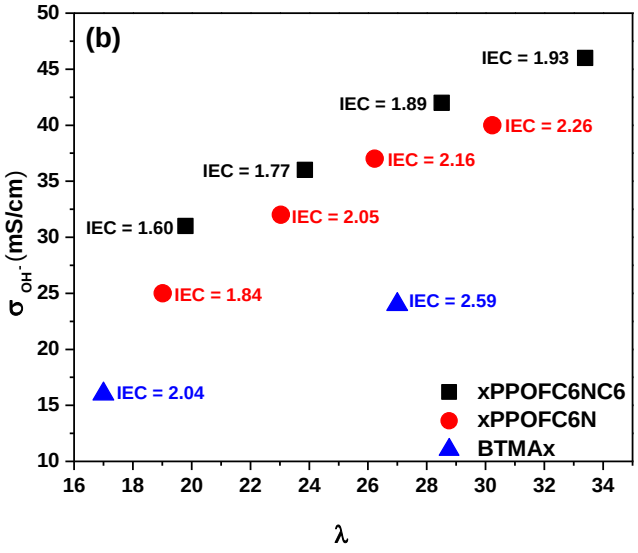

Figure 6.7 Hydroxide conductivity of PPOF and BTMA40 membranes in liquid water at 20 °C as a function of (a) IEC (in mmol/g) and (b) hydration number (λ).

When comparing the ionic conductivity of PPOF and BTMA membranes, the PPOF membranes demonstrated much higher conductivity than that of BTMA samples under the same IEC values. For example, the 60PPOFC6NC6 with IEC = 1.93 mmol/g exhibited the highest OH^- conductivity (46 mS/cm), which was nearly three times higher than that of BTMA30 (16 mS/cm) with IEC = 2.04 mmol/g. We attributed the higher hydroxide conductivities of PPOFC6NC6 to their higher water uptake under the same IEC values (Figure 6.7a). For a better comparison among the different IEC membranes, the hydroxide conductivity was plotted as function of λ in Figure 6.7b (the number of absorbed water molecules per ammonium group). The approximate trend was that the hydroxide conductivity increased with λ due to the increased number of water molecules per ionic site which facilitates the hydroxide transport in the membranes. As shown in Figure 6.7b, PPOF membranes showed much larger hydroxide conductivity than BTMA*x* membranes under a given hydration number (λ). For example, 50PPOFC6NC6 with λ = 28

demonstrated a hydroxide conductivity of 42 mS/cm, while the BTMA40 with λ = 27 showed much lower hydroxide conductivity of 24 mS/cm.

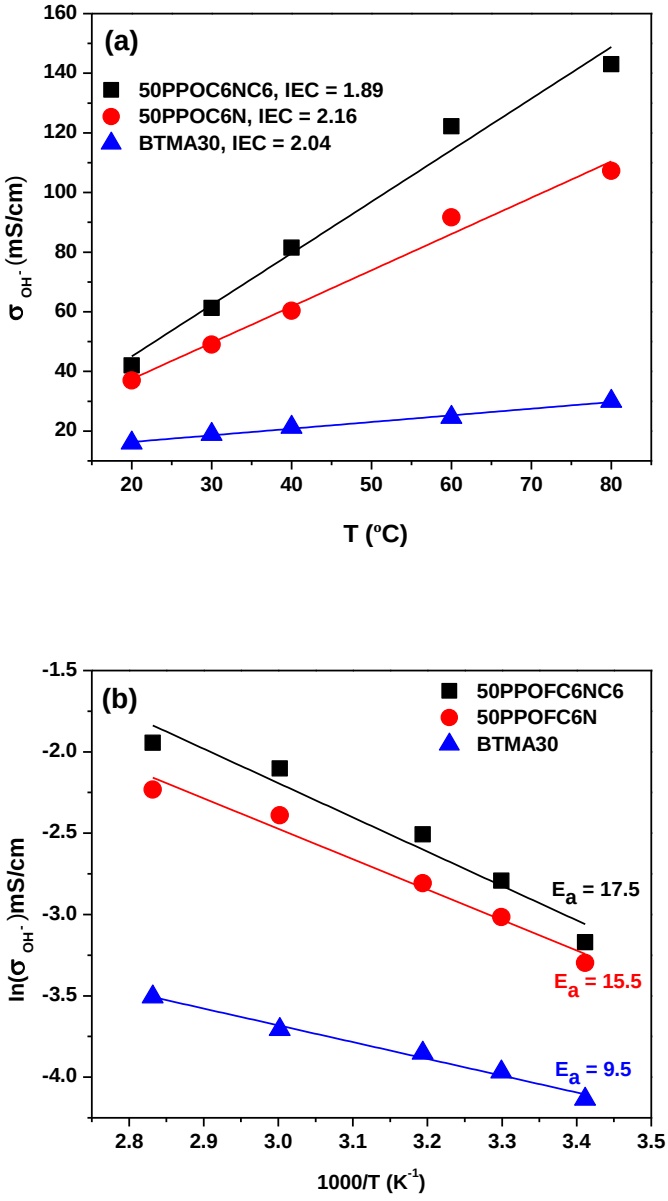

Figure 6.8 Hydroxide conductivity of PPOF and BTMA40 membranes (a) as a function of temperature and (b) Arrhenius-type temperature plot showing activation energies in kJ/mol.

The hydroxide ion conductivity of membranes under the operating temperature of the cell is of significant importance to the performance of the device. The temperature dependence of the OH^- conductivities of PPOF and BTMA30 membranes with similar IEC in water is illustrated in Figure 6.8a. The 50PPOFC6NC6 sample exhibited the highest OH^- conductivity (176 mS/cm) at 80 °C, which was nearly four times higher than that of BTMA40 under the same conditions and significantly higher than in previous reports.[4,10-12] For example, Dang,[10] *et al.* reported phase separated PPO-7Q AEMs exhibiting hydroxide conductivity of 35 mS/cm at 20 °C and higher than 85 mS/cm at 80 °C in water. The fluorene-based AEMs synthesized by Lee,[4] *et al.* exhibited hydroxide conductivity up to 124 mS/cm at 80 °C with IEC = 3.59 mmol/g. The gQAPPO reported by Yang,[11] *et al*. exhibited hydroxide conductivity of 27 mS/cm and 63 mS/cm at 30 and 70 °C, respectively. As shown in Figure 6.8b, the OH^- conductivities of the membranes with similar IEC showed an approximate Arrhenius-type temperature-dependence promoted by the thermal activation of water motion.[18] The apparent activation energy of conduction estimated from the slopes of the ln σ vs 1000/T curves was ~10 kJ/mol and was similar among the measured samples. The apparent activation energy of the tested membranes was comparable or somewhat lower than those of reported AEMs (10 – 23 kJ/mol), indicating that PPOF membranes have similar aqueous OH^- conduction attributes to other membrane samples.[18]

Alkaline stability. Due to its strong nucleophilicity, hydroxide (OH^-) degradation of the cationic groups and polymer backbones are a major concern.[4] Examples of known pathways for the degradation of tetraalkylammonium ions under alkali conditions include β-hydrogen (Hofmann) elimination, direct nucleophilic substitution at the α-carbon, and nitrogen ylide formation.[19-23] We investigated the long-term alkali stability of PPOF membranes by immersing the samples in argon-saturated 1 M NaOH solution at 80 °C.

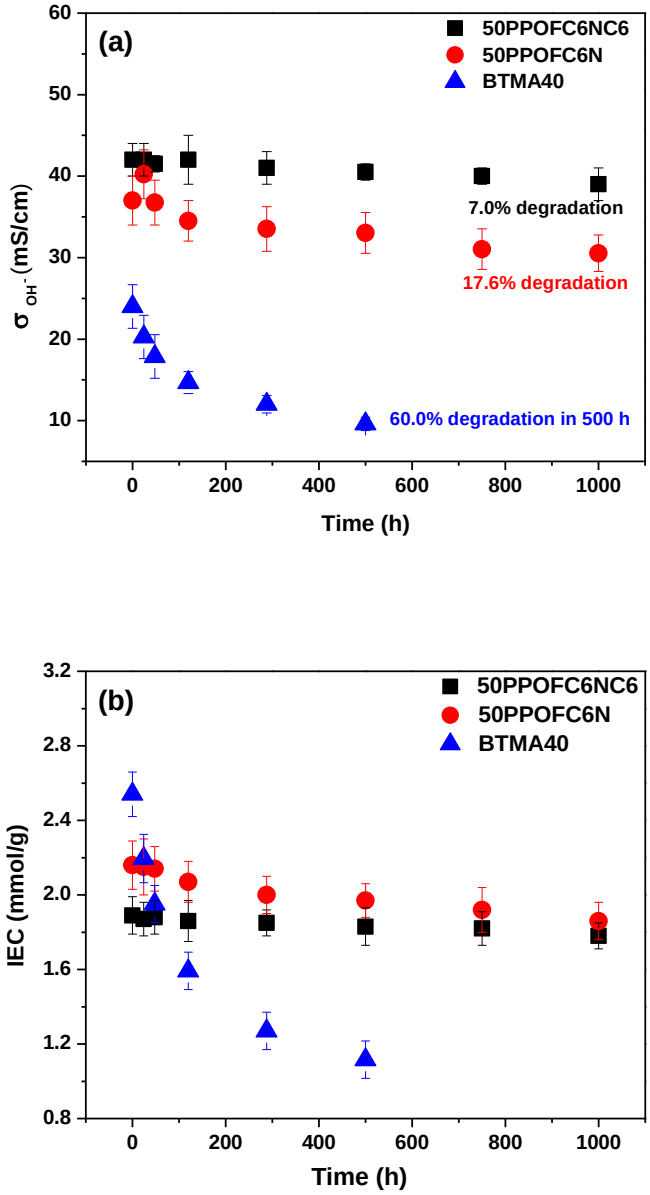

Figure 6.9 Chemical stability of the quaternary ammonium cation in 50PPOC6NC6, 50PPOC6N, and BTMA40 during immersion in 1 M NaOH solution at 80 °C. (a) OH^- conductivity measured at 20 °C and (b) IEC as a function of time.

The degradation of the membranes was evaluated by measuring the change in IEC values and the OH^- conductivities as a function of degradation time. As shown in Figure 6.9a, BTMA40 with tethered benzyltrimethyl ammonium cations exhibited poor chemical stability and lost 60% of its initial ion conductivity after just 500 h of testing. However, the fluorene-containing membranes maintained good hydroxide conductivity even after 1000 h immersion in 1 M NaOH at 80 °C. For example, only 7.0 % hydroxide conductivity degradation in 50PPOC6NC6 was observed after the testing period, which clearly indicates that the fluorene containing AEMs have excellent stability in alkaline conditions. The alkaline stability of the samples was further evaluated by measuring the changes in IEC via titration. As shown in Figure 6.9b, the changes in IEC of the membranes were in good correspondence with the decrease of hydroxide ion conductivity, further suggesting the thermochemical stability of the fluorene-containing AEMs. Compared to BTMA40, the obviously enhanced chemical stability of 50PPOC6N was attributed to the addition of an interstitial spacer since the substitution at the benzyl position was the major degradation route for BTMA40. In addition, the 50PPOFC6NC6 demonstrated higher thermochemical stability than that of 50PPOFC6N because of the addition of the bulky alkyl pendant group, which has been demonstrated previously to enhance AEM stability.[2, 24]

6.4 Conclusions

In summary, we have designed a method for functionalization of PPO by grafting hindered fluorene side chains via a Suzuki-Miyaura cross-coupling reaction using a ligand designed for sterically hindered substrates. Base on the functional PPO, we synthesized fluorene side chain-containing AEMs with attached alkyltrimethyl quaternary ammonium cationic groups Menshutkin reaction. The Suzuki-Miyaura cross-coupling reaction of aryl bromides with fluorene-boronic acids was nearly complete demonstrating the usefulness of this reaction for

polymer post-polymerization modification. Casting from NMP solutions, flexible and tough AEMs were obtained. The 50PPOFC6NC6 sample with an IEC = 1.89 mmol/g showed high OH^- conductivity (176 mS/cm) at 80 °C in liquid water. Compared to BTMA-based AEMs, the PPOF AEMs exhibited good long-term alkaline stability at 80 °C, which is critical for alkaline fuel cell applications. This stability is likely due to the separation of the cationic group from the polymer backbone by an alkyl spacer. Additionally, the presence of long alkyl pendant chains is effective for enhancing the thermochemical stability of the AEMs. The PPOF AEMs showed excellent solubility in solvents such as dimethyl formamide, dimethyl sulfoxide and methanol at room temperature, making them as useful candidates for ionomer materials. The results of this study provide a new approach for functionalization of PPO and design of high performance AEMs for application in alkaline fuel cells.

6.5 References

(1) Lee, W. H.; Mohanty, A. D.; Bae, C. *ACS Macro Lett*. **2015**, *4*, 453.

(2) Li, N.; Leng, Y.; Hickner, M. A.; Wang, C.-Y. *J. Am. Chem. Soc.* **2013**, *135*, 10124.

(3) Tanaka, M.; Fukasawa, K.; Nishino, E.; Yamaguchi, S.; Yamada, K.; Tanaka, H.; Bae, B.; Miyatake, K.; Watanabe, M. *J. Am. Chem. Soc*. **2011**, *133*, 10646.

(4) Lee, W. H.; Mohanty, A. D.; Bae, C. *ACS Macro Lett*. **2015**, *4*, 453.

(5) Seo, D. W.; Hossain, M. A.; Lee, D. H.; Lim, Y. D.; Lee, S. H.; Lee, H. C.; Hong, T. W.; Kim, W. G. *Electrochim. Acta*. **2012**, *86*, 360.

(6) Tanaka, M.; Koike, M.; Miyatake, K.; Watanabe, M. *Macromolecules* **2010**, *43*, 2657.

(7) Han, G. L.; Xu, P. Y.; Zhou, K.; Zhang, Q. G.; Zhu, A. M.; Liu, Q. L. *J. Membr. Sci*. **2014**, *244*, 29.

(8) Lin, B.; Qiu, L.; Qiu, B.; Peng, Y.; Yan, F. *Macromolecules* **2011**, *44*, 9642.

(9) Tomoi, M.; Yamaguchi, K.; Ando, R.; Kantake, Y.; Aosaki, Y.; Kubota, H. *J. Appl. Polym. Sci*. **1997**, *64*, 1161.

(10) Dang, H. S.; Weiber, E. A.; Jannasch, P. *J. Mater. Chem. A*, **2015**, *3*, 5280.

(11) Yang, Z.; Zhou, J.; Wang, S.; Hou, J.; Wu, L.; Xu, T. *J. Mater. Chem. A*, **2015**, *3*, 15015.

(12) Dang, H. S.; Jannasch, P. *Macromolecules* **2015**, *48*, 5742.

(13) Amel, A.; Zhu, L.; Hickner, M.; Ein-Eli, Y. *J. Electrochem. Soc*. **2014**, *161*, F615.

(14) Barder, T. E.; Walker, S. D.; Martinelli, J. R.; Buchwald, S. L. *J. Am. Chem. Soc.* **2005**, *127*, 4685.

(15) Bonfanti, C.; Lanzini, L.; Roggero, A.; Sisto, R. *J. Polym. Sci., Part A: Polym. Chem*. **1994**, *32*, 1361.

(16) Jo, J.; Chi, C.; Höger, S.; Wegner, G.; Yoon, D. Y. *Chem.-Eur. J.* **2004**, *10*, 2681.

(17) Pan, J.; Chen, C.; Zhuang, L.; Lu, J. *Acc. Chem. Res.* **2011**, *45*, 473.

(18) Chen, D.; Hickner, M. A. *Macromolecules* **2013**, *46*, 9270.

(19) Varcoe, J. R.; Slade, R. C. T. *Fuel Cells* **2005**, *2*, 187.

(20) Merle, G.; Wessling, M.; Nijmeijer, K. *J. Membr. Sci.* **2011**, *377*, 1.

(21) Chempath, S.; Einsla, B. R.; Pratt, L. R.; Macomber, C. S.; Boncella,J. M.; Rau, J. A.; Pivovar, B. S. *J. Phys. Chem. C* **2008**, *112*, 3179.

(22) Einsla, B. R.; Chempath, S.; Pratt, L. R.; Boncella, J. M.; Rau, J.; Macomber, C.; Pivovar, B. S. *Electrochem. Soc. Trans.* **2007**, *11*, 1173.

(23) Macomber, C. S.; Boncella, J. M.; Pivovar, B. S.; Rau, J. A. *J. Therm.Anal.Calorim.***2008**, *93*, 225.

(24) Chempath, S., Boncella, J. M., Pratt, L. R., Henson, N., Pivovar, B. S. *J. Phys. Chem. C*, **2010**, *114*, 11977.

Chapter 7

Hydrophilic Robust Anion Exchange Membranes

7.1 Introduction

Compared to their counterpart PEMs, AEMs generally exhibit inferior properties, such as lower mobility of OH^- and less developed phase-segregated morphology of aromatic polymers.[1] In order to enhance the ionic conductivity and maintain an acceptable swelling ratio, researchers have been employed the strategies of cross-linking[1-3] and controlling the phase-segregated morphology to fabricate desirable AEMs.[4-6] In addition, although the rigid aromatic polymer backbones ensure good tensile strength (higher than 20 MPa), the poor flexibility (lower than 30% elongation at break) of the AEMs is unsatisfactory for fuel cell applications.[4] Under low relative humidity, the poor flexibility makes AEMs brittle, causing problems during MEA fabrication.[1] Also, the long-term fuel cell performance is closed related to the flexibility of AEMs since the fuel cell is operated under conditions such as wet-dry cycling.[1,7-12] Herein, we employ a unique approach to toughen AEMs by cross-linking the AEMs using commercial Jeffamine cross-linkers to impart flexibility to AEMs.

7.2 Experimental Section

Materials. Poly(2,6-dimethyl phenylene oxide) was purchased from Sigma-Aldrich and dried under vacuum at room temperature overnight. *N*,*N*-Dimethylhexylamine, *O*,*O'*-bis(2-aminopropyl) polypropylene glycol-block-polyethylene glycol-block-polypropylene glycol 500 (Jeffamine, CAS Number 65605-36-9), *N*-bromosuccinimide, and 2, 2*'*-azobis(2-methylpropionitrile) were obtained from Sigma-Aldrich and used as received. The brominated

PPO polymers with degrees of functionalization (DF) of 60 mol % of the repeat units on the backbone with one benzyl bromide group were synthesized according to the reported literature.[13]

Fabrication of membranes. Brominated PPO with a DF of 60 (2.5 g, 14.88 mmol) was dissolved in 30 mL of *N*-methyl-pyrrolidone (NMP). Then, *N*,*N*-dimethylhexylamine (0.97 g, 7.47 mmol) was added slowly. The mixture was stirred at room temperature for 48 h. The Jeffamine (0.54 g, 0.89 mmol) was added to the resulting mixture. Subsequently, the solution was then cast onto a leveled glass plate, and dried at 82 °C under ambient pressure for 24 h followed by vacuum drying for another 24 h at 80 °C to give a ~100 μm thick, transparent, tough film. The resulting membrane was J10PPO (10% Jeffamine cross-linked) in the bromide form.

7.3 Results and Discussion

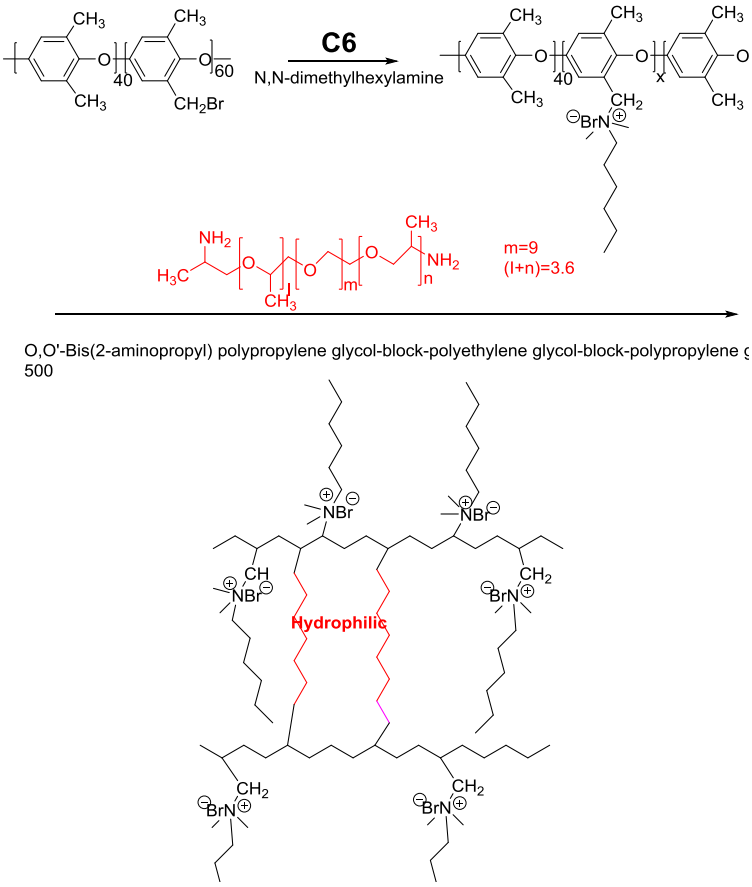

Scheme 7.1 Synthetic route of the Jeffamine cross-linked AEMs.

The synthetic route of the Jeffamine cross-linked AEMs was shown in Scheme 7.1. Br-PPO possessing a degree of bromination (DB) of 60 mol % at the benzyl position was synthesized using *N*-bromosuccinimide and 2, 2*'*-azobis(2-methylpropionitrile) in a refluxing chlorobenzene solution for 3 h according to our previous reports.[4] Then, a series of cross-linkable comb-shaped ionomers were achieved by the Menshutkin reaction of the olefinic primary amine (N,N-dimethylhexylamine shown above) with the bromo group of Br-PPO as shown in Scheme 7.1. Subsequently, the cross-linked samples were fabricated by the reaction of the remaining bromo

groups of Br-PPO with the secondary amine groups of the Jeffamine cross-linker during membrane casting. The DB of Br-PPO was maintained at 60 to obtain samples with calculated IECs ranging from 1.67 to 2.51 mmol/g (Table 7.1).

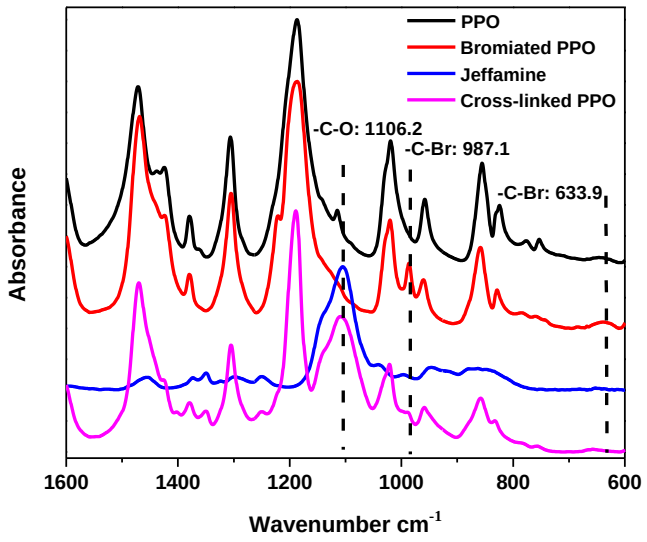

Figure 7.1 FTIR spectra of PPO, brominated PPO, Jeffamine and cross-linked membranes.

FTIR was used to confirm the reaction of the C-Br with the -NH_2 to form the cross-linked network. Compared to the PPO, as shown in Figure 7.1, there were distinct *v* (C-Br) peaks at 634 and 987 cm^{-1} for the brominated PPO, which appeared after bromination.[14-15] Both of the peaks assigned to *v* (C-Br) disappeared after cross-linking. In the spectrum of complete cross-linked membranes by the Jeffamine cross-linker, the new peaks at 1106 cm^{-1} associated with *v* (C-O) verified the presence of Jeffamine cross-linker in the cross-linked AEMs.[16] Considering these results, a strong covalent cross-linking network was formed by bromine and the secondary amine reaction which was further confirmed by the gel fraction (>80%) in NMP, Table7.1.

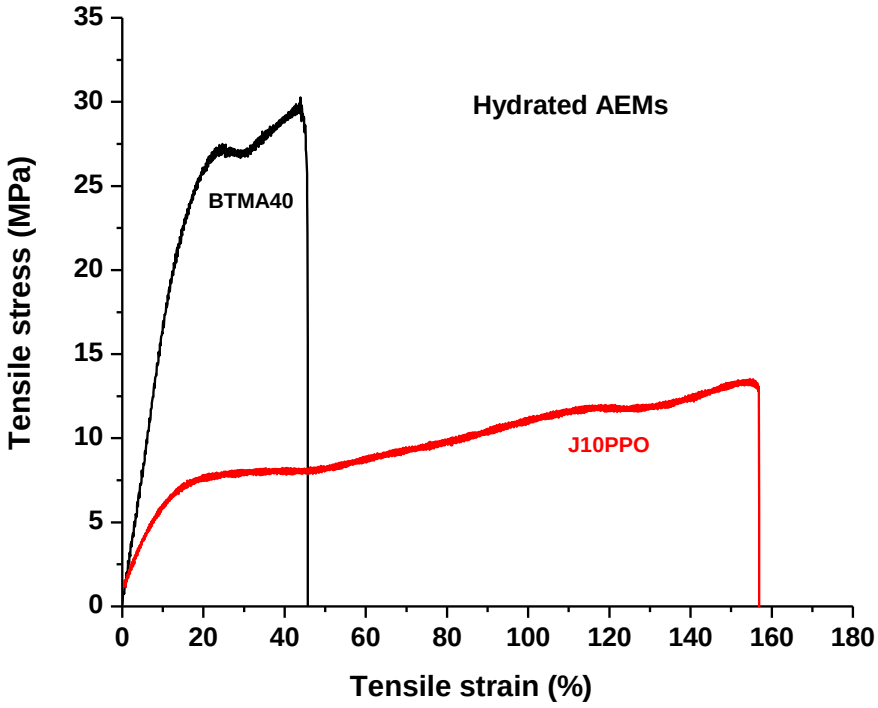

Figure 7.2 Stress-strain curves for J10PPO and BTMA40 hydrated AEMs.

Mechanical Properties. The comparison of mechanical properties between J10PPO and BTMA40 hydrated AEMs are shown in Figure 7.2. As conventional rigid AEM, BTMA40 exhibited high tensile strength (24 MPa), but possessed a low flexibility (51.7 % elongation at break). Compared to the BTMA40 membrane, the J10PPO demonstrated significantly higher elongation at break. To be specific, the hydrated BTMA40 membrane showed a 51.7% elongation at break, while the J10PPO had a 166.8 % elongation at break. Clearly, the introducing of hydrophilic cross-linked network greatly enhanced the toughness of the AEMs.

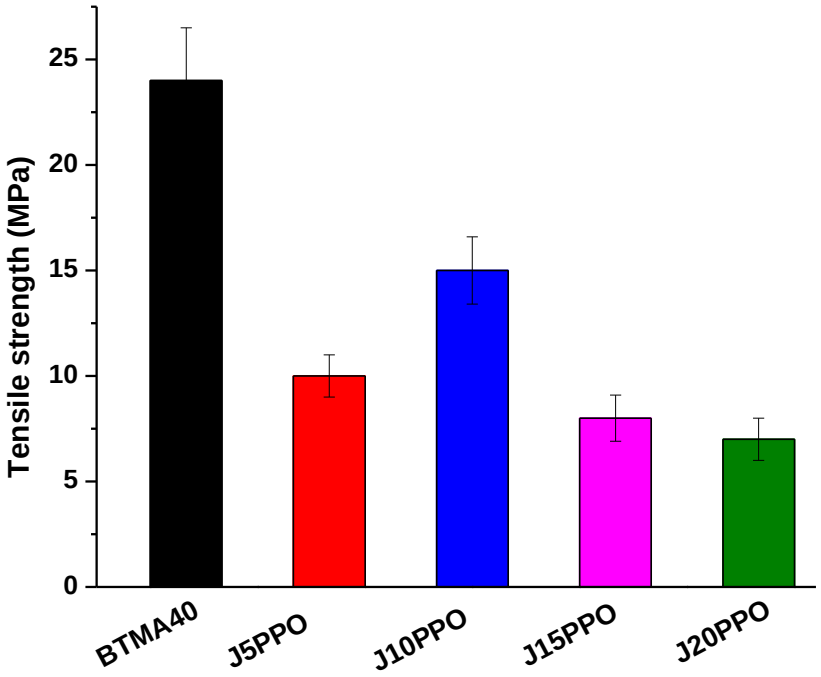

Figure 7.3 Maximum tensile stress for Jeffamine cross-linked and BTMA40 hydrated AEMs.

The comparison of tensile strength between Jeffamine cross-linked and BTMA40 hydrated AEMs are shown in Figure 7.3. The tensile strength decreased by increasing the content of Jeffamine cross-linker due to the flexible and hydrophilic properties of the cross-linker. In addition, the increase in the Jeffamine cross-linker reduced the content of rigid PPO backbones, which decreased the strength of the AEMs as well. Compared with J5PPO, the J10PPO showed a higher tensile strength due to the trade-off between decreased of content of rigid backbones and IEC.

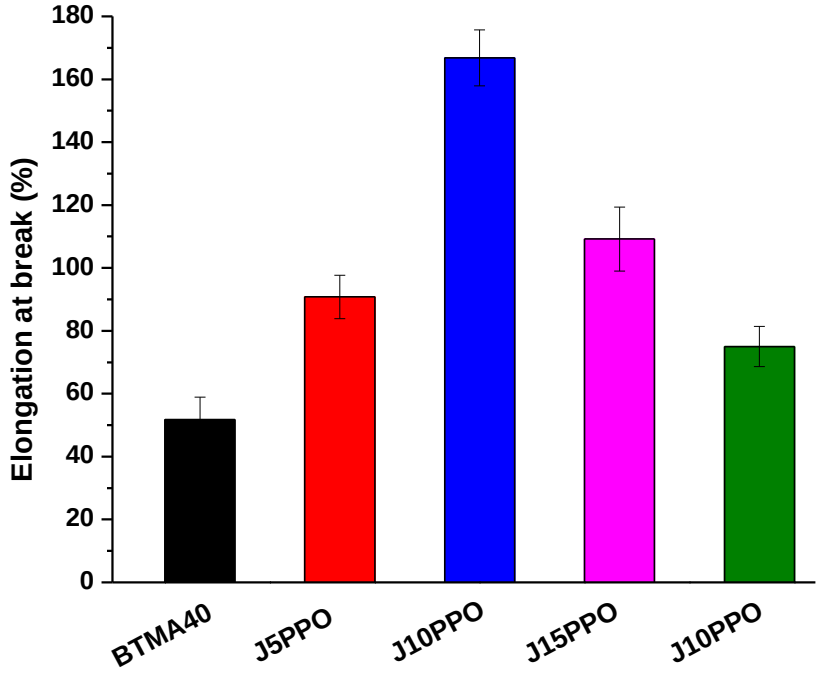

Figure 7.4 Maximum elongation at break for Jeffamine cross-linked and BTMA40 hydrated AEMs.

The comparison of elongation at break between Jeffamine cross-linked and BTMA40 hydrated AEMs are shown in Figure7.4. When the degree of cross-linking increased from 0 to 10%, the elongation at break increased by increasing the content of Jeffamine cross-linker. For example, J10PPO exhibited a 177% elongation at break, while the BTMA 40 showed only 52 %. However, the elongation decreased as degree of cross-linking increased from 10 to 20% due to the trade-off between content of Jeffamine cross-linker and degree of cross-linking.

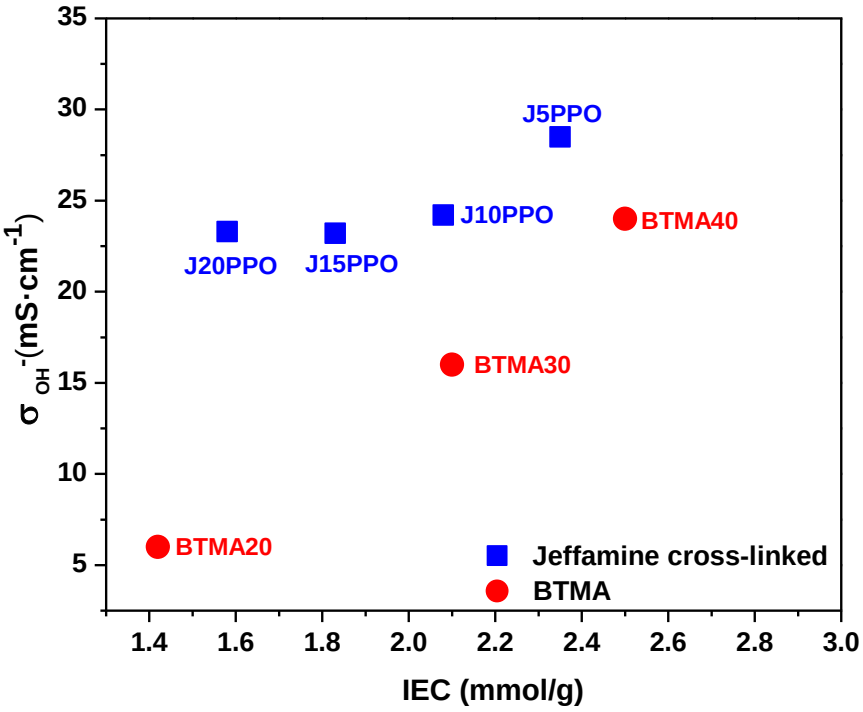

Figure 7.5 Hydroxide conductivity of Jeffamine cross-linked and BTMA AEMs in liquid water at 20 °C as a function of IEC.

High ionic conductivity is one of the most important properties for the application of AEMs in devices. To study ion transport behaviors inside of the Jeffamine cross-linked AEMs, OH^- conductivities of the AEMs with different IECs were measured. As expected, for the same type of AEM, the ionic conductivity decreased with decreasing IEC (Figure 7.5). As shown in Figure 7.4, the J5PPO membrane displayed OH^- conductivity of 29 mS/cm at room temperature with an IEC of 2.35 mmol/g, compared to 24 mS/cm for BTMA40 (IEC = 2.50 mmol/g) under the same testing conditions.

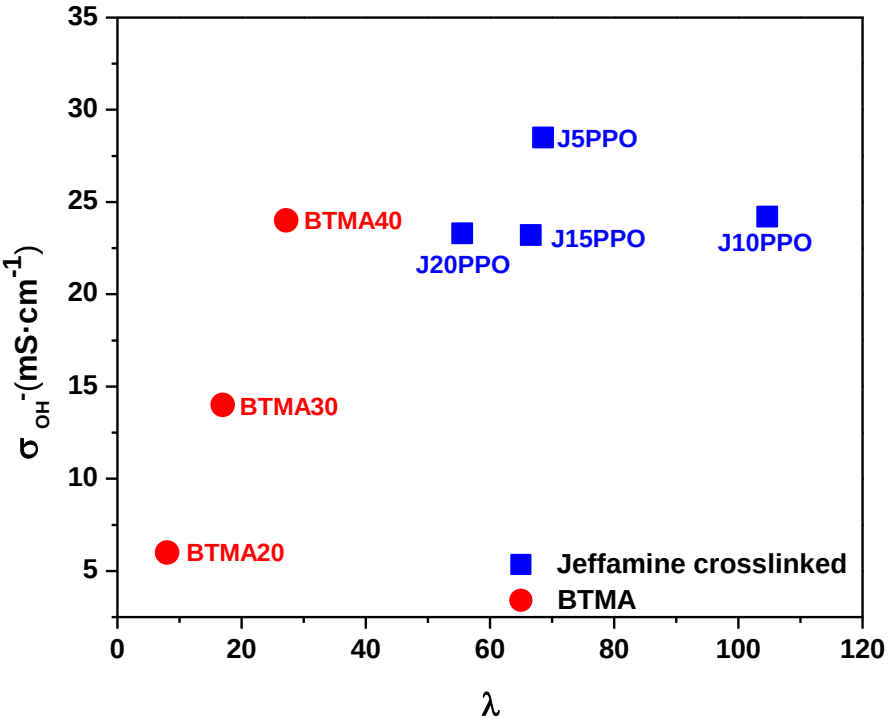

Figure 7.6 Hydroxide conductivity of Jeffamine cross-linked and BTMA AEMs in liquid water at 20 °C as a function of hydration number (λ).

For a better comparison among the different IEC membranes, the hydroxide conductivity was plotted as function of λ in Figure 7.6 (the number of absorbed water molecules per ammonium group). For the BTMA membranes, the approximate trend was that the hydroxide conductivity increased with λ due to the increased number of water molecules per ionic site which facilitates the hydroxide transport in the membranes. For Jeffamine cross-linked membranes, they showed similar hydroxide conductivity as BTMA*x* membranes under much higher hydration number (λ). For example, J15PPO demonstrated a hydroxide conductivity of 23 mS/cm with λ = 67, while the BTMA40 showed similar hydroxide conductivity of 24 mS/cm with λ = 27. This result is attributed to the introducing of hydrophilic cross-linker.

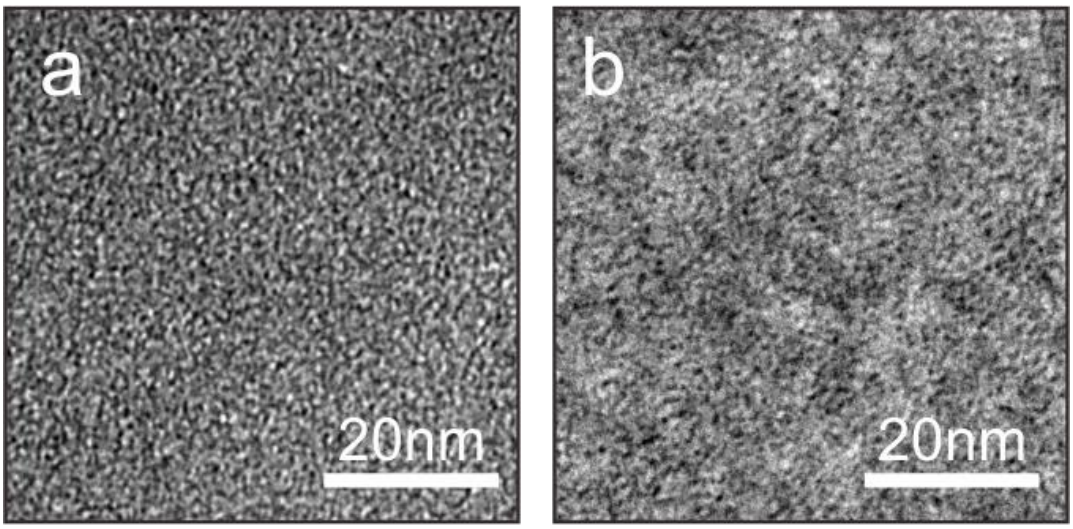

Figure 7.7 TEM images of dry membranes in the bromide form (a) BTMA40; (b) J10PPO.

As shown in the transmission electron micrographs in Figure 7.6, the dark areas represent the ionic domains stained by ruthenium tetroxide, while the bright areas represent the non-ionic domains. As shown in Figure, for the J10PPO membrane, ion aggregation in the TEM image was obvious hydrophilic/hydrophobic phase separation was observed tying the increased conductivity of these samples to their better-developed morphologies. In contrast, no obvious ion aggregation was observed in the TEM image for BTMA 40.

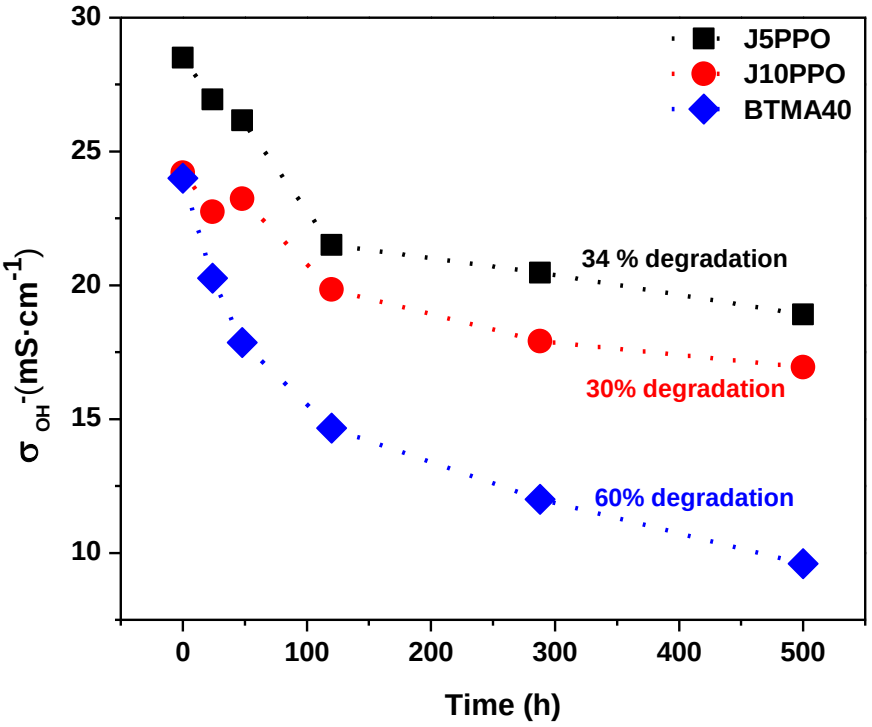

Figure 7.8 Chemical stability of the quaternary ammonium cation of Jeffamine cross-linked and BTMA40 samples in 1 M NaOH solution at 80 °C, OH^- conductivity as a function of duration time measured at 20 °C.

To evaluate the long-term alkaline stability of the AEMs, Jeffamine cross-linked and BTMA40 samples were immersed in Argon-saturated 1 M NaOH solution at 80 °C for 500 hours, with replacement of the 1 M NaOH every 3 days during the testing period. Figure 7.8 illustrates the changes in IEC and OH^- conductivity during stability testing of the samples. During the 500 h test, J10PPO exhibited the greatest cation stability. The OH^- conductivity of this membrane decreased by 30 %. In contrast, the OH^- conductivity of BTMA40 decreased to 9.6 mS/cm at 20°C, which 60 % lower than the value measured for the sample before the stability test. Better stability of Jeffamine cross-linked was demonstrated due to the cross-linking network and an

increase in the microphase separation of hydrophilic and hydrophobic domains, which is in good agreement with other reported results.[17]

7.4 Conclusions

A unique approach was employed to toughen AEMs by cross-linking the AEMs using commercial Jeffamine. Compared to the BTMA40 membrane, the Jeffamine cross-linked membrane demonstrated significantly higher elongation at break. To be specific, the hydrated BTMA40 membrane showed a 51.7% elongation at break, while the 10% Jeffamine cross-linked membrane had a 166.8 % elongation at break. Clearly, the introducing of hydrophilic cross-linked network greatly enhanced the toughness of the AEMs. In addition, Compared to BTMA-based AEMs, Jeffamine cross-linked membrane exhibited higher hydroxide conductivity and better long-term alkaline stability, which is critical for alkaline fuel cell applications.

Table 7.1 Ion exchange capacity, water uptake, ionic conductivity and mechanical properties of Jeffamine cross-linked AEMs.

sample	Jeffamine (mol %)	IEC (mmol/g)[a]	IEC (mmol/g)[b]	WU (wt%) (OH^-)[c]	σ (mS/cm) (OH^-)[c]	λ (OH^-)	Tensile strength (MPa)[d]	Elongation at break (%)[d]	Gel fraction (%)
J5PPO	5	2.51	2.35	295 ± 15	29 ± 2	68	10 ± 1	91 ± 7	79
J10PPO	10	2.22	2.08	425 ± 20	24 ± 1	105	15 ± 2	177 ± 9	81
J15PPO	15	1.94	1.83	259 ± 11	23 ± 1	67	8 ± 1	109 ± 10	84
J20PPO	20	1.67	1.58	208 ± 9	23 ± 1	56	7 ± 1	75 ± 6	85
BTMA40	-	2.66	2.50	116 ± 8	24 ± 2	27	24 ± 3	52 ± 7	-

[a]Calculated from the polymer composition and the degree of bromination. [b]Titrated values. [c]Measured at room temperature in liquid water. [d] For the hydrated samples.

7.5 References

(1) Pan, J.; Zhu, L.; Han, J.; Hickner, M. A. *Chem. Mater.* **2015**, *27*, 6689**.**

(2) Robertson, N. J.; Kostalik IV, H. A.; Clark, T. J.; Mutolo, P. F.; Abruña, H. D.; Coates, G. W. *J. Am. Chem. Soc.* **2010**, *132*, 3400.

(3) Pan, J.; Li, Y.; Zhuang, L.; Lu, J. *Chem. Commun.* **2010**, *46*, 8597.

(4) Li, N.; Leng, Y.; Hickner, M. A.; Wang, C.-Y. *J. Am. Chem. Soc.* **2013**, *135*, 10124.

(5) Pan, J.; Chen, C.; Li, Y.; Wang, L.; Tan, L.; Li, G.; Tang, X.; Xiao, L.; Lu, J.; Zhuang, L. *Energy Environ. Sci*. **2014**, *7*, 354.

(6) Tanaka, M.; Fukasawa, K.; Nishino, E.; Yamaguchi, S.; Yamada, K.; Tanaka, H.; Bae, B.; Miyatake, K.; Watanabe, M. *J. Am. Chem. Soc*. **2011**, *133*, 10646.

(7) He, S. S.; Strickler, A. L.; Frank, C. W. *ChemSusChem* **2015**, *8*, 1472.

(8) Song, F.; Fu, Y.; Gao, Y.; Li, J.; Qiao, J.; Zhou, X.-D.; Liu, Y. *Electrochim. Acta* **2015**, *177*, 137.

(9) Park, A. M.; Turley, F. E.; Wycisk, R. J.; Pintauro, P. N. *Macromolecules* **2014**, *47*, 227.

(10) Li, X.; Yu, Y.; Liu, Q.; Meng, Y. *ACS Appl. Mater. Interfaces* **2012**, *4*, 3627.

(11) Lin, B.; Qiu, L.; Qiu, B.; Peng, Y.; Yan, F. *Macromolecules* **2011**, *44*, 9642.

(12) Lin, B.; Qiu, L.; Lu, J.; Yan, F. *Chem. Mater.* **2010**, *22*, 6718.

(13) Li, N.; Yan, T.; Li, Z.; Thurn-Albrecht, T.; Binder, W. H. *Energy Environ. Sci.* **2012**, *5*, 7888.

(14) Ong, A. L.; Saad, S.; Lan, R.; Goodfellow, R. J.; Tao, S. J. Power Sources **2011**,*196*, 8272.

(15) Yang, Y.; Knauss, D. M. Macromolecules **2015**, *48*, 4471.

(16) Pucić, I.; Jurkin, T. *Radiat. Phys. Chem*. **2012**, *81*, 1426.

(17) Zhou, J. F.; Unlu, M.; Anestis-Richard, I.; Kohl, P. A. *J. Membr. Sci.* **2010**, *350*, 286.

Chapter 8

Summary and Future Research Directions

8.1 Summary and Conclusions

The research in this thesis has demonstrated strategies to produce cross-linked quaternary ammonium functionalized poly(2,6-dimethyl-1,4-phenylene oxide) AEMs synthesized via thiol-ene click chemistry and how the cross-linking strategy can boost both the dimensional and chemical stability of comb-shaped AEMs. Additionally, AEMs with multiple cations per side chain site were synthesized to study how the side chain cation motif can boost both the conductivity and stability of poly(2,6-dimethyl-1,4-phenylene oxide)-based AEMs. The triple-cation AEMs with proper arrangement of cations on the side chain exhibited high conductivity and chemical stability because of their low DF and better-developed morphologies compared to double or single cation samples. New synthetic routes for poly(2,6-dimethyl-1,4-phenylene oxide)-based AEMs with fluorene side chains were employed to study how introducing pendant alkyltrimethylammonium groups enhanced the conductivity and stability of PPO-based AEMs. By cross-linking the AEMs using commercial Jeffamine cross-linkers, toughened AEMs were obtained to show how the hydrophilic cross-linkers impart flexibility to the membranes. This thesis has not only clarified the properties of a number of novel AEMs, but has also employed newly designed and synthetized polymer materials to obtain insight to provide pathway for the development of next-generation AEM materials.

8.1.1 Cross-linking of Comb-Shaped Polymer Anion Exchange Membranes via Thiol-ene Click Chemistry

To produce anion conductive and durable polymer electrolytes for alkaline fuel cell applications, a class of cross-linkable, comb-shaped copolymers for stable anion exchange membrane applications were synthesized. The cross-linked comb-shaped membranes were achieved by thiol-ene click chemistry and the degree of cross-linking was readily controlled by tuning the amount of alkene-containing side chains pendant to the polymer backbone. The obtained cross-linked AEMs displayed a nanoscale phase-separated morphology, which was responsible for the higher ion conductivity of these materials compared to conventional BTMA AEMs. The cross-linking of the membranes enhanced both the chemical and dimensional stability of the membranes. The ATR-FTIR spectra clearly demonstrated that the major degradation pathway of the quaternary ammonium functionalized poly(2,6-dimethyl-1,4-phenylene oxide)s under alkaline conditions was β-hydrogen (Hofmann) elimination. The combination of the good solubility of the precursor and the highly efficient thiol-ene click chemistry enables this cross-linking strategy as a promising technology for preparing attractive AEM materials for fuel cells applications.

8.1.2 MultiCation Side Chain Anion Exchange Membranes

Side-chain containing AEMs with one, two or three cations per side chain were designed and synthesized, enabling a systematic study of how the degree of polymer backbone functionalization and arrangement of cations on the side chain impact AEM properties. Systematic improvements in ion conduction, swelling resistance, and long-term alkaline stabilities were observed, when the charge number on the cation side chain increased from one to three. Compared with typical AEMs based on the benzyltrimethyl ammonium motif and pendant

benzyldimethylhexyl ammonium single cationic group, the muti-cation side chain membranes exhibited much higher ionic conductivity but lower water uptake, due to the phase separation of the hydrophobic domains at low DF and larger ionic clusters induced by the presence of the side chains. Based on the high-performance triple-cation side chain AEM, a Pt-catalyzed fuel cell with a peak power density of 364 mW/cm^2 was achieved at 60 °C under 100% related humidity.

8.1.3 Poly(2,6-dimethyl-1,4-phenylene oxide)s With Fluorene Side Chains for Anion Exchange Membranes

Fluorene side chain-containing AEMs with attached alkyltrimethyl quaternary ammonium cationic groups were designed and synthesized. The AEMs were prepared by grafting fluorene units onto a PPO backbone via a Suzuki-Miyaura cross-coupling reaction using a ligand designed for sterically hindered substrates. The Suzuki-Miyaura cross-coupling reaction of aryl bromides with fluorene-boronic acids was nearly complete demonstrating the usefulness of this reaction for polymer post-polymerization modification. Compared to BTMA-based AEMs, the PPOF AEMs exhibited good long-term alkaline stability at 80 °C, which is critical for alkaline fuel cell applications. This stability is likely due to the separation of the cationic group from the polymer backbone by an alkyl spacer. Additionally, the presence of long alkyl pendant chains is effective for enhancing the thermochemical stability of the AEMs. The PPOF AEMs showed excellent solubility in solvents such as dimethyl formamide, dimethyl sulfoxide and methanol at room temperature, making them as useful candidates for ionomer materials. The results of this study provide a new approach for design of high performance AEMs for application in alkaline fuel cells.

8.1.4 Jeffamine cross-linked robust Anion Exchange Membranes

A unique approach was employed to toughen AEMs by crosslinking the AEMs using commercial Jeffamine, an amine end-functionalized PEO-PPO copolymer (CAS Number 65605-36-9). Compared to the BTMA40 membrane, the Jeffamine cross-linked membrane demonstrated significantly higher elongation at break. To be specific, the hydrated BTMA40 membrane showed a 51.7% elongation at break, while the 10% Jeffamine cross-linked membrane had a 166.8 % elongation at break. Clearly, the introducing of hydrophilic cross-linked network greatly enhanced the toughness of the AEMs. In addition, Compared to BTMA-based AEMs, Jeffamine cross-linked membrane exhibited higher hydroxide conductivity and better long-term alkaline stability, which is critical for alkaline fuel cell applications.

8.2 Future Research Direction

The concentration of the future work will focus on further enhancing the chemical stability of AEMs for long-lasting purpose in electrochemical devices and designing mechanically robust AEMs with high hydroxide conductivity. The multication side chain and fluorene side chain containing AEMs need to be reinforced to obtain mechanically robust AEMs via introducing flexible cross-linked networks. In addition, the ^{1}H NMR and 2D NMR need to be employed to investigate the degradation mechanism of the AEMs, providing more information and direction for future design and development of advanced AEMs. This thesis has demonstrated a number of methods to obtain high conductivity materials, but degradation stability at 80 °C and higher must be pursued to obtain materials that do not degrade over 100s of hours of accelerated testing.

VITA

Liang Zhu

Liang Zhu was born and raised in Jiangxi, China, and attended Pingxiang Number 2 High School where she graduated with honors in 2004. Liang continued your education at the Tianjin Polytechnic University, where she pursued Materials Science and Engineering. He graduated in 2008, receiving a Bachelor of Science in Materials Science and Engineering. He received his master of science in Polymer Chemistry and Physics from Zhejiang University in 2012. He began graduate school in August of 2012 at The Penn State University, and began working under the tutelage of Dr. Michael A. Hickner in June of 2013. His PhD dissertation involved in the synthesis of side-chain containing anion exchange membranes for fuel cell application.